

https://dspace.org/

Profiling gene expression pattern changes in HIV-1-associated kidney disease

Mpye, Keleabetswe Lerato

2016-02-22
http://hdl.handle.net/10539/19677

Downloaded from a DSpace repository. https://dspace.org/

1. BACKGROUND

1.1. Kidneys: An overview

Human kidneys are a pair of 10 to 13 centimeter long organs located posteriorly in the abdomen. The primary functions of the kidney are to filter blood as a means of removing waste products from plasma thereby, controlling the body's fluid balance and maintaining electrolyte and acid-base balance, and to produce key hormones such as erythropoietin and parathormone (Ebert and Bunn, 1999; Drueke and Eckardt; 2002). Thus, urine production starts in the renal glomerulus (Figure 1). The glomerular filtration barrier consists of three layers, notably; the endothelium, the glomerular basement membrane (GBM) and the podocytes (Figure 2), each of which contributes to the selective permeability of the filter.

Glomerular endothelial cells are flattened cells that separate the blood and tissue compartments. These cells are highly fenestrated, and thus, extremely permeable to water and small solutes. Although the precise function of this first layer is still unclear in the glomerular filter system, it has been shown to regulate vasomotor tone, trafficking of leukocytes and hemostasis (Ballermann, 2005). An earlier study assessed the effects of oxidative stress on the endothelium and revealed that damage to the endothelial surface layer resulted in proteinuria even if the GBM and podocytes remained intact (Kawabara *et al.*, 2010). The resulting increase in glomerular permeability suggested that the endothelium is involved in regulating the permselectivity of macromolecules.

The GBM is a dense structure of extracellular matrix synthesized and maintained by the podocytes (Pavenstadt *et al*., 2003). This second layer of the glomerular filter is composed of collagen type IV, laminins, nidogen and proteoglycans. The GBM serves as both structural support for the capillary wall to be able to maintain local high blood pressure and also for selective permeability of the filtration barrier (Levidiotis and Power, 2005). The capillary wall is

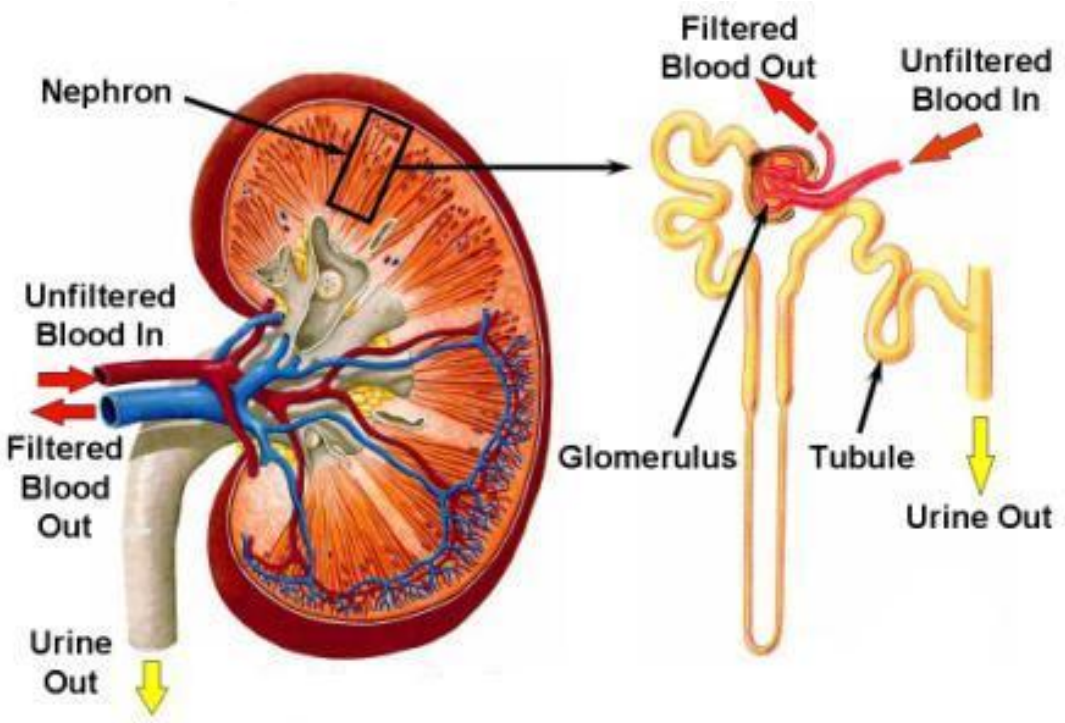

Figure 1: Kidney cross-section

A kidney's functional unit is called a nephron. Through the nephron, a kidney controls the body's fluid balance and maintaining electrolyte and acid-base balance by filtering blood, i.e., removing waste products from plasma and excreting in urine. Urine production starts in the renal glomerulus

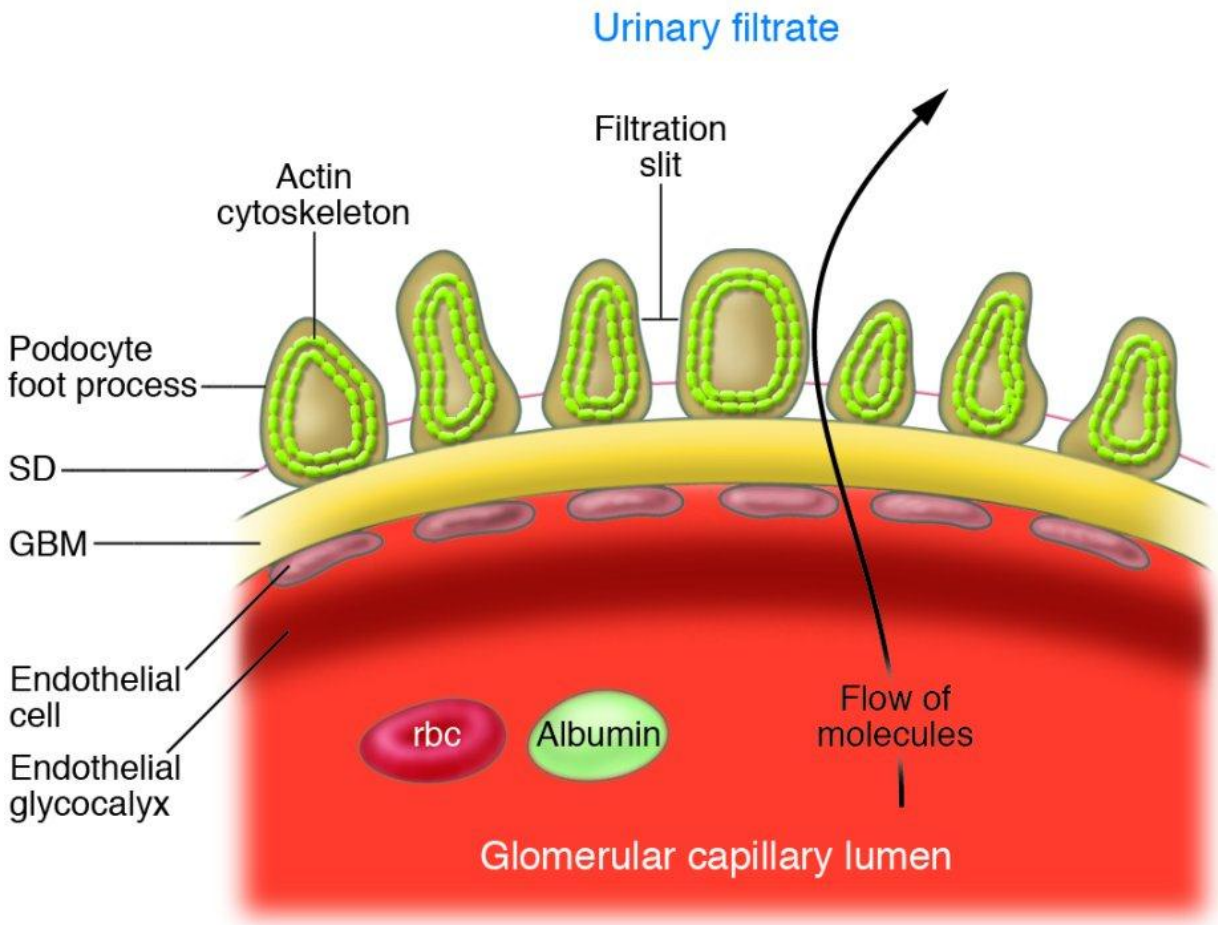

Figure 2: Glomerular filtration barrier

The three layers of the glomerular filter responsible for the selective permeability of the filter. The filter is composed of the glomerular endothelium, glomerular basement membrane (GBM) and visceral epithelium or podocytes. The actin-based cytoskeleton maintains the structural integrity of the foot processes. Foot processes of neighboring podocytes interdigitate to form slit pores (filtration slits) that are linked by an extracellular structure called the slit diaphragm (SD). Waste products are removed from the filtered blood and form part of what is excreted as urine (urinary filtrate). Water, small molecules and ions are filtered through the glomerular capillary wall, whereas albumin, red blood cells and other large molecules are retained. Photo adapted from Ronco (2007), with permission from the publishers (License number: 3587010816195; Appendix).

permeable to water, small molecules and ions but impermeable to plasma proteins and other large molecules (Figure 2) (Reiser *et al*., 2000). Due to its constituents, the GBM was initially believed to be the most vital component of the glomerular filter until several novel proteins for size-selective glomerular permeability were discovered in the glomerular podocytes. The GBM accounts for the charge-selective permeability of the glomerular filter (Drumond and Deen, 1994).

The third layer, comprising podocytes or visceral epithelial cells, constitutes the main part of the glomerular filtration barrier. It covers the exterior basement surface of the glomerular capillary and maintains an immense filtration surface. Structurally, podocytes are highly specialized, terminally differentiated cells composed of three different segments; cell body, major processes and foot processes. The former two segments float freely in the Bowman's space and are not in direct contact with GBM whereas, the foot processes extend into the cytoplasm and are attached to the outer surface of the GBM through cell membrane receptors (Figure 3) (Kretzler, 2002). The cell body, located in the center of the cell bulging into the urinary space, possesses thick extensions that branch to form pedicles called foot processes. Foot processes of neighboring podocytes interdigitate to form filtration slits (slit pores) that are linked by an extracellular structure called the slit diaphragm (Figure 2). Podocyte shape is maintained through the cytoskeleton encompassing actin, myosin, α-actinin, talin, paxillin, filamin and vinculin (Drenckhahn and Franke, 1988; Mundel and Kriz, 1995). These proteins link the GBM to the intracellular cytoskeleton via the heterodimeric transmembrane receptors, integrins (Mundel and Kriz, 1995). The cytoskeleton not only enables the continuous formation and adaptation of the podocytes, but also opposes the high hydrostatic pressure necessary for glomerular filtration by supporting the glomerular capillary wall (Kriz *et al*., 1994). Functionally, podocytes are responsible for synthesizing and maintaining the GBM, secreting vascular endothelial growth factor A, and similar to the GBM, podocytes are responsible for selective permeability, based on size, of the glomerular filter (Farquhar, 1975; Tanner, 2009). Jointly with their foot processes, podocytes maintain the ultrafiltration barrier and prevent urinary protein loss (i.e., proteinuria). Transmembrane and adaptor proteins such as zonulaoccludens-1, CD2-associated protein, podocin, nephrin and P-cadherin link the slit diaphragm to the podocyte cytoskeleton, thus playing a pivotal role in maintaining the structural and functional integrity of the glomerular filtration barrier (Figure 3) (reviewed in detail by Mundel and Shankland, 2002).

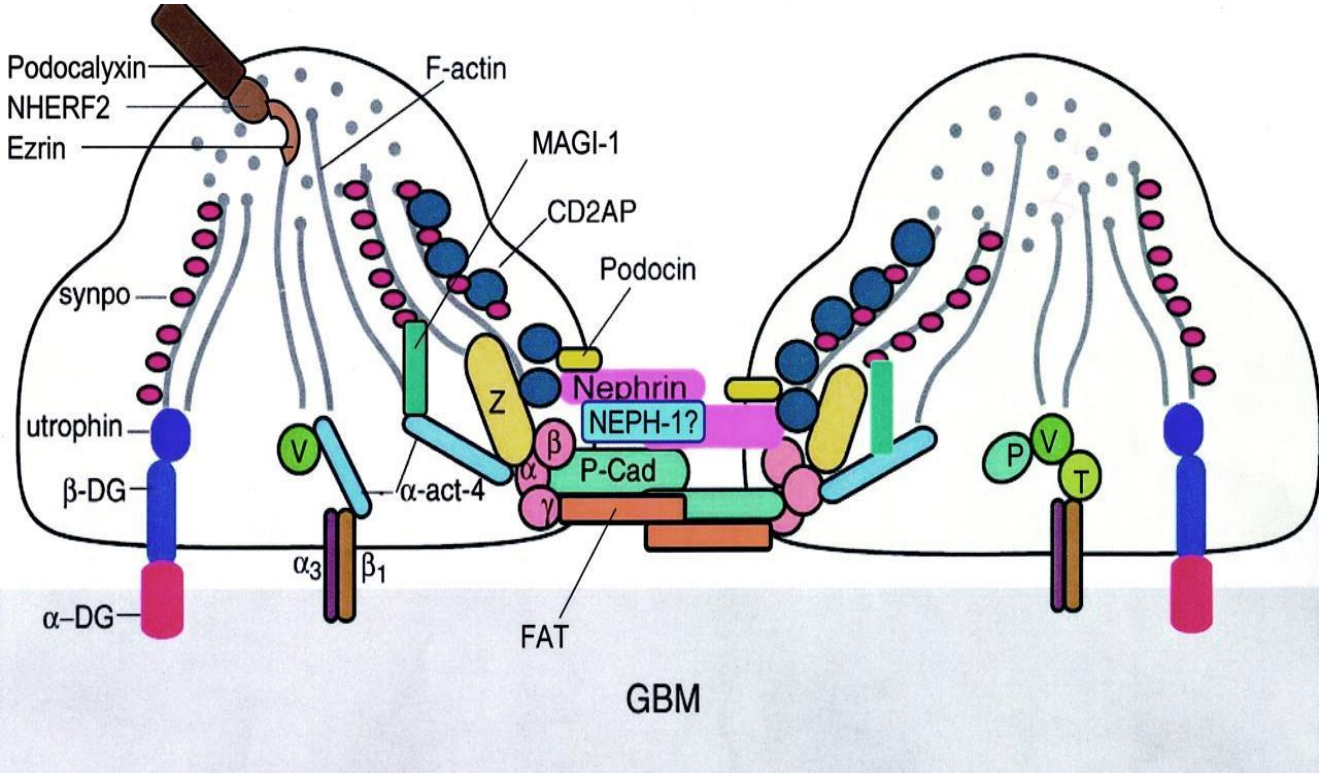

Figure 3: Schematic representation of actin-based podocyte cytoskeleton

Foot processes extend from the podocytes into the cytoplasm to increase the surface area critical for the efficiency of ultrafiltration. Podocyte shape is maintained through the cytoskeleton composed of actin, myosin, α-actinin, synaptopodin (synpo), talin, paxillin and vinculin. The cytoskeleton enables the continuous formation and adaptation of the podocytes and also opposes the high hydrostatic pressure necessary for glomerular filtration by supporting the glomerular capillary wall. In lipid rafts, a surface receptor nephrin transmits extracellular signals from the slit diaphragm to the cytoskeketon through interactions with podocin and CD2AP. Nephrin and podocin are anchored to the actin filaments by binding CD2AP. Foot processes are attached to the outer surface of the GBM through cell membrane receptors. Photo adapted from Mundel and Shankland, 2002. Reproduced with permission from the publisher (License number: 3585300486244; Appendix)

1.2. Kidney diseases

Epidemiological studies have listed kidney disease amongst the top 10 leading causes of death in the American population and affecting over 10 % of the adult population (Centers for Disease Control and Prevention, 2014 - http://www.cdc.gov, accessed February 2015). The risk of developing cardiovascular disease is increased by up to 30 % in chronic kidney disease patients (Sarnak *et al*., 2003). Like most other diseases, kidney disease can be primary, arising from diseases specific for the kidneys. These are mostly genetically inherited and include focal glomerulosclerosis, minimal change nephropathy and membranous nephropathy (Tryggvason *et al*., 2006a). Conversely, secondary glomerular disease occurs as a result of a systemic condition for examples, following diabetes mellitus, lupus erythematosus, amyloidosis, preeclampsia or bacterial, protozoal or viral infections (Hepatitis and HIV). Glomerular injury is marked by hematuria and proteinuria, and structural and histological abnormalities detected by imaging and microscopy (National Institute for Health and Care Excellence, 2015 - http://www.nice.org.uk, accessed February 2015). Along with genetic mutations, changes in the podocyte foot processes and actin-based cytoskeleton components may lead to nephrotic syndrome (Smoyer *et al*., 1997; Takeda *et al*., 2001; Tryggvason *et al*., 2006). Disruption of the podocyte cytoskeleton architecture through dysregulation of its principal element, actin, or its associated proteins, has been demonstrated to be the cause of foot process effacement and proteinuria. The majority of these proteins are susceptible to proteolysis by a lysosomal cysteine protease, cathepsin-L (Figure 4) (Sever *et al*., 2007; Faul *et al*., 2008; Yaddanapudi *et al*., 2011). Host genes implicated in nephrotic syndrome are discussed in Section 1.6. Malfunctioning of the kidney may result in build-up of waste products in the blood, causing complications such as nerve damage, high blood pressure and cardiovascular disease. Progression of kidney diseases may lead to terminal kidney failure/end-stage renal disease, requiring dialysis or transplantation. Focal segmental glomerulosclerosis and HIV-associated nephropathy, representing primary and secondary renal diseases, respectively, were chosen for the purpose of the current study and are discussed further in Sections 1.2.1 and 1.2.3. The two share a common histology and are clinically characterized by progression to end-stage renal disease.

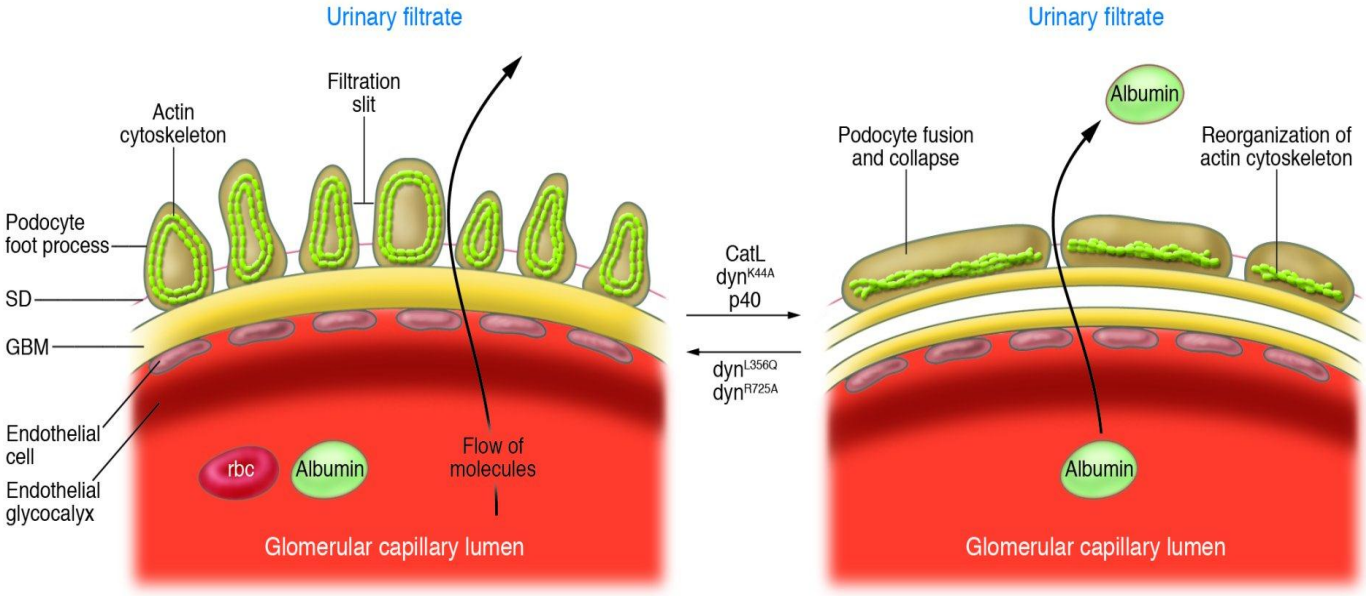

Figure 4: Re-organization of the Podocyte cytoskeleton and proteinuria

The onset of proteinuric renal diseases manifests through re-organization of the podocyte cytoskeleton architecture. Proteolysis of the actin-associated protein, i.e., dynamin, CD2AP or synaptopodin, by a lysosomal cysteine protease cathepsin-L leads to foot process effacement and proteinuria. Proteinuria is characterized by excretion of large molecules as part of the urinary filtrate. Image reproduced with permission from the publisher (License number: 3587010816195; Appendix) (Ronco, 2007).

1.2.1. Chronic kidney disease

Chronic kidney disease (CKD) is a global public health problem with increasing prevalence. The disease has been classified into 5 stages, by the U.S. National Kidney Foundation, according to estimated glomerular filtration rate (Levey *et al*., 2003). Normal glomerular filtration rate (GFR) ranges between 90 and 120 ml/min/1.73 m^2, depending on age, as GFR decreases with age. Stages 1 to 3 of CKD are described by kidney damage characterized by abnormal urinary sediment (proteinuria, hematuria) or structural abnormalities plus normal to moderately decreased GFR (GFR 30 - 90 ml/min/1.73 m^2), whereas stages 4 and 5 present with severely decreased GFR, between 15 and 29 ml/min/1.73 m^2 and less than 15 ml/min/1.73 m^2, respectively. Of the 11 % (19.2 million) U.S. population suffering from chronic kidney disease, 0.22 % have end-stage renal disease (ESRD), i.e., stage 5 of CKD (Coresh *et al*., 2003). The prevalence of ESRD is steadily growing and it is estimated to rise to over 20 % of the CKD population by the year 2030 (Schoolwerth *et al*., 2006). End-stage renal disease is an irreversible condition arising due to, but not limited to, hypertension, obesity, glomerulonephritis and most commonly diabetic nephropathy, with patients ultimately requiring renal replacement therapy in the form of dialysis and renal transplantation. Studies have reported that ESRD patients have four to fivefold increased risk of developing renal cancer (Birken *et al*., 2000, Mandayan and Shahinian, 2008).

1.2.2. Focal segmental glomerulosclerosis

Focal segmental glomerulosclerosis (FSGS) refers to a pathologically diverse group of glomerular lesions with heterogeneous clinical manifestations. Nearly 10 % of primary FSGS patients progress to ESRD and about 25 % of transplant patients develop recurrent FSGS following surgery (D'Agati *et al*., 2011). In primary FSGS, five variant forms of the disease have been defined according to the Columbia FSGS classification system. Notably, the collapsing variant, cellular variant, tip lesion variant, perihilar variant and the not otherwise specified variant. As the name suggests, the collapsing variant is histologically characterized by collapse of the glomerular tuft. This FSGS variant presents with decreased renal function and rapid progression to renal failure (Detwiler *et al*., 1994). The cellular variant of FSGS is characterized

by endocapillary hypercellularity and cells in a segment of glomerular capillary tuft with lumen occlusion. Cellular FSGS occurs at a very low frequency in the population. Tip lesion FSGS variant has a more benign course than other FSGS variants and responds well to corticosteroid therapy (Howie and Brewer, 1984). Perihilar variant is histologically defined by glomeruli with perihilar hyalinosis. This variant of FSGS is usually accompanied by glomerulomegaly (enlargement of glomeruli) and often presents in association with obesity or compromised functional renal mass (Kambham *et al*., 2001). The not otherwise specified variant is histologically characterized by segmental capillary wall collapse and/or segmental sclerosis. However, researchers agree that some of these variants are difficult, almost impossible, to distinguish histologically (Meyrier, 2001; Chun *et al*., 2004; Stokes *et al*., 2006).

1.2.3. HIVAN and HIVICK

HIV-1 infected individuals are at risk of developing clinically and morphologically diverse renal complications. Most of the resulting renal complications are similar to those observed in non-HIV patients while some are limited to HIV patients. Two to ten percent of patients infected with HIV-1 ultimately suffer from chronic kidney disease due to HIV-associated nephropathy (HIVAN) (Rao *et al*., 1984; Bourgoignie and Pardo, 1991). This chronic kidney disease arises due to expression of viral genes in podocytes and parietal epithelial cells, tubular epithelial cells and mesangial cells, and causes loss of adherence of foot processes (Bruggeman *et al*., 2000; Husain *et al*., 2002). HIVAN may also result from dysregulation of certain host cellular pathways; these include pathways involved in cell cycle and apoptosis (He *et al*., 2004). Infection of tubular cells results in tubular cell apoptosis, characterized by alterations in expression levels and patterns of characteristic cellular markers (Rosenstiel *et al*., 2008). Clinically, HIVAN presents with heavy proteinuria, azotemia and enlarged kidneys. Collapsing focal segmental glomerulosclerosis (FSGS) and proliferation of renal tubular, parietal and visceral epithelial cells are amongst other prominent pathologic characteristics of a well-progressed HIVAN. Tubular cell hypertrophy, microcystic tubular dilation and irregular cell division, portrayed by increased chromosome number, together with interstitial inflammation are amongst the remarkable features observed in HIVAN patients (Rosenstiel *et al*., 2008). Proteinuria serves as an early sign of HIVAN, and may be used as a tool to monitor HIV

patients. Prior to the era of antiretroviral treatment, HIVAN was characterized by rapid progression to end-stage renal disease, thus necessitating dialysis for patients. HIVAN was profiled as the third leading cause of end-stage renal disease, after diabetes and hypertension, in the African-American population and was almost exclusively restricted to black patients (Cantor *et al*., 1991; Winston *et al*., 1998). This marked racial predilection suggested that genetic factors played a crucial role in the pathogenesis of HIVAN. Patients with genetic polymorphisms in the myosin heavy chain 9, non-muscle (*MYH*9), *apolipoprotein L*1 (*APOL*1), CD2-associated protein (CD2AP) and *nephrosis 2, idiopathic steroid-resistant* (podocin) (*NPHS*2) genes were identified to be at high risk. Contributions of each of the abovementioned genetic polymorphisms are reviewed section 1.6.

Similarly to HIVAN, HIV immune complex kidney disease (HIVICK) is characterized by leakage of large amounts of protein from the blood stream into the urine. However, unlike HIVAN, the onset of HIVICK does not require expression of viral genes in renal compartments and the disease may not be improved or prevented by antiretroviral therapy (Foy *et al*., 2013). The disease had been predominantly reported in patients of Asian and European descent (Nochy *et al*., 1993), and subsequently it has been reported in patients of African ancestry (Gerntholtz *et al*., 2006; Foy *et al*., 2013). Immune response to viral proteins, i.e., activation of B cells, with immune complex formation was proposed to be the cause of this disease (Bruggeman and Nelson, 2009). HIV immune complex kidney disease usually presents with a group of symptoms that include nephrotic syndrome with microscopic hematuria in HIV-positive patients. These clinicopathologic features resemble those observed in other glomerular diseases such as HIVAN, membrano-proliferative glomerulonephropathy, membranous nephropathy, glomerulonephritis and “lupus-like” glomerulonephritis (Haas *et al*., 2005; Cohen *et al*., 2008).

1.3. Human immunodeficiency virus

By the end of 2013, over 35 million people were infected with the human immunodeficiency virus (HIV) globally, with a mortality rate of above 23 % of the infected population (World Health Organization, 2015 - http://www.who.int/gho/hiv/en, accessed February 2015). The HIV-pandemic continues to grow in sub-Saharan Africa, with over 70 % of global infections localized to this region. Human immunodeficiency virus type 1 (HIV-1) is a highly mutable lentivirus whose infection is responsible for the development of an acquired immune deficiency syndrome (AIDS) (Weiss *et al*., 1985; Gallo and Montagnier, 1988, Gallo, 1988). HIV-1 encodes structural genes (*gag*, *pol* and *env*), regulatory genes (*tat* and *rev*) and accessory genes (*vif*, *vpr*, *vpu*, and *nef*) (Figure 5). Similarly to most retroviruses, the main or structural genes are expressed as zymogens (inactive polyprotein precursors) that are later hydrolyzed by protease enzymes to yield mature structural and functional proteins essential for viral assembly, maturation and continued infection (Coffin *et al*., 1997; Vogt, 1996; Louis *et al*., 1999). Proteolysis of the *gag* region gives rise to the structural proteins; N-terminal matrix protein (p17), the capsid protein (p24), the nucleocapsid (p7) and the C-terminal p6 (Luban *et al*., 1993). The two envelope glycoproteins, gp41 and gpl20, in the golgi apparatus are encoded in the *env* gene and are processed in the final stages of the HIV-1 life-cycle to produce infectious virion particles (Debouck *et al*., 1987; Niu, 2008). HIV-1 *pol* gene processing yields three viral enzymes; namely, the protease (p10), reverse transcriptase (p66 and p51) and integrase (p32) crucial for viral maturation and propagation. Figure 5 highlights the genomic arrangement of HIV-1 and the proteolytic results thereof. HIV-1 infection leads to a compromised immune system as a result of depletion of CD4+ T cells, a clinical characteristic of AIDS. This renders the infected individuals susceptible to an array of secondary or opportunistic infections including tuberculosis and viral infections such as cytomegalovirus, with a frequent clinical presentation with kidney failure (Johnson *et al*., 2001; Lawn and Wood, 2005). Renal failure accounts for about 10 % of deaths associated with HIV-1 infection (Zhong *et al*., 2005). Several of the HIV-1 genes are implicated in the onset of HIV-associated nephropathy (HIVAN) (explained in detail in section 1.2.3).

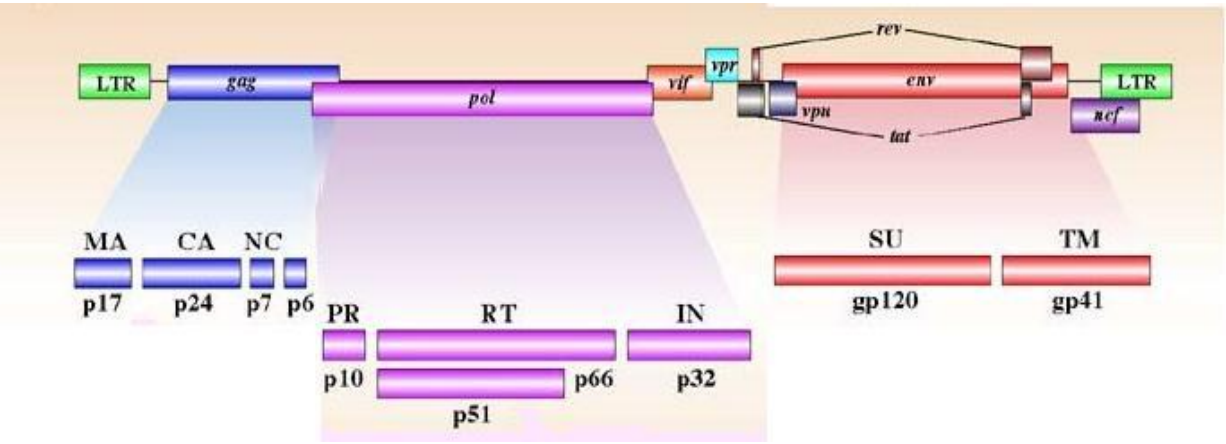

Figure 5: Genomic organization of HIV-1

Structural genes, *gag*, *pol* and *env*, encode several proteins and enzymes that are responsible for multiplication and continued infection of the virus. LTR: long terminal repeats, MA: matrix protein, CA: capsid protein, NC: nucleocapsid protein, PR: protease enzyme, RT: reverse transcriptase enzyme, IN: intergrase enzyme, SU: gp120 subunit envelope glycoprotein and TM: gp41 transmembrane envelope glycoprotein. Photo credits: (UNAIDS)

1.4. HIV-1 acquisition in renal cells

HIV-1 infection of host cells is initiated by sequential binding of the viral gp120 to host receptors (CD4) and chemokine co-receptors (CCR5 or CXCR5). However, in the case of renal cell infection, where neither receptors nor the co-receptors are expressed on the cell surface, the mechanism of HIV-1 acquisition is not yet clearly understood (Eitner *et al*., 2000). Several research groups have made efforts to elucidate the mechanism of infection of renal cells by HIV-1. Two possible mechanisms of HIV-1 acquisition by kidney cells have been reported. The first mechanism studied hypothesized the usage of lipid rafts whereby HIV-1 infection of podocytes was drastically hindered upon treatment of cells with methyl-β-cyclodextrin. The compound disrupts lipid channels within the membranes by removing cholesterol from cell membranes. This study concluded that HIV-1 acquisition was through lipid rafts embedded in the cell membranes (Mikulak and Singhal, 2010). However, this contradicted reports from other studies (Percherancier *et al*., 2003; Popik and Alce, 2004). The second mechanism hypothesized cell to cell adhesion as the favorable method of infecting kidney cells by HIV-1. Renal cells were co-cultured with CD4+ T cells infected with tagged HIV-1. Stable cell to cell adhesion through cell surface heparin sulfate proteoglycans (attachment receptors) resulted in viral RNA direct transfer from CD4+ T cells into kidney cells (Chen *et al*., 2011). The cell-cell transfer method has been supported and proven valid by numerous successive research groups using renal tubular epithelial cells incubated with HIV-infected macrophages (Hubner *et al*., 2009; Connell and Lortat-Jacob, 2013; Costiniuk and Jenabian, 2014).

Renal cross-transplantation experiments and phylogenetic comparative analysis have revealed evidence of tissue-specific viral evolution that lead to nephropathy, independently of the circulating viral proteins (Marras *et al*., 2002; Bruggeman *et al*., 2009). This was further emphasized by a case where a patient with virus suppressed in the peripheral blood following anti-retroviral therapy still had detectable levels of HIV-1 mRNA in the renal tissue and went on to develop HIVAN (Winston *et al*., 2001). HIV-1 proviral DNA and mRNA were detected in epithelial cells of the kidneys in such patients. These findings demonstrated the existence of a renal viral reservoir.

HIV-1 mortality has been markedly reduced following the introduction of highly-active antiretroviral treatment (HAART) (Lawn and Wood, 2005; Montaner *et al*., 2006). Subsequently, the prevalence of HIVAN and progression to ESRD was curbed in HAART settings (Lucas *et al*., 2004). Studies using Tg26 transgenic mouse revealed that HIVAN was still as prevalent in HAART patients with undetectable plasma viral RNA (Winston *et al*., 2001). Thus, infected renal epithelium serves as a distinct compartment from the blood and viral expression in the kidneys is sufficient to cause HIVAN (Medapalli *et al*., 2011). Biopsy specimens from HIVAN patients were analyzed to assess the prevalence of HIV in the human kidney (Marras *et al*., 2002).

1.5. HIV-1 genes implicated in HIVAN manifestation

Up to 10 % of HIV-1 infected individuals die from HIVAN (Zhong *et al*., 2005). From studying HIVAN biopsies, it was discovered that a well-progressed HIVAN is characterized by collapsing focal and segmental glomerulosclerosis (FSGS). HIVAN severely affects the renal podocyte cytoskeleton by altering its filtering capacity, resulting in heavy proteinuria and without HAART, rapid progression to end-stage renal disease. HIV-1 mRNA is expressed in renal tubular cells and replicates within the renal compartments. However, a study using an HIV-1 transgenic rat lacking viral structural genes (*gag* or *pol*) has revealed that viral replication is not necessary for the pathogenesis of HIVAN, however they may play a role in disease progression (Reid *et al*., 2001). Other studies have demonstrated that expression of viral accessory genes in renal compartments is crucial in the development of kidney disease and results in HIVAN pathology (Zhong *et al*., 2005; Rosenstiel *et al*., 2008). In a study by Zhong *et al*., (2005) the role of podocyte-restricted HIV-1 gene expression in progression of HIVAN was determined by generating transgenic mice expressing non-structural genes (*vif*, *vpr*, *vpu*, *tat*, *rev* and *nef*) in podocytes. Using *in-situ* hybridization, HIV-1 RNA was localized to podocytes. After 2 weeks, podocytes had a cuboidal morphology. In the third week, proteinuria had developed and podocyte damage and damage to other glomerular cells was evident. Eventually, collapsing FSGS and microcystic tubular dilation was observed after 4 weeks (Zhong *et al*., 2005). This implicated the HIV-1 accessory gene *nef* in the pathogenesis of HIVAN. *Nef* plays a crucial role in various steps of the viral life cycle and its pathogenesis, including lymphocyte T cell

activation, promotes viral transcription and activation of cell signaling pathways (Laguette *et al*., 2010). In podocytes, *nef* induces dedifferentiation and proliferation through MAPK1, 2 and Stat3 pathways activation (He *et al*., 2004). Elimination of Stat3 activity in HIV-1 transgenic mice prevented the occurrence of HIVAN (Gu *et al*., 2013).

Another study, assessing the effects of HIV *vpr* gene in glomerulosclerosis, reported that *vpr* plays an important role when associated with *nef* expression in podocytes, and further worsens renal tubular pathology (Rosenstiel *et al*., 2008). To validate this hypothesis, the effects of *vpr* expression on renal tubular epithelial cell function following transduction with a pseudotyped lentivirus vector carrying HIV-1 *vpr* and control genes were determined. The study reported that *vpr* expression in cell culture impaired cytokinesis, causing cell enlargement and multinucleation. This correlated with *in vivo* experiments in HIVAN mouse models and human HIVAN biopsies. Collectively, these studies provided evidence of new clinical phenotypes in HIVAN, resulting from *vpr* ability to alter cytokinesis. In tubular epithelial cells, *vpr* induces caspase 8-mediated apoptosis through activation of the ERK signaling (Snyder *et al*., 2010). In the viral life cycle, *vpr* promotes translocation of the viral pre-integration complex to the host nucleus for genome integration and similarly to *nef*, *vpr* promotes viral transcription through cell arrest at G2/M phase, inhibiting cell growth (Laguette *et al*., 2010; Sharifi *et al*., 2012). However, the exact mechanism by which *vpr* induces glomerular injury is still unclear.

1.6. Host genes and gene products implicated in renal disease

Despite the limitation of not always fully mimicking their human counterparts, the use of experimental animal models has played a crucial role in enhancing the understanding of various aspects of diseases. Similarly, kidney diseases have been thoroughly studied using transgenic mice and rats models. It was with the aid of animal studies that a relationship between host predisposition alleles and viral proteins was shown to induce alterations in the podocyte gene expression pattern. The HIVAN phenotype is highly dependent upon a genetic background. Several studies hypothesized that HIVAN is linked to susceptibility loci within genes. Genetic predisposition alleles for HIVAN were identified in transgenic mice (Gharavi *et al*., 2004; Papeta

et al., 2009). The size-selective barrier of the glomerular podocytes, slit diaphragm, is functionally controlled by a number of proteins that interact with the actin filaments inside these structures. These proteins work synergistically to maintain the structural and functional integrity of the podocytes (Schwarz *et al*., 2001; Asanuma and Mundel, 2003). Alterations in expression patterns of one or more of the genes encoding these fundamental proteins lead to proteinuria, indicative of glomerular injury. Some of these causal genes and their products are discussed in sections 1.6.1 to 1.6.5 below; only genes that were assessed in the current study are briefly reviewed below.

1.6.1. Dynamin

In eukaryotic cells, membrane transport between two compartments requires proteins that promote the budding and scission of newly formed vesicles from one compartment as well as their targeting and fusion with another. Dynamins are scission molecules tailored to function at various cellular compartments and pathways. However, these proteins have also been identified in non-fission pathways, notably in mitochondrial fusion reaction (Wong *et al*., 2003), in podosome formation (Orth and McNiven, 2003), in tubulation during cytokinesis (Verma, 2001) and in macrophage fusion during osteoclast formation (Verma *et al*., 2014). This protein superfamily has been shown to be involved in vesicle scission, organelle division and fusion, cytokinesis, and pathogen resistance, amongst other pathways. Dynamin was also identified as a substrate for protein kinase C in neural tissue (Robinson *et al*., 1991) and cathepsin-L in kidney podocytes (Figure 4) (Sever *et al*., 2007). The neuronal isoform of dynamin, dynamin I, has been shown to be phosphorylated by protein kinase C, suggesting a neuronal-specific function for such phosphorylation reaction. In the kidney, dynamin is crucial for maintaining the ultrafiltration barrier through regulation of the actin mechanism in podocytes. Although the precise mechanism of action of dynamins is still unknown, it has been shown to possess a catalytic arginine residue that plays a pivotal role in GTP hydrolysis. Mutation of this arginine residue rendered dynamin defective in GTP hydrolysis (Sever *et al*., 1999). Dynamins and dynamin-related proteins are distinguished from the rest of the GTPases by their larger GTPase domain and the presence of the GTPase effector domain, which is responsible for the oligomerization and regulation of the GTPase activity. Dynamin also contains a pleckstrin

homology domain involved in membrane binding and a C-terminal proline-rich domain which contains a number of thiol-binding sites for signal transduction. The proline-rich domain binds other proteins and either stimulates GTPase activity of dynamin or targets dynamin to the plasma membrane. Dynamins are designed in a way that enables them to interact with lipid membranes through phosphoinositides and thus, making membrane transport easier (Salim *et al*., 1996; Klein *et al*., 1998).

1.6.2. Cathepsin-L

Lysosomal cysteine proteases cathepsins are mainly of three types B, L and S, all of which share a conserved active site with other cysteine protease superfamily members. The active site is a three-dimensional pocket composed of cysteine, histidine and asparagine residues. Cysteine protease cathepsins are produced as inactive proenzymes which are proteolytically processed to yield the matured enzymes that are stable in acidic cellular compartments, notably lysosmes and endosomes. Although generally recognized as lysosomal proteases, cathepsins are also secreted (Mason *et al*., 1987). They are chiefly responsible for the catabolism of proteins in lysosomes, with their extracellular secretion associated with pathological processes (McCoy *et al*., 1988; Goretzki *et al*., 1992). *In vitro* and clinical data revealed that cysteine cathepsins are mainly expressed in cardiorenal system cells, particularly cardiac myocytes, interstitial myofibroblasts, intracoronary smooth muscle cells and endothelial cells, renal tubules and podocytes. Expression and secretion of cysteine cathepsins in cardiac and renal compartments is significantly enhanced in disease states, consequently inducing these cathepsins to exhibit their collagenolytic and elastolytic capabilities (Senatorski *et al*., 1998; Bauer *et al*., 2011). Research using human models evaluated the use of serum cathepsin levels as diagnostic tools for renal disease. These studies revealed that serum cystatin-C and cathepsin-L are sensitive predictors of potential kidney injury and that increased urinary cathepsin-B levels are associated with membranous glomerulonephritis (Senatorski *et al*., 1998; Bauer *et al*., 2011; Takeuchi *et al*., 2011). Expression and activity of cathepsins is regulated at a cellular level by natural inhibitors including cystatin-C (Sloane *et al*., 1990) and stefin-B (Hall *et al*., 1995; Turk *et al*., 1995). The former has been pronounced to have a predictive value as a functional marker in patients with coronary artery disease and heart and renal failure (Cheng *et al*., 2006). Fluctuations in cardiac

cathepsin-B levels were demonstrated to occur as a result of cardiac injury and failure (Crie *et al*., 1983; Ge *et al*., 2006). Cathepsin-L has been shown to be involved in (i) the manifestation of cardiac disease through dilation of the cardiac chamber, thus resulting in impaired cardiac function (Stypmann *et al*., 2002); (ii) allowing cancer cells to invade locally and metastasize to distant sites by catalyzing interstitial matrix and basement membranes, thus (Gottesman and Cabral, 1981); (iii) and the onset of proteinuric renal diseases through proteolysis of dynamin, consequently collapsing the ultrafiltration barrier (Figure 4) (Server *et al*., 2007). Studies in human and mice models have revealed that increased levels of cathepsin-S were associated with severe diabetes, obesity and atherosclerosis (Cheng *et al*., 2006). As demonstrated by its involvement in various cellular events, cathepsin-L, a broad-spectrum enzyme, cleaves several extracellular proteins, serum proteins and cytoplasmic proteins and nuclear proteins (Barrett and Kirscke, 1981; Maciewicz *et al*., 1987; Mason, 1989). Furthermore, cathepsin-L was shown to be involved in the degradation events of the ovulation process (Robker *et al*., 2000) as well as the progressive loss of lung elastin in progression of pulmonary emphysema (Chapman *et al*., 1994; Taggart *et al*., 2001). Altintas *et al*., (2014) recently demonstrated that the proteolytic activity of renal cathepsin-L can be attenuated by alkalinizing the acidic cytoplasmic environment of the podocytes using glutamine, thereby, protecting the cytoskeleton and reducing proteinuria.

1.6.3. Synaptopodin

Hyperproliferation of podocytes, marked by the expression of the proliferation marker Ki-67 and the loss of differentiation markers (CALLA, GLEPP-1, WT-1 and synaptopodin), have also been identified as one of the most prominent pathologic features of HIVAN (Barisoni *et al*., 1999). Synaptopodin is a key marker of the differentiated podocyte phenotype. This actin-associated protein is a member of the proline-rich family of proteins expressed in the brain, dendritic spine and renal podocytes (Mundel *et al*., 1997; Deller *et al*., 2000; Deller *et al*., 2007). The proline-rich c-terminus promotes postsynaptic targeting and α-actinin binding in the spine apparatus and podocytes, respectively. *In vivo*, the expression of synaptopodin is differentiation-specific in all three regions and signifies postmitotic differentiated podocytes (Mundel *et al*., 1991). The same study demonstrated that together with α-actinin, synaptopodin plays a crucial role in regulating the integrity of the podocyte cytoskeleton and foot processes. Using synaptopodin-deficient mice

models, Asanuma *et al*., (2005) showed that podocyte structure is not altered in the absence of this marker protein though an impaired reformation of the actin filaments was evident in synaptopodin-deficient podocytes. This impaired plasticity of the actin-based podocyte cytoskeleton is implicated in the manifestation of proteinuria and nephrotic syndrome. In the podocyte cytoskeleton (Figure 3) and spine apparatus, synaptopodin regulates synaptic plasticity by binding both F-actin and α-actinin (Yamazaki *et al*., 2001; Asanuma *et al*., 2005).

1.6.4. CD2-associated protein

CD2-associated protein (CD2AP) was initially identified in T cell activation as a promoter of receptor patterning and cytoskeletal polarity (Dustin *et al*., 1998). In the actin-based podocyte cytoskeleton, CD2AP binds and anchors slit diaphragm proteins, i.e., nephrin and podocin, to the actin filaments (Figure 3). The thiol-rich adapter protein, CD2AP, is bound at the carboxyl terminus by the nephrin cytoplasmic domain and in turn binds to the carboxyl terminus of podocin (Shih *et al*., 2001; Schwarz *et al*., 2001). This association is crucial for maintaining the cytoskeleton integrity and proper signaling at the slit diaphragm (Shih *et al*., 1999; Schwarz *et al*., 2001). CD2AP knockout mice develop congenital nephrotic syndrome and die from podocyte-associated lesions after six to eight weeks (Shih *et al*., 1999). Knocking-out CD2-AP promotes TGF-β expression in glomerular podocytes of mice models (Woroniecki *et al*., 2006). Enhanced TGF-β1 expression induces cathepsin-L protease expression through nuclear dendrin, and in turn, down-regulates CD2-AP and other enzymatic substrates of cathepsin-L cleavage, i.e., dynamin and synaptopodin (Asanuma *et al*., 2007; Yaddanapudi *et al*., 2011). Nuclear dendrin serves as a transcription factor for enhancing renal cathepsin-L expression. Down-regulation thereof has been shown to restore formation of the stress fibers and focal adhesions within cell bodies that connect actin filaments (Yaddanapudi *et al*., 2011). Using transgenic mice, Grunkemeyer *et al*., (2005) reported that the effect of cytosolic cathepsin-L activity is alleviated when podocyte CD2-AP expression is induced.

1.6.5. NPHS1 *and* NPHS2

Nephrin and podocin, encoded by the *NPHS1* and *NPHS2* genes, respectively, are expressed in the glomerular podocytes and play an integral role in maintaining foot process integrity and slit diaphragm permeability (Routsalainen *et al*., 1999; Boute *et al*., 2000). During kidney development, the expression of podocin and nephrin is similar. Using immunoelectron microscopy, Schwarz *et al*., (2001) traced the localization of podocin at the lipid rafts of the foot process membrane where it interacts with CD2AP and nephrin (Figure 3). Localization of nephrin and CD2AP was previously identified in the podocyte foot processes (Li *et al*., 2000; Shih *et al*., 2001). A member of the immunoglobulin superfamily, nephrin, serves as a surface receptor, transmitting extracellular signals from the slit diaphragm to the podocyte cytoskeketon. This transmembrane protein forms *cis* and *trans* bonds with other nephrin molecules through its extracellular domain and interacts with other adaptor proteins through its cytoplasmic domain (Barletta *et al*., 2003). The role of these protein associations in facilitating nephrin signaling is reviewed by Huber and Benzing (2005). Association of nephrin with the adaptor proteins, i.e., CD2AP, podocin and Nck, also play a pivotal role in regulating the functional and structural integrity of the slit diaphragm (Tryggvason *et al*., 2006b). The association of protein complexes in the actin-based cytoskeleton and the slit diaphragm is thoroughly reviewed by Faul *et al*., (2007). Podocin, a hairpin-like member of the stomatin family, interacts with nephrin in the lipid rafts and promotes nephrin signaling (Huber *et al*., 2003). Mutations and down-regulated expression of the *NPHS1* gene were initially implicated in the manifestation of congenital nephrotic syndrome of the Finnish type (Kestila *et al*., 1998; Lenkkeri *et al*., 1999), whereas mutations in the *NPHS2* gene were associated with the pathogenesis of autosomal recessive steroid-resistant nephrotic syndrome and sporadic focal segmental glomerulosclerosis in adults (Boute *et al*., 2000; Caridi *et al*., 2003). The former is a severe renal disorder that cannot be remedied by immunosuppressant or steroid therapy, and rapidly progresses to ESRD. The condition can only be corrected by renal transplantation.

1.7. HIV renal disease and treatment

As most HIV renal diseases manifest through proteinuria, regimens employed for treatment of the majority of these kidney disorders are focused on curbing proteinuria and viral loads. This is often achieved through highly active antiretroviral therapy. Highly active antiretroviral therapy has proven to have beneficial effects by potentially reducing the progression rate of HIVAN and mortality of HIV-1-related renal diseases (Ifudu *et al*., 1995; Wali *et al*., 1998; Szczech *et al*., 2002). HIV-related ESRD mortality rate was significantly reduced following initiation of HAART in 1995, from 69 % in 1991 to 24 % in 2002 (Schwartz *et al*., 2005). Steroid therapy has also been demonstrated to be beneficial in delaying development of ESRD in HIV-1 patients. Cortico-steroid therapy functions by reducing the interstitial inflammation through a decrease in NF-κB, a transcription factor that is significantly up-regulated in HIV-infected cells (Smith *et al*., 1996). Angiotensin-converting enzyme (ACE) inhibitors and statins are other regimens with the potential to have an impact in this regard (Burns *et al*., 1997; Wei *et al*., 2003).

1.8. Antiretroviral drug-induced nephrotoxicity

The introduction of HAART has played a crucial role in curbing the progression of HIV-1 and the ultimate development of opportunistic infections. Despite the beneficial effects of HAART, some of the drugs employed in the regimen have been implicated in the initiation of kidney disease. Highly active antiretroviral therapy is an intense regimen that uses a combination of antiretroviral (ARV) drugs that target and inhibit various stages/processes in the viral cycle. These drugs inhibit functions of the three HIV-1 enzymes (integrase, reverse transcriptase and protease) used by the virus for its maturation and continued infection, as illustrated in Figure 6. No significant renal toxicity has been reported thus far following fusion inhibitors and integrase inhibitors regimen. However, administration of nucleoside reverse transcriptase inhibitors (NRTI) has been shown to lead to the development of mitochondrial cytopathies that perturb the proximal tubule. Toxicity of NRTI drugs is due to co-administration with other ARV drugs, especially protease inhibitors (PIs) that hamper the excretion of NRTIs (Rockwood *et al*., 2011). Accumulation of the NRTIs in the proximal tubules leads to enlarged cells, with dysmorphic mitochondria and eosinophilic inclusions. Tenofovir is an NRTI with a well profiled potential for

renal toxicity. Additionally, NRTIs have been proven to cause lactic acidosis and electrolyte abnormalities, notably hyperuricemia, hypermagnesemia, hypokalemia and hyponatremia (Patel and Hedayati, 2006; Ifudu and Friedman, 2009). On their own, PIs may cause kidney stones, crystalluria and chronic interstitial diseases in HIV patients. The stones usually resolve following cessation of the PI regimen (Rockwood *et al*., 2011). Nephrotoxicity may also arise from some drugs used to treat opportunistic infections in HIV-1 disease (Lucas *et al*., 2004; Sweet, 2005; Fine *et al*., 2008).

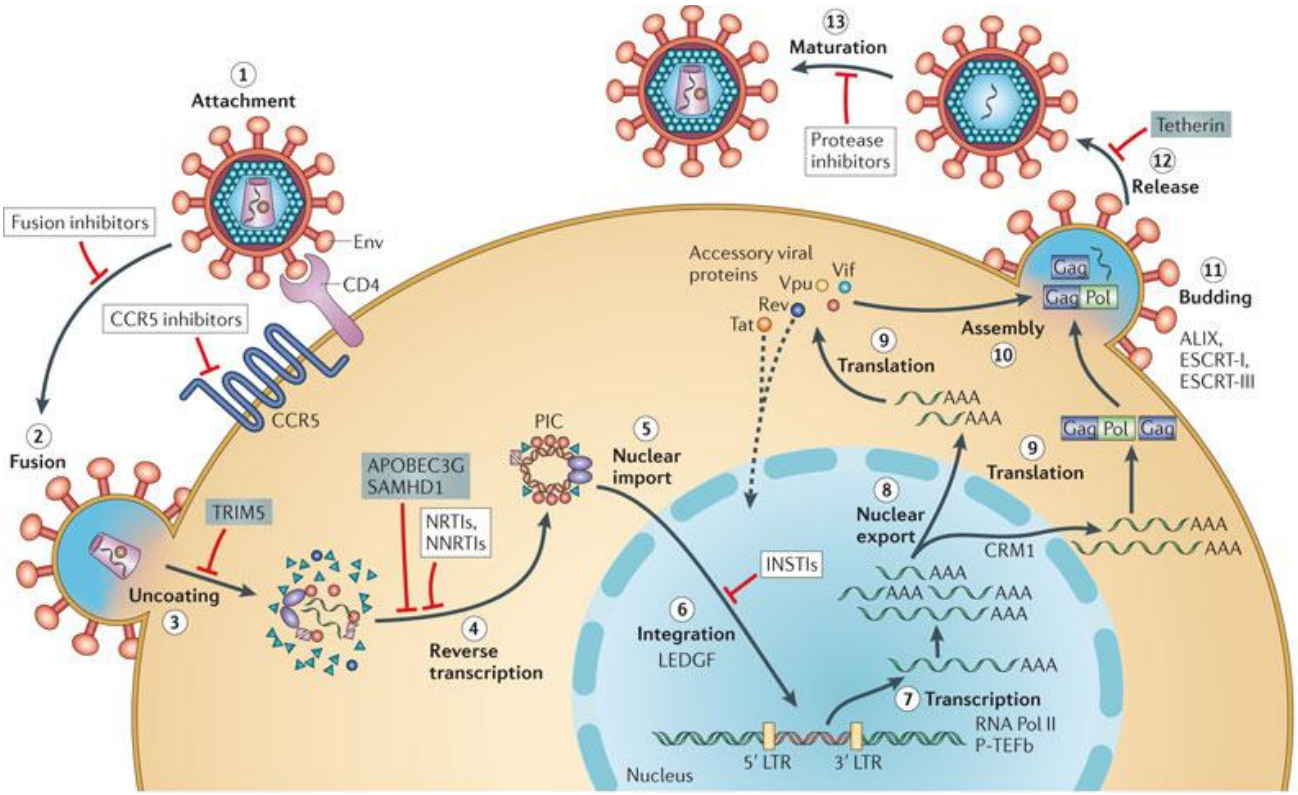

Figure 6: HIV-1 life-cycle

Production of mature and infectious viral particles is achieved through synergistic contribution of the *gag-pol* gene products as depicted above. Briefly, HIV infects T cells that carry the CD4+ antigen on their surface. The viral RNA is reverse-transcribed to DNA by the viral reverse transcriptase upon entering the cell. The viral DNA is then integrated into the genetic material of the cell by a second virally encoded enzyme, the integrase, in the nucleaus. Messenger RNA, transcribed from the viral DNA upon host cell activation, is consequently translated into viral proteins. The third virally encoded enzyme, the protease, enzymatically catalyzes a viral polyprotein precursor into individual mature proteins at this stage. The viral RNA and proteins gather at the cell surface to form new virions, which bud from the cell and are released to infect another cell. Cell death occurs upon damage from destruction of host's genetic system to the budding and release of virions. Photo adapted from Engelman and Cherepanov, 2012, with permission from the publisher (License number: 3587040500655; Appendix).

Study hypothesis

We hypothesize that enzymatic activity of the over-expressed cysteine cathepsin-L in the glomeruli compromises the actin-based podocyte cytoskeleton integrity through cleavage of its substrate dynamin, thus inducing proteinuria. Moreover, various metabolic pathways and host-response genes are altered following HIV infection in proteinuric kidney disease.

Aim

To profile gene expression pattern changes in HIV-1-associated kidney disease.

Objectives

i. Localize and quantify cathepsin-L and dynamin in proteinuric renal tissue
    - Probe using immunohistochemistry.

ii. Assess various isoforms of cathepsin-L and dynamin to delineate the isoforms implicated in proteinuria observed in HIVAN and HIV negative FSGS
    - Analyse using real time quantitative PCR experiments
        - Validate using western-blotting.

iii. Evaluate the expression patterns of other previously documented genes that play a key role in maintaining the structural and functional integrity of the actin-based podocyte cytoskeleton i.e., nephrin, podocin, CD2AP and synaptopodin using real time quantitative PCR.

iv. Evaluate the toll-like receptor and HIV-host response gene expression pattern changes induced in HIVAN and HIV negative FSGS
    - Assess using RT^2 Profiler PCR arrays
        - Validate using real time quantitative PCR and western-blotting.

2. MATERIALS AND METHODS

2.1. Sample acquisition

Kidney biopsy specimens were attained through Prof. Martin Hale and Dr. Pulane Mosiane of the Anatomical Pathology Department of the National Health Laboratory Services, Charlotte Maxeke Johannesburg Academic Hospital, University of the Witwatersrand, Johannesburg. Formalin-fixed, paraffin-embedded (FFPE) kidney tissue was acquired as blocks for RNA extraction and fixed on slides (2 micron sections) for immunohistochemistry experiments. Four healthy non-proteinuric controls, seven focal segmental glomerulosclerosis (FSGS), six HIV-associated nephropathy (HIVAN) and four minimal change disease (MCD) samples were compared. Healthy non-proteinuric nephrectomy tissue, acquired from trauma victims, was used as controls. There were major difficulties in acquiring both healthy and proteinuric renal tissue hence, tissues used in this study was not matched for age, gender, race or other factors. However, the study omitted samples from minors, younger than 18 years of age. Ethics clearance (Clearance certificate number M131062, attached in the appendix) was obtained from the Human Research Ethics Committee (Medical) of the University of the Witwatersrand, Johannesburg.

2.2. Immunohistochemistry

Immunohistochemistry (IHC), a technique in which antigens in tissue sections are localized using specific labeled antibody through antigen-antibody interaction, is widely used in clinical diagnostics and medical research. As the name suggests, immunohistochemistry integrates three fields of science, notably, immunology, histology and chemistry. Since the development and introduction of IHC, using fluorescent-labeled antibodies to identify antigens in tissue sections, the technique has expanded to using chromogenic enzyme labels such as horseradish peroxidase and alkaline phosphatase (Nakane and Pierce, 1967; Mason and Sammons, 1978). The antibody-antigen interactions are visualized using 3,3-diaminobenzidine tetrachloride (DAB) or 5-Bromo-4-chloro-3-indolyl phosphate/Nitro blue tetrazolium chloride (BCIP/NBT), respectively. These

chromogens produce a brown-colored precipitate that enables the antigen-antibody interaction to be visible.

Expression of the markers, dynamin and cathepsin-L, was assessed in human kidney tissue sections embedded in paraffin. Immunohistochemistry was initialized by deparaffinizing and rehydrating the sections through saturation of slides in xylene twice for 5 minutes each, twice in absolute alcohol for 2 minutes each and lastly in 95 % alcohol for 2 minutes. The slides were washed while stirring for 1 minute in distilled water. Fixation agents such as formalin have cross-linking abilities, thereby forming protein cross-links that reduce or mask the accessibility of antibody-binding epitopes on the antigen surface. To enhance the intensity of the antibody staining, protein cross-linking was broken and the antigen epitopes unmasked by heating the Tris-EDTA-immersed slides at medium heat in a microwave for 6 minutes. Tris-EDTA epitope retrieval buffer was replaced with a fresh buffer and slides reheated for an additional 6 minutes at medium heat. Slides were then allowed to cool in the same buffer for approximately 30 minutes at room temperature before aspirating excess liquid and marking tissue sections with a Dako pen. The Dako pen circles around sections create a water repelling barrier that serves as a dam to solutions applied to the sections and thus, reducing the volume of reagents added. The slides were washed with PBS thrice for 2 minutes each while stirring. Endogenous peroxidase activity was quenched by saturating slides in 3 % H_2O_2 solution for 10 minutes. This reduces the false positives and high background staining.

Tissue sections were rinsed with PBS twice for 5 minutes, excess liquid aspirated, serum-blocked for 30 minutes, aspirated and incubated in primary antibody overnight at 4 °C, in that order. Although antibodies are directed to specific epitopes on the target antigen, partial or weak binding to nonspecific sites may occur, expressing the need for blocking such sites. Nonspecific antibody binding cause high background staining that can mask the detection of target antigen. Goat serum and rabbit serum (Santa Cruz Biotechnology, Anatech Instruments) were used at 1 % dilution for dynamin and cathepsin-L, respectively, to block epitopes on tissue samples that would otherwise result in nonspecific binding of either the primary or secondary antibodies in the respective experiments. Target antigens on the human kidney tissue were detected using initially optimized concentrations of the primary and secondary antibodies. Dynamin (H-300)

(Santa Cruz Biotechnology, Anatech Instruments) and cathepsin-L (C-18) (Santa Cruz Biotechnology, Anatech Instruments) were used at 4.0 µg/mℓ and 6.6 µg/mℓ, respectively. Dynamin (H-300) maps an epitope corresponding to amino acid 567-866 at the C-terminus of dynamin 2 of human origin and may be used to detect dynamin 1, 2 and 3 of human, mouse and rat origin. Cathepsin-L (C-18) maps an epitope at the C-terminus of cathepsin-L of human origin and may be used to detect cathepsin-L, L2 and S of human, mouse and rat origin. Tissue sections were subsequently incubated in secondary antibody for 1 hour following a 2 times 2 minutes rinse in PBS. Rinsing the sample in between antibody applications is critical to remove unbound antibodies and also to remove antibodies that are weakly bound to nonspecific sites. Goat anti-rabbit IgG HRP-conjugated (Santa Cruz Biotechnology, Anatech Instruments) and rabbit anti-goat IgG HRP-conjugated (Santa Cruz Biotechnology, Anatech Instruments) were used for dynamin and cathepsin-L, respectively. Secondary antibodies were used at a dilution of 1:500. Fifty microlitres of the antibody solution was added per tissue section. Slides were rinsed twice with PBS, excess liquid aspirated and the antibody-antigen interactions visualized by adding 50 µℓ DAB (Roche chemicals) per tissue section for 5 minutes exactly for reproducible results. DAB was rinsed off with PBS followed by water before tissue sections were dehydrated and mounted with coverslip. Dehydration of the tissue sections was performed in 5 steps as follows; 2 minute incubation in 95 % alcohol, 2 times 2 minutes incubation in absolute alcohol and 2 times 5 minutes incubation in xylene. Sections were immediately mounted using coverslips and Entellan® (Merck Millipore).

The images were captured on Zeiss Axio-Cam HRC camera and Axiovision 4.8.1 software. Quantities of cathepsin-L and dynamin localization in the kidney were quantified using CellProfiler software (Lamprecht *et al*., 2007). Quantification is initiated by converting the original image to a grayscale image that is used to identify areas of interest for analysis. The program grades the intensity of selected area from zero (dark) to one (light), whereby, zero denotes a highly concentrated localization and one a diffusely localized protein. Multiple areas were selected from each sample, their intensities averaged and statistically analyzed using Statistica 12.5.192.5 software (StatSoft).

2.3. RNA isolation, purification and quantification

RNA was extracted from FFPE renal tissue of HIVAN, FSGS, MCD and healthy control biopsies using the AllPrep DNA/RNA FFPE kit (QIAgen, Whitehead Scientific) as per manufacturer's instruction (Protocol is detailed in the appendix). Briefly, tissue sections were deparaffinized, pelleted and dried in an eppendorf tube. Tissue was resuspended in lysis buffer to lyse the tissue and the DNA-containing pellet was precipitated by centrifugation. RNA-containing supernatant was transferred onto an RNeasy MinElute spin column, placed in a 2 mℓ collection tube, for total RNA purification. Sample was passed through the spin column by centrifugation. RNA, bound to the column, was washed by adding washing buffer to the RNeasy MinElute spin column and centrifuged. Contaminating DNA was subsequently digested by adding DNase I solution directly onto the column membrane and incubated for 15 minutes at room temperature. RNeasy MinElute spin column was placed in a new collection tube and spun to dry residual ethanol from the column membrane. Following incubation of the spin column with 20 µℓ RNase-free water for 1 minute at room temperature, RNA was eluted into a new 1.5 mℓ collection tube by centrifugation at 12 000 x g for 1 minute. RNA-containing eluate was re-applied to the column, to retrieve residual RNA from the column, and centrifuged for a minute at 12 000 x g.

Concentration of extracted RNA was estimated by measuring absorbance ratio (A_{260}/A_{280}) using NanoDrop spectroscopy (Thermo Scientific). RNA purity was evaluated by calculating RNA integrity number (Fleige and Pfaffl, 2006) using the RNA 6000 Pico Kit and the Agilent Bio-Analyzer (Agilent Technologies), following manufacturer's guidelines. RNA was stored at -80 °C prior to downstream application.

RNA was subjected to off-column genomic DNase digestion prior to cDNA synthesis. Genomic DNA contamination causes background noise in qPCR experiments. Contaminating genomic DNA was eliminated by resuspending 10 µg RNA in 1 × DNase Reaction Buffer (New England Biolabs, The Scientific Group) to a final concentration of 100 µℓ. Two units of DNase I (New England Biolabs, The Scientific Group) for 10 minutes were pipetted into the mix, thoroughly

mixed by vortexing and incubated at for 10 minutes 37 °C before adding EDTA to a final concentration of 5 mM. The genomic DNA elimination mix was heat inactivated at 75 °C for 10 minutes. RNA concentration was estimated using A_{260}/A_{280} reading from a NanoDrop spectrophotometer (Thermo Scientific) and integrity quantified using RNA 6000 Pico Kit and Agilent Bio-Analyzer (Agilent Technologies), precise protocol attached in the appendix. RNA with the same RNA integrity numbers (RIN) was used in subsequent experiments. Acceptable RNA integrity has 28S:18S ratio of ~2.0 and A_{260}/A_{280} ratio ranged between 1.6 and 2.0. Purified RNA was reverse transcribed to yield single-stranded cDNA, as described in Section 2.4, for use as a template in real time qPCR experiments in Section 2.6.

2.4. Template preparation

cDNA was reverse transcribed from total RNA using High Capacity cDNA Reverse Transcription kit (Applied Biosystems) according to manufacturers' instructions. Protocol is detailed in the appendix**.** Briefly, cDNA reverse transcription (RT) reaction was prepared as indicated in Table 1. RT master mix was aliquoted accordingly and diluted to 1 × reaction mix by pipetting equal volume of extracted RNA sample from section 2.3. The reaction mix was subjected to thermal cycling under the conditions outlined in Table 2. For transcription control (NRT) experiments, reverse transcriptase was omitted and volume made-up with nuclease-free water. Non-reverse transcriptase (NRT) controls were included to monitor genomic DNA contamination. RNA samples were used at final concentration of 200 ng in all RT experiments. At the end of the run the reverse transcription reaction (cDNA) was removed from the thermocycler and stored at -20 °C prior to use.

Table 1: Preparation of the High Capacity cDNA 2 × reverse transcription master mix

Component	Volume/reaction (µℓ)
10 × RT buffer	2.0
25 × dNTP mix (100 mM)	0.8
10 × RT random primers	2.0
MultiScribe™ reverse transcriptase	1.0
Nuclease-free water	4.2
Total	**10**

Reaction volumes of 20 µℓ were made-up by adding 10 µℓ of nuclease free water to each reaction mix. RNA was used at final concentration of 200 ng in each RT experiment.

Table 2: Thermo-cycling conditions for cDNA synthesis using High Capacity cDNA reverse transcription kit

	Phase 1	**Phase 2**	**Phase 3**	**Phase 4**
Temperature (°C)	25	37	85	4
Time (minutes)	10	120	5	∞

2.5. Primer design

All primers were designed and purchased from the Integrated DNA Technologies (IDT) (http://www.idtdna.com, Whitehead Scientific). Real time primers were designed based on intercalating dye chemistry (SYBR green) and mRNA transcript sequence information of the gene of interest. Primers were designed based on the Gene Bank accession numbers BC_012612, AB_019534 and BC_160188 for Cathepsin-L 1, 2 and 3, and NM_004408, BC_054501 and NM_015569 for Dynamin 1, 2 and 3, respectively (primer sequences are listed in Table 3). Primers for renal specific reference genes were designed based on the Gene Bank accession numbers NM_012423, NM_004168 and NM_003406 for RPL13A, SDHA and YWHAZ, respectively (Table 4). The nucleotide sequence of the gene was blasted and the best forward and reverse primers for each gene were selected using the criteria: (i) ΔG of hairpins at the 3' end was ≤ 2 and ≤ 3 in structure. (ii) ΔG of self-dimers at the 3' end was ≤ -8 and ≤ 6 in structure and (iii) low to no self-complementarity to avoid primer dimers. Amplicons were kept between 50 and 200 base pairs.

2.6. Real-time quantitative polymerase chain reaction for assessing cathepsin-L and dynamin expression

Real-time quantitative polymerase chain reaction (qPCR) employs fluorescence-based chemistry to monitor the accumulation of DNA synthesized as the PCR reaction progresses. The fluorescent signal generated is increased in direct proportion to the amount of DNA produced at each cycle. Changes in gene expression patterns of renal cathepsin-L and dynamin in proteinuric conditions (HIVAN, FSGS and MCD) were compared to healthy non-proteinuric controls in qPCR experiments. Cathepsin-L and dynamin primers were used in qPCR experiments with cDNA reverse transcribed from RNA, from Sections 2.3 and 2.4, and Brilliant II SYBR green (Agilent Technologies). A qPCR reaction master mix (Sabax water, 1 × Brilliant II SYBR, 200 nM forward primer and 200 nM reverse primer) was prepared for each primer set and aliquoted into each reaction well (Table 5). cDNA from the reverse transcription reaction was added into appropriate wells to a final concentration of 5 ng. Reaction volumes were set at 25 μℓ and the

Table 3: Primer sequences of cathepsin-L and dynamin genes

Gene	Primer	Sequence
CTS-L 1	Forward	5' - TTGCTAATGACACCGGCTTTGTGG - 3'
	Reverse	5' - ACAGGAAGGACTCATGACCTGCAT - 3'
CTS-L 2	Forward	5' - TCAGAGGCTTGTTTGCTGAG - 3'
	Reverse	5' - CCAGGACGAGCGAAAGAT T - 3'
CTS-L 3	Forward	5' - GCTACGTGACTCCTGTGAAGG - 3'
	Reverse	5' - TTCTCAGTTTTCCTAACATCTGTC - 3'
DYN 1	Forward	5' - CCGTTAGACAGTGCACCAAG - 3'
	Reverse	5' - GCTCCATCTCCTCCCGTAG - 3'
DYN 2	Forward	5' - GGAAGTCGATCCCCAAGG - 3'
	Reverse	5' - CCTCGTCCATCAGGTCAAG - 3'
DYN 3	Forward	5' - CTCCTGGATACAGCACTCTCG - 3'
	Reverse	5' - TTAGTGTTGGCCTCCTTTGG - 3'

CTSL-1: isoform 1 of *Homo sapiens* cathepsin-L; CTSL-2: isoform 2 of *Homo sapiens* cathepsin-L; CTSL-3: isoform 3 of *Homo sapiens* cathepsin-L; DYN-1: isoform 1 of *Homo sapiens* dynamin; DYN-2: isoform 2 of *Homo sapiens* dynamin; DYN-3: isoform 3 of *Homo sapiens* dynamin; Primers were designed based on the Gene Bank accession number BC_012612, AB_019534 and BC_160188 for CTSL1, 2 and 3, and NM_004408, BC_054501 and NM_015569 for DYN-1, 2 and 3, respectively. Primers were designed for intercalating SYBR-based real-time PCR using the Integrated DNA Technologies (IDT) Primer Quest design tool (http://www.idtdna.com/primerrequest) and purchased (Whitehead Scientific).

Table 4: Primer sequences of reference genes

Gene	Primer	Sequence
RPL13A	Forward	5' -CCTGGAGGAGAAGAGGAAAGAGA - 3'
	Reverse	5' - TTGAGGACCTCTGTGTATTTGTCAA - 3'
SDHA	Forward	5' -TGGGAACAA GAG GGC ATC TG - 3'
	Reverse	5' - CCACCACTGCATCAAATTCATG - 3'
YWHAZ	Forward	5' - ACTTTTGGTACATTGTGGCTTCAA - 3'
	Reverse	5' - CCGCCAGGACAAACCAGTAT - 3'

RPL13A: *Homo sapiens* ribosomal protein L13a; *SDHA*: *Homo sapiens* succinate dehydrogenase complex, subunit A, flavoprotein; *YWHAZ*: *Homo sapiens* tyrosine 3-monooxygenase/tryptophan 5-monooxygenase activation protein, zeta polypeptide. Primers were designed based on the Gene Bank accession number NM_012423, NM_004168 and NM_003406 for *RPL13A*, *SDHA* and *YWHAZ*, respectively. Primers were designed for intercalating SYBR-based real-time PCR using the Integrated DNA Technologies (IDT) Primer Quest design tool (http://www.idtdna.com/primerrequest) and purchased (Whitehead Scientific).

Table 5: Preparation of real time quantitative PCR reaction mix using Brilliant II SYBR

Component	Concentration/reaction
Sabax water	9.0 µℓ
2 × Brilliant II SYBR Master mix	1 ×
Forward primer	200 nM
Reverse primer	200 nM
cDNA	5 ng

Reaction volumes were set at 25µℓ.

reaction mix was centrifuged to eliminate air bubbles and loaded onto the qPCR machine. Gene expression was evaluated through 40 amplification cycles using AB 7500 Real Time PCR System (Applied Biosystems). Cycling conditions are outlined in Table 6. NRT controls for each transcribed template were also subjected to qPCR to assess genomic DNA contamination. SYBR green binds to the minor grooves of double stranded DNA that is produced as a PCR reaction progresses. However, SYBR green also binds primer dimers and non-specific PCR products. Bound SYBR green emits fluorescent light that is interpreted as qPCR signal. To assess the composition of the amplified product, melting curves were performed with every qPCR run. For a reliable qPCR assay with controlled variations in extraction yield, reverse transcription yield and amplification efficiency, enabling mRNA concentration comparison across various samples; samples were normalized against internal controls (Huggett *et al*., 2005). Expression of internal controls is consistent and not altered in the conditions under investigation. Variations in expression levels of reference genes are attributed to experimental variation and are compensated for during normalization. Three renal disease validated genes, i.e., *Homo sapiens* ribosomal protein L13a (*RPL13A*), *Homo sapiens* succinate dehydrogenase complex, subunit A, flavoprotein (*SDHA*) and *Homo sapiens* tyrosine 3-monooxygenase/tryptophan 5-monooxygenase activation protein, zeta polypeptide (*YWHAZ*), were employed in all qPCR experiments for normalization as calculated according to Equations 1 to 4 (Livak and Schmittgen, 2001; Romanowski *et al*., 2007; Lisowski *et al*., 2008).

Table 6: Thermo-cycling conditions for real time quantitative PCR reaction using Brilliant II SYBR

Phase	Cycles	Temperature (°C)	Time (minutes)
1	1	95	10
2	40	95	0.5
		60[##]	1
3 (Melting curve)	1	95	0.25
		60	1
Ramp at 1 % [##]		95	0.5

[##] denotes data collection point. Melting curves were performed to determine the composition of the reaction product since SYBR green non-specificity may result in bound primer dimers and non-specific PCR products.

$$\boldsymbol{Geometric\ Mean\ (GM) = (a_1 \times a_2 \times \ldots \times a_n)^{\frac{1}{n}}} \qquad \textbf{Equation 1}$$

where a is C_q value of the reference gene and n is the number of reference genes used.

$$\boldsymbol{\Delta C_q = C_{q(GoI)} - GM_{(Ref)}} \qquad \textbf{Equation 2}$$

where GoI (gene of interest) is the gene whose expression is under investigation and $GM_{(Ref)}$ is the geometric mean of the reference genes as determined in Equation 1. These values are used to calculate $-\Delta\Delta C_q$ that is subsequently used to calculate fold-change as indicated below.

$$\boldsymbol{-\Delta\Delta C_q = -(\Delta C_{q(q)} - \Delta C_{q(c)})} \qquad \textbf{Equation 3}$$

where (q) represents any sample, i.e. MCD, FSGS or HIVAN in this case, and (c) a calibrator sample, i.e. healthy non-proteinuric. Fold-change is defined by the equation:

$$\boldsymbol{Fold\ change = 2^{-\Delta\Delta C_q}} \qquad \textbf{Equation 4}$$

For statistical analyses, the Log_{10} of the fold-change was used. No template controls, in which cDNA was omitted, were included for each primer set to check for contamination. All experiments were performed in duplicate and in accordance with the *Minimum information for publication of quantitative real-time PCR experiments* (MIQE) guidelines (Bustin *et al*., 2009). Renal cathepsin-L and dynamin expression was computed using AB 7500 v2.0.5 software and statistically quantified using Statistica 12.5.192.5 software (StatSoft).

2.7. Determining expression levels of podocyte cytoskeleton proteins

Proteolysis of the actin-associated proteins, in the podocytes slit diaphragm, by cathepsin-L in renal cells leads to compromised cytoskeleton integrity and podocytes foot process effacement, and ultimately proteinuria. mRNA expression patterns of these actin-associated proteins were assessed in proteinuric kidney diseases relative to the healthy non-proteinuric control group. Primers were designed using Integrated DNA Technologies Primer Quest design tool and purchased through Whitehead Scientific. Primer sequences (Table 7) were based on the Gene Bank accession numbers BC069444, NM_000609, NM_002984 and AF499136 for CD2AP, nephrin, podocin and synaptopodin, respectively. Quantitative real-time PCR experiments were carried out as described for cathepsin-L and dynamin (Section 2.6).

2.8. PCR arrays

Changes in gene expression patterns of host kidney cells were determined using RT^2 Profiler PCR arrays (SABiosciences, Whitehead Scientific) in real-time qPCR experiments. The RT^2 Profiler PCR Arrays incorporate a panel of relevant optimized primers for monitoring pathway- or disease-focused gene expression patterns in cells and tissues. The two arrays selected for this study are Human Toll-Like Receptor and HIV Host Response panels. The PCR array profiles are explained in the appendix. PCR array experiments were divided into 3 parts, notably first-strand cDNA synthesis, cDNA target template pre-amplification and real-time qPCR.

The protocol was initialized by eliminating genomic DNA from the RNA isolated as outlined in Section 2.3. Genomic DNA elimination mix was prepared by adding 5 µℓ RNase-free water and 2 µℓ buffer GE (PreAMP cDNA Synthesis kit, QIAgen) to 250 ng RNA. The mixture was gently mixed by pipetting up and down, briefly centrifuged, heated at 42 °C for 5 minutes and placed on ice. Reverse transcription mix (4 µℓ 5 x buffer BC3, 1 µℓ control P2, 1 µℓ cDNA Synthesis Enzyme Mix, 1 µℓ RNase inhibitor and 3 µℓ RNase-free water; PreAMP cDNA Synthesis kit, QIAgen) was added to the 250 ng RNA in the genomic DNA elimination mix, gently mixed by

Table 7: Primer sequences used for actin-associated cytoskeleton gene products.

Gene	Primer	Sequence
CD2AP	Forward	5' GTGGCTGGAAGGAGAACTAAA 3'
	Reverse	5' CGTTTGATGGGCAAACTGTC 3'
Nephrin	Forward	5' AGGACCGAGTCAGGAACGAAT 3'
	Reverse	5' CTGTGAAACCTCGGGAATAAGACA 3'
Podocin	Forward	5' GCTGTGCAATTCCTTGTGCAAACC 3'
	Reverse	5' CTTTGCATCTTGGGCGATGCTCTT 3'
Synaptopodin	Forward	5' AAACCCAACCAGAACCTCTC 3'
	Reverse	5' GGCTTGAAGACTCGATGACATA 3'

CD2AP: *Homo sapiens*: CD2-associated protein. Primers were designed based on the Gene Bank accession number BC069444, NM_004646, NM_014625 and AF499136 for CD2AP, nephrin, podocin and synaptopodin, respectively. Primers were designed for intercalating SYBR-based real-time technology using the Integrated DNA Technologies (IDT) Primer Quest design tool (http://www.idtdna.com/primerquest) and purchased (Whitehead Scientific).

pipetting then briefly spun to remove air bubbles. The mixture was incubated at 42 °C for 30 minutes before the reaction was stopped by incubating at 95 °C for 5 minutes before placing on ice. The Pre-AMP step was carried-out to reverse transcribe the RNA and yield cDNA that was to be used in real-time quantitative PCR.

Either the HIV disease- or Toll-Like Receptor pathway-specific RT^2 PreAMP primer mix (SABiosciences, Whitehead Scientific), 7.5 μℓ, and its compatible RT^2 PreAMP PCR Mastermix (SABiosciences, Whitehead Scientific), 12.5 μℓ, were added to 5 μℓ of cDNA synthesis reaction in a 0.2 mℓ PCR tube. Pre-amplification mix was subjected to thermocycling as tabulated (Table 8). At the end of the cycling, 2 μℓ Side Reaction Reducer was added to the PCR tube placed on ice. The pre-amplification reaction was gently mixed, incubated at 37 °C for 15 minutes before heat inactivated at 95 °C for 5 minutes. The reaction mix was then diluted by adding 84 μℓ nuclease-free water and mixed well before proceeding to real-time qPCR arrays protocol.

The PCR components mix was prepared by adding 102 μℓ of the pre-amplification reaction to 1.275 mℓ of RT^2 qPCR Master Mix containing SYBR Green-optimized primers, before adding 1.173 mℓ of RNase-free water. Equal volumes, i.e., 25 μℓ, of the mixture was added to each well of RT^2 Profiler PCR Array, with tips changed for every well to avoid cross-contamination. Arrays were tightly sealed, to prevent evaporation during cycling, before centrifuging at 1000 x g for 3 minutes to remove air bubbles. Real-time PCR cycling of the arrays was performed under the conditions outlined in Table 9. To verify PCR specificity, 1 cycle of dissociation curve was performed at 95 °C for 15 seconds and 1 minute at 65 °C. qPCR was carried-out using the AB7500 Real Time PCR System (Applied Biosystems) and data collected for analysis using the AB7500 real-time cycler software v2.0.5 and web-based software package (RT^2 PCR Profiler Array System v4.0; SABiosciences, QIAgen). Catalogued PCR Arrays used for HIV Host Response Panel and Toll-Like Receptor are PAHS-051Z and PAHS-018Z, respectively.

Table 8: Real-time PCR cycling conditions for pre-amplification of cDNA target template used in RT^2 PCR array experiments

Phase	Cycles	Temperature (°C)	Time (minutes)
1	1	95	10
2	8	95	0.25
		60	2
Hold		4	

Reaction volumes of 25 µℓ were used.

Table 9: Real-time cycling conditions used for RT^2 PCR array experiments

Phase	Cycles	Temperature (°C)	Time (minutes)
1	1	95	10
2	40	95	0.25
		60	1
3 (Melting curve)	1	95	0.25
		65	1
Ramp at 1 %		95	0.5

Reaction volumes of 25 µℓ were used. Melting curves were performed to determine the composition of the reaction product since SYBR green non-specificity may result in bound primer dimers and non-specific PCR products.

2.9. Validation of PCR arrays

Expression patterns of genes that were either up- or down-regulated from the PCR Profiler arrays were further assessed at a transcriptional level by designing primers specific for each gene and used in real time quantitative PCR experiments. Gene expression patterns in proteinuric groups were compared to the healthy non-proteinuric controls.

2.9.1. Validation of altered HIV-host response genes

From the HIV-host response panel of qPCR arrays, expression of 3 genes (*CCL4*, *CXCL12* and *SLPI*) was altered in HIVAN as compared to the HIV negative FSGS (Figure 16 in the results section). Additionally, expression of 5 other genes (*CCL3*, *CDKN1A*, *SERPINA1*, *STAT1* and *TNFSF10*) was altered in both HIV negative FSGS and HIVAN, relative to the healthy non-proteinuric control group, and one more (*TGF-β1*) was only over-expressed in HIV negative FSGS but not in HIVAN (Figure 19 in the results section). Primers for all 9 genes were designed using Integrated DNA Technologies Primer Quest design tool and purchased (Whitehead Scientific) for use in qPCR experiments to elucidate the effect of HIV-1 infection on expression of these genes and to validate the array results. Primer sequences (Table 10) were based on the Gene Bank accession numbers NM_000609, NM_002984 and NM_003064 for *CXCL12*, *CCL*4 and *SLPI*, respectively. Primer sequences (Table 11) were based on the Gene Bank accession numbers NM_002984, NM_001220777, BC015642, GU211347, BC032722 and NM_000660 for *CCL3*, *CDKN1A*, *SERPINA1*, *STAT1*, *TGF-β1* and *TNFSF10*, respectively. Quantitative real-time PCR experiments were carried out as described for cathepsin-L and dynamin (Section 2.6).

Table 10: Primer sequences for up- or down-regulated HIV-host response genes in HIVAN compared to HIV negative FSGS

Forward and reverse primers for down-regulated *CXCL12* and up-regulated *CCL4* and *SLPI* genes from HIV Host Response panel of arrays.

Gene	Primer	Sequence
CCL4	Forward	5' GCCTGCTGCTTTTCTTACAC 3'
	Reverse	5' CTTGCTTGCTTCTTTTGGTTTG 3'
CXCL12	Forward	5' GAAGGCAAACCCATCAACAAA 3'
	Reverse	5' AGTAAAGATCCCTCAGGCTCTA 3'
SLPI	Forward	5' AAATCTGCCCAGTGCCTTAG 3'
	Reverse	5' ACAAGTGTCAGGACAACATCTC 3'

CCL4: *Homo sapiens* Chemokine (C-C Motif) Ligand 4; *CXCL12*: *Homo sapiens* Chemokine (C-X-C Motif) Ligand 12; *SLPI*: *Homo sapiens* Secretory Leukocyte Peptidase Inhibitor. Primers were designed based on the Gene Bank accession numbers NM_000609, NM_002984 and NM_003064 for *CXCL12*, *CCL4* and *SLPI*, respectively. Primers were designed for intercalating SYBR-based real-time technology using the Integrated DNA Technologies (IDT) Primer Quest design tool (http://www.idtdna.com/primerquest) and purchased (Whitehead Scientific).

Table 11: Primer sequences for altered HIV-host response genes in HIVAN and HIV negative FSGS compared to the healthy controls

Gene	Primer	Sequence
CCL3	Forward	5’ GTACGTGTATGACCTGGAACTG 3’
	Reverse	5’ AGTCCTGAGTATGGAGGAGATG 3’
CDKN1A	Forward	5’ CCAGCCTCTGGCATTAGAATTA 3’
	Reverse	5’ CGGGATGAGGAGGCTTTAAATA 3’
SERPINA1	Forward	5’ CGTGAAGGTGCCTATGATGAA 3’
	Reverse	5’ TGGCATTGCCCAGGTATTT 3’
STAT1	Forward	5' CACCTACGAACATGACCCTATC 3'
	Reverse	5' GCTGTCTTTCCACCACAAAC 3'
TGF-β1	Forward	5' CGTGGAGCTGTACCAGAAATAC 3'
	Reverse	5' CACAACTCCGGTGACATCAA 3'
TNFSF10	Forward	5' CAGAGAGTAGCAGCTCACATAAC 3'
	Reverse	5' CCTTGATGATTCCCAGGAGTTT 3'

Primers for the *Homo sapiens* genes were designed based on the Gene Bank accession numbers NM_002984, NM_001220777, BC015642, GU211347, BC032722 and NM_000660 for *CCL3*, *CDKN1A*, *SERPINA1*, *STAT1*, *TGF-β1* and *TNFSF10*, respectively. Primers were designed for intercalating SYBR-based real-time using the Integrated DNA Technologies (IDT) Primer Quest design tool (http://www.idtdna.com/primerquest) and purchased (Whitehead Scientific). *CCL3*: Chemokine (C-C motif) ligand 3; *CDKN1A*: Cyclin-dependent kinase inhibitor 1A; *SERPINA1*: Serpin peptidase inhibitor, clade A (alpha-1 antiproteinase, antitrypsin), member 1; *STAT1*: Signal transducer and activator of transcription 1; *TGF-β1*: Transforming growth factor beta; TNFSF10: Tumor necrosis factor (ligand) superfamily, member 10.

2.9.2. Validation of altered TLR genes

In HIVAN kidneys, expression of seven genes from the Toll-Like Receptor Array was altered as compared to the HIV negative FSGS (Figure 20 in the results section). The altered genes included *HMGB1*, *LY96*, *PELI1*, *SIGIRR*, *MAP3K1*, *MAP4K4* and *MAPK8*. When gene expression pattern in proteinuric kidney diseases was compared to the healthy non-proteinuric controls, 2 more genes, notably *CCL2* and *REL1*, were shown to be altered in proteinuric kidney diseases. Validation of the altered MAPK pathway genes was assessed using the anti-SAPK/JNK and anti-phospho-SAPK/JNK (T183/Y185) antibodies (Cell Signaling Technology, Anatech Instruments) in western-blotting experiments (Section 3.4.2.1). Primers for the altered *CCL2* and *REL1* genes were designed and ordered for use in real-time quantitative PCR experiments to validate the expression patterns of these genes. The primers were designed using Integrated DNA Technologies Primer Quest design tool and purchased through Whitehead Scientific. Primer sequences (Table 12) were based on the Gene Bank accession numbers NM_002982 and NM_006509 for CCL2 and REL1, respectively. Quantitative real-time PCR experiments were performed as described for cathepsin-L and dynamin (Section 2.6).

Table 12: Primers for altered TLR genes in FSGS and HIVAN compared to healthy controls

Gene	Primer	Sequence
CCL2	Forward	5' TCATAGCAGCCACCTTCATTC 3'
	Reverse	5' CTCTGCACTGAGATCTTCCTATTG 3'
REL1	Forward	5' CTGCGGATTTGCCGAATTAAC 3'
	Reverse	5' ACACCACTGATATGTCCTCTTTC 3'

CCL2: *Homo sapiens* Chemokine (C-C Motif) Ligand 2; *REL1*: V-rel reticuloendotheliosis viral oncogene homolog (avian). Primers were designed based on the Gene Bank accession number NM_002982 and NM_006509 for *CCL2* and *REL1*, respectively. Primers were designed for intercalating SYBR-based real-time using the Integrated DNA Technologies (IDT) Primer Quest design tool (http://www.idtdna.com/primerquest) and purchased (Whitehead Scientific).

2.10. Protein extraction

Protein was isolated from human FFPE kidney biopies according to the method of Addis *et al*., (2009), with slight modifications. Briefly, tissue was deparaffinized by heating for 10 minutes at 56 °C in deparaffinization solution (QIAgen, Whitehead Scientific)) before the tissue was weighed and crushed in an Eppendorf tube. Minced tissue was resuspended in 20 % w/v extraction buffer (20 mM Tris-HCl, pH 8.8, 2 % SDS and 200 mM DTT) and subjected to higher temperatures, i.e., 100 °C for 20 minutes followed by 80 °C for 2 hours, with shaking. The extract was clarified by centrifugation at 12 000 x g for 15 minutes at 4 °C using a HERMLE Z216 MK centrifuge. Protein contained in the supernatant was harvested into a new Eppendorf tube and quantified. Protein concentration was estimated using the BCA Protein Assay kit (Pierce Biotechnology, Thermo Scientific) and integrity determined using SDS-PAGE. Protein was aliquoted, snap-frozen and kept at -80 °C until use.

2.11. Western-blotting

To correlate the gene expression patterns observed in quantitative real-time PCR with protein expression in the tissue, western-blotting experiments were conducted. The technique is used in molecular biology to locate and identify proteins based on their ability to bind to a panel of predefined antibodies. Specific antibodies are employed to probe the presence and concentration of the protein of interest. Cathepsin-L (C-18) goat and dynamin (H-300 (Santa Cruz Biotechnology, Anatech Instruments) were used to probe the protein concentration of cathepsin-L and dynamin, respectively. Anti-SAPK/JNK and anti-phospho-SAPK/JNK (T183/Y185) monoclonal antibodies were purchased (Cell Signaling Technology, Anatech Instruments) and used to detect the amount of JNK signaling pathway-specific protein present in various proteinuric disease states relative to healthy non-proteinuric controls. To normalize the levels of protein detected, loading controls are often included in western-blotting experiments. Loading controls are used to assess uniform loading of the samples across wells and confirm that band intensity variations observed in investigated proteins are due to varied expression of the proteins. Molecular weight of the loading control must be different from the protein of interest in order to distinguish and cut the bands with ease. Cathepsin-L, dynamin amd JNK proteins have molecular

weights ranging between 30 and 100 kDa. Hence, anti-Histone H3 antibody (Abcam, BIOCOM biotech) was used as a loading control, based on the very low molecular weight of the protein (~18 kDa) and its expression throughout the cell cycle, independent of DNA synthesis. Western-blotting was performed according to the well-documented protocol (Towbin *et al*., 1979). Briefly, proteins were separated by loading 150 µg of total purified protein sample from section 2.10 per lane onto 10 % sodium dodecyl sulphate polyacrylamide gel electrophoresis (SDS-PAGE) as outlined in the appendix (Laemmli, 1970). SDS-PAGE-resolved samples were removed from the running plates and incubated in transfer buffer for 15 minutes. Gel, placed on polyvinylidene difluoride (PVDF) transfer membrane, was stacked between six layers of filter paper, previously equilibrated in transfer buffer. Immun-Blot® PVDF membrane, 0.2 µM, (Bio-Rad) was activated by soaking in methanol for 10 minutes followed by equilibration in transfer buffer before use to immobilize protein. Protein samples, on the gel, were transferred and immobilized onto the PVDF membrane using a wet transfer system (Bio-Rad) under the following parameters; constant voltage at 250 volts and increasing current, initially set at 0.04 amperes for a single gel transfer. Protein sizes were estimated in relation to a protein molecular weight marker consisting of a set of standard proteins, of known molecular weight, electrophoresed and transferred under the same conditions (Precision Plus Protein™ Dual Color Standards, Bio-Rad). Following 90 minutes of transfer, the protein-containing membrane was removed from the sandwich and incubated in blocking buffer for 1 hour at room temperature to block non-specific binding sites. Milk quenched much of the signal of the SAPK-JNK antibody thus; fat-free milk was substituted with 5 % BSA in these experiments. Blocking buffer was washed off, 3 times with 5 minutes washes on a shaker, using TTBS. All subsequent washes were carried out in this manner. All buffer components are listed in the appendix. Membrane was incubated overnight in primary antibody (1:50 for Phospho-SAPK/JNK (T183/Y185), 1:100 for cathepsin-L, dynamin and SAPK/JNK, and 1:10 000 for Histone H3), prepared in blocking buffer, at 4 °C. The membrane was washed to remove excess/unbound primary antibody and incubated in secondary antibody for 1 hour at room temperature. HRP-linked goat anti-mouse IgG was used for Phospho-SAPK/JNK (T183/Y185) detection whereas HRP-linked goat anti-rabbit was used for dynamin, SAPK/JNK and Histone H3. Cathepsin-L was detected using rabbit anti-goat HRP-conjugated IgG. Secondary antibodies were prepared in blocking buffer containing 5 % milk for all antibodies to reduce background noise and were used at a final

concentration of 1:10 000. Following secondary antibody incubation, the membranes were washed and reaction developed using an enhanced chemiluminescent substrate for HRP (SuperSignal® WestPico kit, Thermo Scientific). The substrate was diluted1:1 with laminol before adding onto the blot for 5 minutes at room temperature. The chemiluminescence reaction was analyzed using clear blue X-Ray film (CL-XPosure^{TM}, ThermoScientific) which was exposed to the blotting membranes for 2 minutes and developed in the dark.

2.12. Data analysis

2.12.1. Immunohistochemistry quantification

Intensities of localized immune marker proteins were quantified from gray scale images of renal FFPE biopsies using CellProfiler (Lamprecht *et al*., 2007). Objects to be characterized, i.e., renal tubules and glomeruli, were identified manually and intensity measured. Intensities of selected areas were quantified using a scale of zero (dark) to one (light), whereby, zero denotes a highly concentrated localization and one a diffusely localized protein (CellProfiler software). Four objects were selected per case and intensities averaged and statistically analyzed using Statistica 12.5.192.5 software (StatSoft).

2.12.2. Statistical analysis of qPCR data

For real time qPCR assays, samples were deemed positive when the emitted fluorescence signal was higher than the threshold value automatically calculated as C_q value by the qPCR software (AB 7500, Applied Biosystems). Cq values were exported to a Microsoft Excel worksheet and the relative gene expression level of target gene calculated according to Equations 1 to 4 and presented as Log_{10} ($2^{-\Delta\Delta Cq}$). Statistical analyses of duplicated experiments were performed using Statistica 12.5 (StatSoft). A two-way analysis of variance (ANOVA, Kruskal-Wallis) and Mann-Whitney U-test were employed to test for significance. Samples were deemed significantly different when *p-value* < 0.05. Data were represented on Box-Whiskers plotted using median values of Log_{10} ($2^{-\Delta\Delta Cq}$) of each of the experimental groups as determined from the Kruskal-Wallis ANOVA test.

3. RESULTS

3.1. Immune-markers, cathepsin-L and dynamin, localization

The current study examined kidney biopsy sections from 21 patients, four of whom were healthy controls (trauma victims with neither renal injury nor kidney failure). Expression of immunohistochemical markers, notably cathepsin-L and dynamin, in kidney tubules and glomeruli amongst proteinuric kidney disease populations were assessed. Target antigens on tissue sections were probed using anti-cathepsin-L and anti-dynamin antibodies in respective experiments. Following immunostaining of the human kidney tissue sections, as detailed in the protocol (Section 2.2), slides were analyzed for the presence and quantity of immonohistochemical marker proteins under the light microscope (Figure 7 to Figure 9). Three proteinuric disease states, notably minimal change disease (MCD), focal segmental glomerulosclerosis (FSGS) and HIV-associated nephropathy (HIVAN), were studied relative to healthy controls. Contribution of the immunohistochemical markers in proteinuric disease was characterized by the amount of labeling in the respective tissue sections. Immunolabelling was quantified using the CellProfiler software (Lamprecht *et al*., 2007). Staining intensities in the pre-selected areas were determined from gray scale images (a representative is shown in Figure 10), whereby zero denotes a darker/concentrated localization and one a light/no protein expression detected. Median intensity values for each study group were compared to one another and to the healthy non-proteinuric control group using the Mann-Whitney U-test (Statistica analysis software, StatSoft) (Figure 8, Figure 11, Table 13 and Table 15).

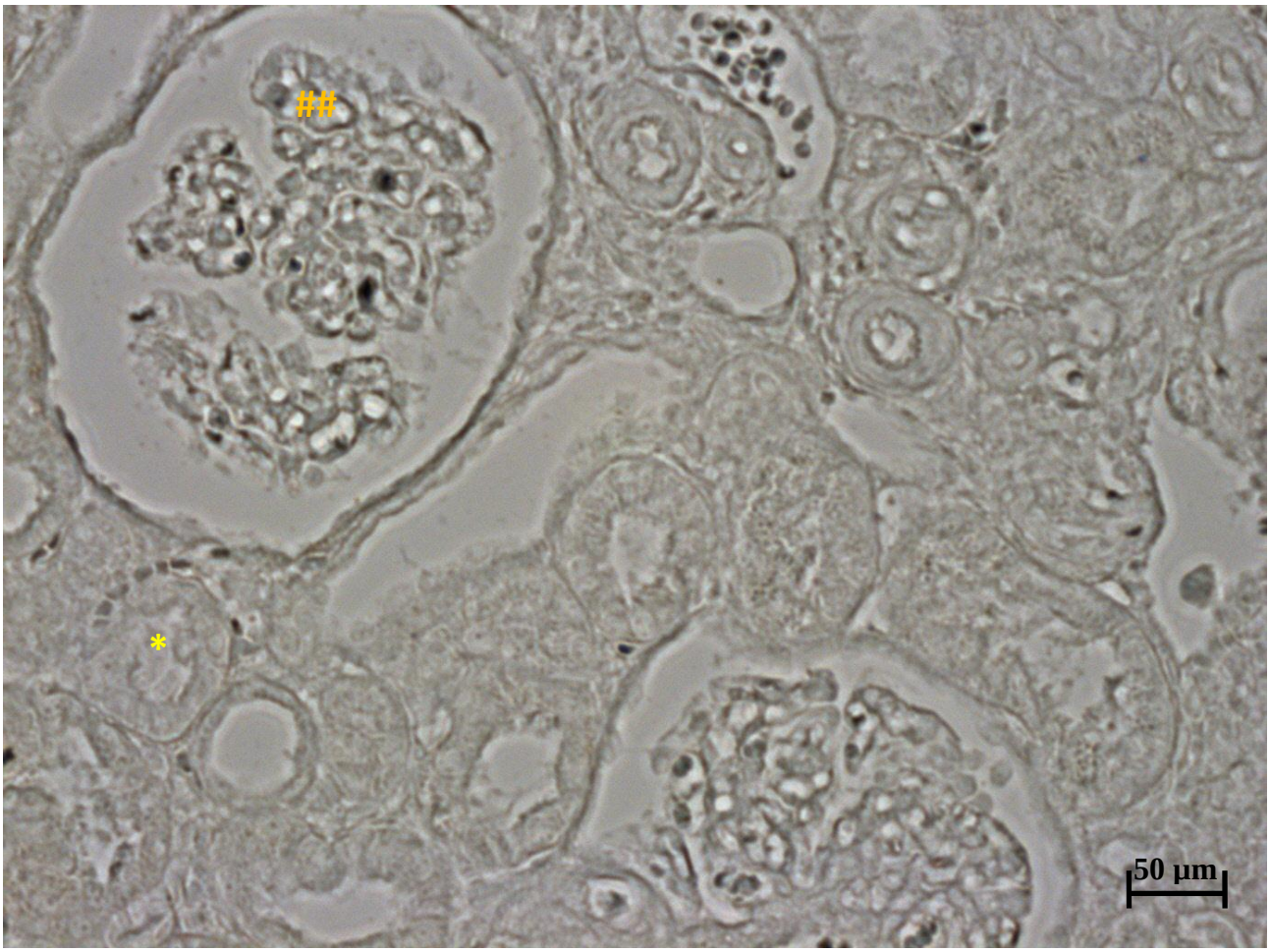

Figure 7: A representative of a light microscopy section of negative control kidney tissue

Representative of negative control experiments when the primary antibody directed towards the antigen of interest (either dynamin or cathepsin-L) was omitted. Expression of the marker proteins was assessed in the renal tubules (*) and glomeruli (##). The image was captured at 40 × magnification using Zeiss Axio-Cam HRC camera and Axiovision 4.8.1 software.

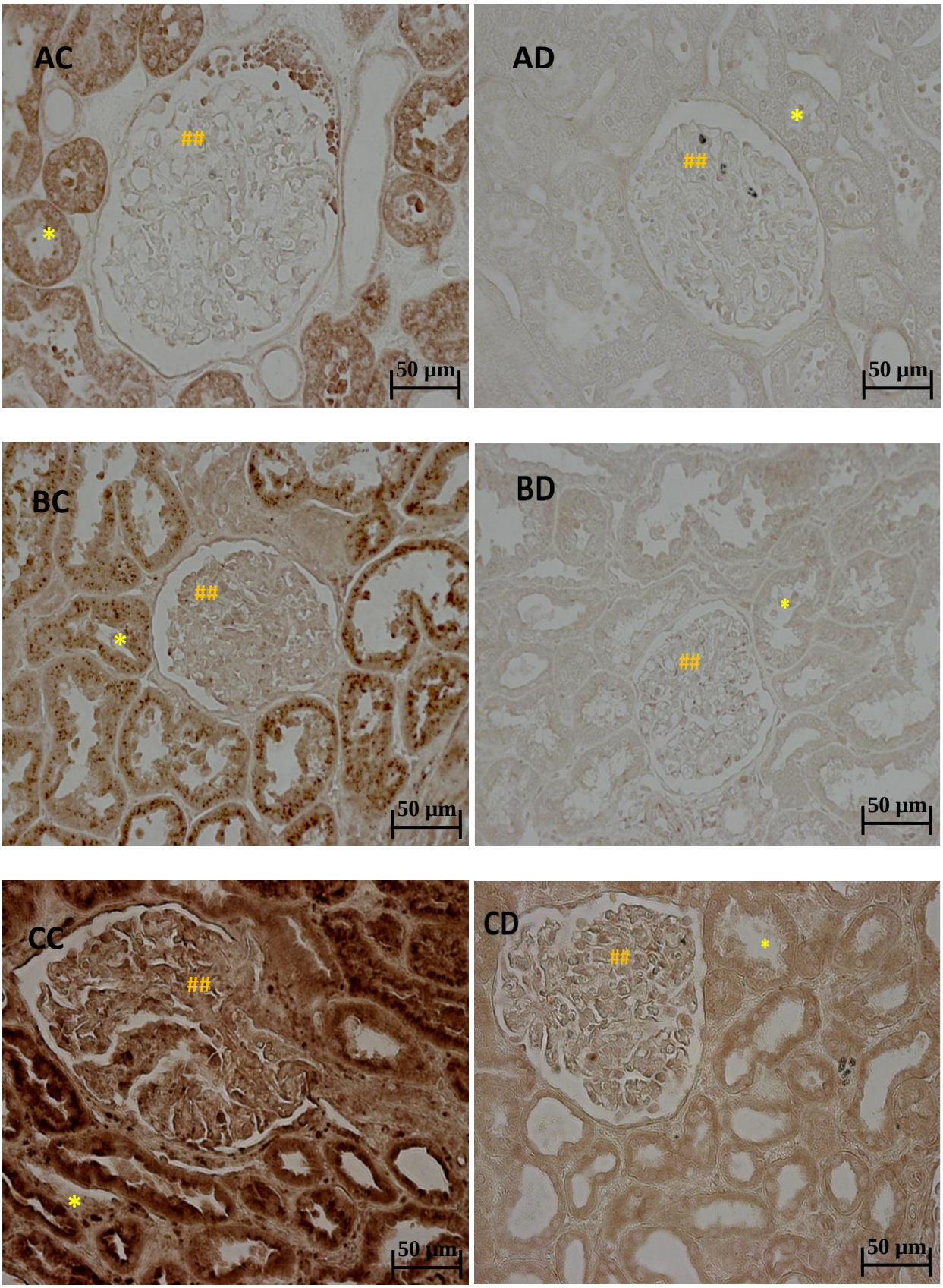
AC
##
*
50 µm
AD
*
##
50 µm
BC
##
*
50 µm
BD
*
##
50 µm
CC
##
*
50 µm
CD
##
*
50 µm

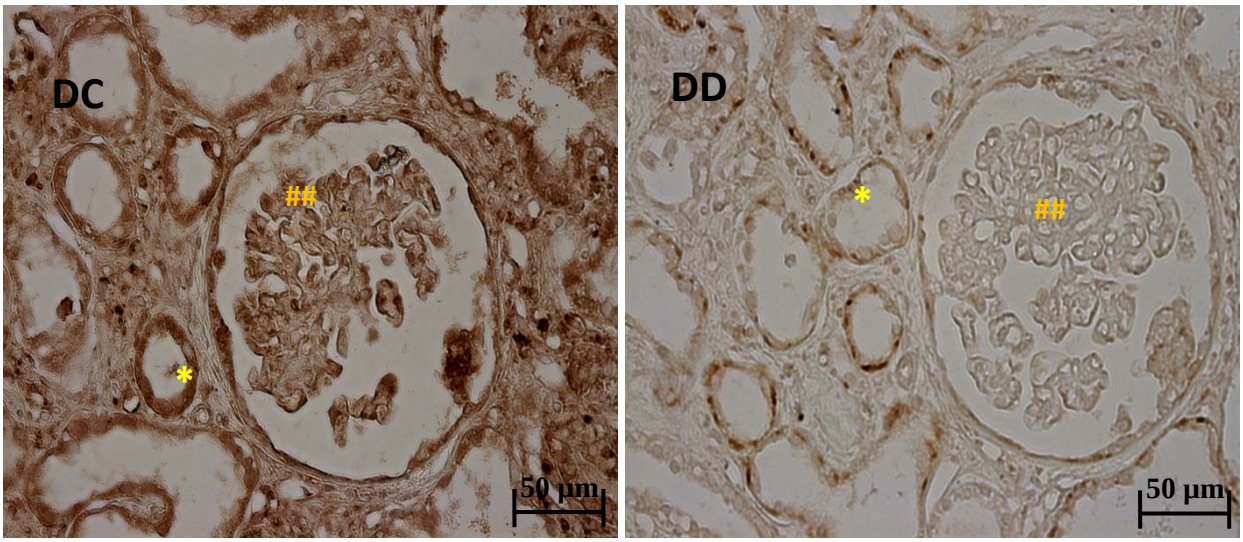

Figure 8: Probing cathepsin-L and dynamin expression and localization in renal tissue

Representatives of immunohistochemistry results of paraffin-fixed human kidney tissue probing the presence and location of cathepsin-L (C - left panel) and dynamin (D - right panel). The immunohistochemical markers were localized using cathepsin-L goat polyclonal IgG and dynamin rabbit polyclonal IgG, respectively. The antibody-antigen reactions were visualized by adding 3, 3-diaminobenzidine tetrachloride which exudes a brownish color upon interaction with the antibody-antigen complex. Expression of the marker proteins was assessed in the renal tubules (*) and glomeruli (##) from three disease (proteinuric) groups and a control group. **A**) healthy control; **B**) Minimal change disease – proteinuric control with histologically normal glomeruli on light microscopy; **C**) Focal-segmental glomerulosclerosis kidney tissue **D**) HIV-associated nephropathy kidney tissue. Images were captured at 40 × magnification using a Zeiss Axio-Cam HRC camera and Axiovision 4.8.1 software.

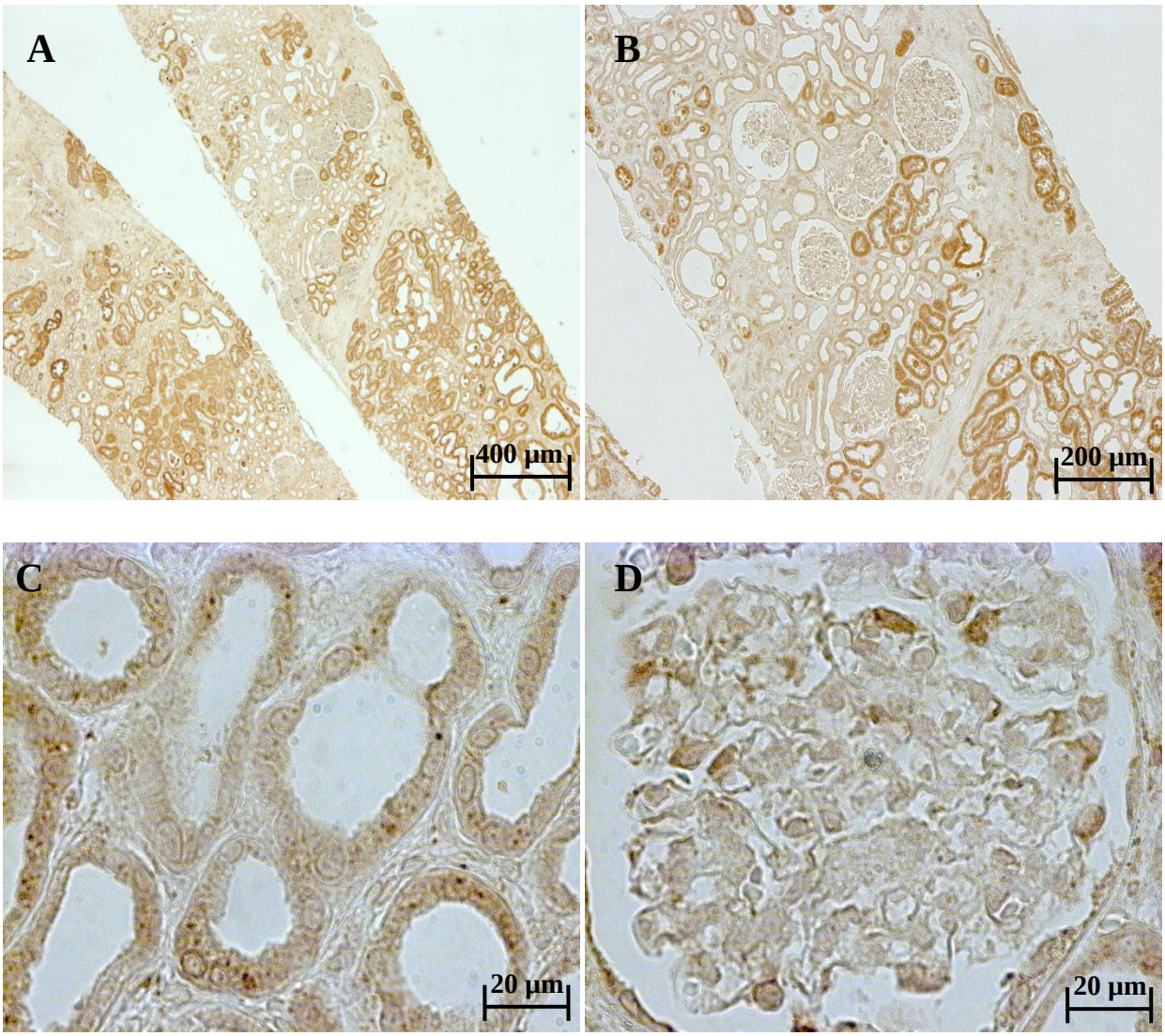

Figure 9: Comprehensive analysis of cathepsin-L and dynamin distribution within the kidney

Presence and localization of cathepsin-L and dynamin within proteinuric human kidneys was probed in immunohistochemistry experiments. Images were captured at various magnifications to illustrate the biomarker distribution within the human kidney. An overall localization pattern is presented in (**A**) 5 × and in (**B**) 10 × magnification. Focused images of the tubules and glomerulus were captured under oil immersion at 100 × magnification (Bottom panel). Cathepsin-L distribution within the kidney was dominant in tubular epithelial cells (**C**) and within the glomerulus (**D**). A Zeiss Axio-Cam HRC camera and Axiovision 4.8.1 software were used to capture the images.

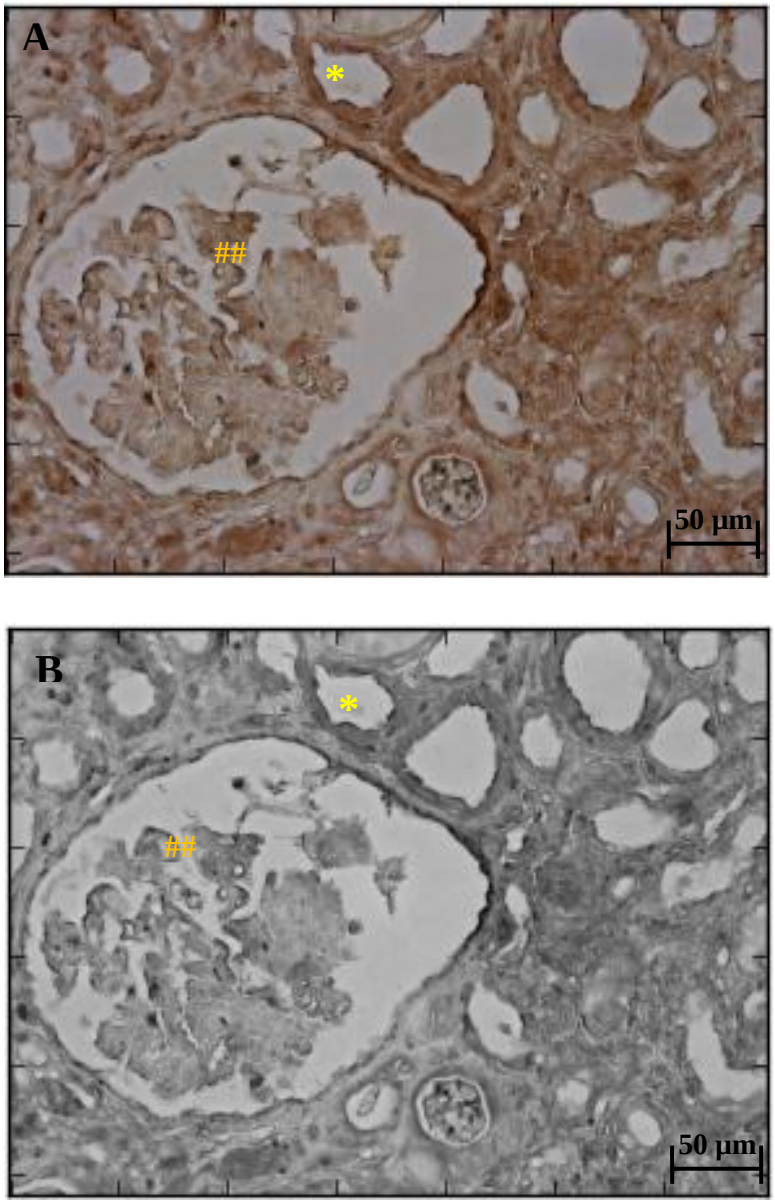

Figure 10: CellProfiler analyzed images

Cathepsin-L and dynamin expression was quantified using CellProfiler and data analysed using Statistica 12.5.192.5 software (StatSoft). The original image (A) was initially converted to a grayscale image (B) that was then used to identify areas of interest for analysis, renal tubules (*) and glomeruli (##). The program grades the intensity of selected area from zero (dark) to one (light).

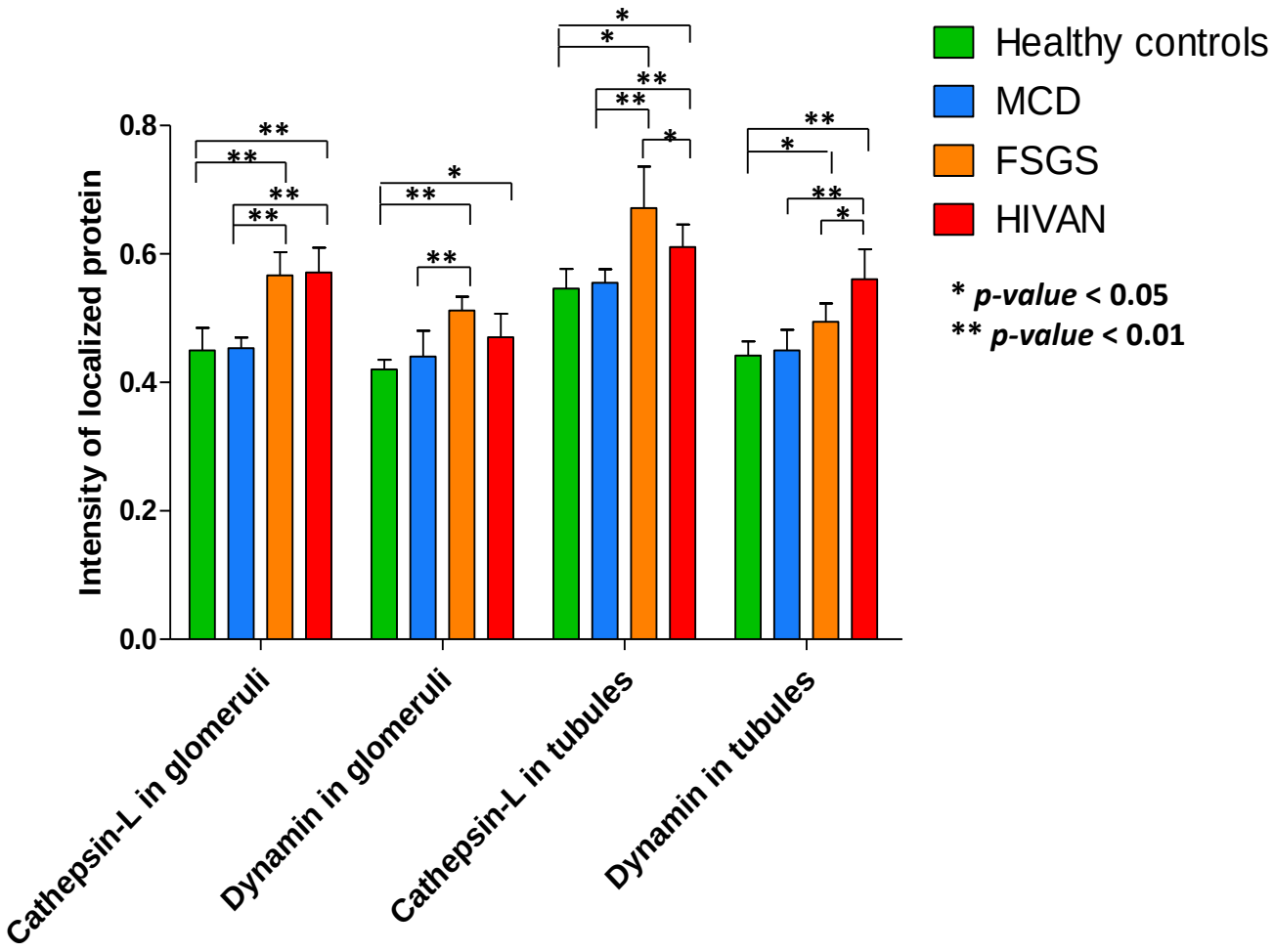

Figure 11: Quantification of immunohistochemical marker localization

Expression of cathepsin-L and dynamin in the renal tubules and glomeruli were compared amongst HIVAN, HIV negative FSGS, MCD and healthy controls. The intensity of localized cathepsin-L and dynamin is represented as reciprocal of the CellProfiler data. Immuno-labeled human kidney tissue sections were quantified using CellProfiler software and resultant data analyzed using Statistica 12.5.192.5 software (StatSoft). The graph was plotted using Graph Pad Prism 5 software.

Table 13: Comparison of glomerular cathepsin-L and dynamin localization intensities between disease states

***p-values* between groups**								
Glomeruli								
	Cathepsin-L				**Dynamin**			
	Normal	**MCD**	**FSGS**	**HIVAN**	**Normal**	**MCD**	**FSGS**	**HIVAN**
Normal	1.0000				1.0000			
MCD	0.9047	1.0000			0.5555	1.0000		
FSGS	**0.0015****	**0.0040****	1.0000		**0.0025****	**0.0242***	1.0000	
HIVAN	**0.0015****	**0.0040****	0.8784	1.0000	**0.0101***	0.1636	0.0728	1.0000

Mann-Whitney U-test was used to compare two independent groups. Samples marked with asterisk had protein expression levels that are significantly different from each other. * *p-value* < 0.05; ** *p-value* < 0.01. Normal: healthy controls; MCD: minimal change disease; FSGS: focal and segmental glomerulosclerosis; HIVAN: human immunodeficiency virus-associated nephropathy. Normal n= 4; MCD n= 4; FSGS n= 8; HIVAN n=8

Table 14: Comparison of tubular cathepsin-L and dynamin localization intensities between disease states

***p-values* between groups**								
Tubules								
	Cathepsin-L				**Dynamin**			
	Normal	**MCD**	**FSGS**	**HIVAN**	**Normal**	**MCD**	**FSGS**	**HIVAN**
Normal	1.0000				1.0000			
MCD	0.5555	1.0000			0.7302	1.0000		
FSGS	**0.0108***	**0.0080****	1.0000		**0.0480***	0.0727	1.0000	
HIVAN	**0.0186***	**0.0090****	**0.0498***	1.0000	**0.0025****	**0.0060****	**0.0174***	1.0000

Mann-Whitney U-test was used to compare two independent groups. Samples marked with asterisk had protein expression levels that are significantly different from each other. * *p-value* < 0.05; ** *p-value* < 0.01. Normal: healthy controls; MCD: minimal change disease; FSGS: focal and segmental glomerulosclerosis; HIVAN: human immunodeficiency virus-associated nephropathy. Normal n= 4; MCD n= 4; FSGS n= 8; HIVAN n=8

Intensity of localized cathepsin-L and dynamin was evaluated in renal tubules and glomeruli of HIVAN, FSGS, MCD and healthy controls. Expression of the immune markers varied across disease states and location (Figure 11). However, the labeling pattern observed in minimal change disease and healthy controls was similar (Figure 8A and B). Cathepsin-L was more diffusely localized in the glomeruli than in the tubules of healthy controls and MCD patients. In contrast, a significant amount of cathepsin-L labeling was observed in both the renal tubules and glomeruli of HIVAN and FSGS patients (Figure 8C and D). Healthy controls and MCD populations demonstrated a low expression of dynamin in both target locations with FSGS showing a moderate expression in both structures (Figure 11). To further quantify the intensity of localized target antigens in disease states, median values of each of the three proteinuric kidney disease groups were individually compared to each other and to a healthy control group, consisting of the non-proteinuric population. The groups were compared based on *p-values* obtained using Mann-Whitney U-test from a statistical analysis program (StatSoft). Relative to healthy non-proteinuric and MCD groups, HIVAN and FSGS expression of cathepsin-L and dynamin in the glomeruli was significantly increased, *p-values* ≤ 0.01, for (Table 13), whereas there was no significant difference observed between MCD and the healthy controls. A similar trend for expression of cathepsin-L was observed in renal tubules (Table 14). However, the intensity of localized cathepsin-L and dynamin differed significantly between HIVAN and FSGS with *p-values* of 0.0498 and 0.0174, respectively (Table 14). Dynamin expression in tubules and glomeruli of HIVAN and MCD kidneys was not statistically different, *p-values* of 0.1636 and 0.0727, respectively. In the HIVAN population, enhanced localization of dynamin was observed in the tubules compared to the glomeruli (Figure 11).

3.2. Cathepsin-L and dynamin expression patterns

3.2.1. Transcriptional mRNA expression of cathepsin-L and dynamin

RNA was reverse transcribed and yielded good quality cDNA that was used as a template in subsequent qPCR assays. Contaminating genomic DNA was successfully eliminated from RNA samples as indicated by no signal detected from qPCR of non-reverse transcriptase (NRT) controls. Real time qPCR was employed to assess the expression levels of renal cathepsin-L and dynamin in proteinuric kidney diseases. Gene expression in HIVAN, FSGS and MCD were compared to healthy non-proteinuric controls. mRNA expression patterns were profiled in qPCR experiments using cDNA and primers specific for the genes. To control for variability in the efficiency of reverse transcription, qPCR expression data was normalized against three kidney specific reference genes, notably *RPL13A, SDHA* and *YWHAZ*. No amplification was detected from the "no template controls", indicative of no contamination. Melting curves were performed with each run to determine the composition of the amplification product since SYBR green non-specificity may result in bound primer dimers and non-specific PCR products.

Our results, as presented in Table 15 and Figure 12, revealed that relative to healthy non-proteinuric controls, expression of cathepsin-L 1 in MCD is marginally enhanced. Expression of cathepsin-L 1 in MCD was significantly increased relative to HIVAN and FSGS, *p-value* < 0.05. Expression of cathepsin-L 2 was down-regulated across all proteinuric kidney disease states, significantly so in HIVAN relative to the healthy controls, *p-value* of 0.0317. Cathepsin-L 3 expression was down-regulated in MCD and enhanced in HIVAN and FSGS relative to healthy controls, though the differences were statistically insignificant.

Table 15: Comparison of qPCR expression levels of cathepsin-L in the kidneys of proteinuric groups and the healthy non-proteinuric controls.

Groups	*p-values* between groups											
	CTSL-1				*CTSL-2*				*CTSL-3*			
	Normal	**MCD**	**FSGS**	**HIVAN**	**Normal**	**MCD**	**FSGS**	**HIVAN**	**Normal**	**MCD**	**FSGS**	**HIVAN**
Normal	1.0000				1.0000				1.0000			
MCD	0.7857	1.0000			0.1428	1.0000			0.7857	1.0000		
FSGS	**0.0480***	**0.0166***	1.0000		0.0732	0.6666	1.0000		0.3434	0.0666	1.0000	
HIVAN	**0.0173***	**0.0238***	0.1375	1.0000	**0.0317***	0.7857	0.3434	1.0000	0.5368	0.3809	0.1375	1.0000

Mann-Whitney U-test was used to compare two independent groups. Significantly different protein localization in each group is marked: * *p-value* < 0.05; ** *p-value* < 0.01; *** *p-value* < 0.001. Normal: healthy controls; MCD: minimal change disease; FSGS: focal and segmental glomerulosclerosis; HIVAN: human immunodeficiency virus-associated nephropathy. Normal n= 4; MCD n= 4; FSGS n= 7; HIVAN n=6.

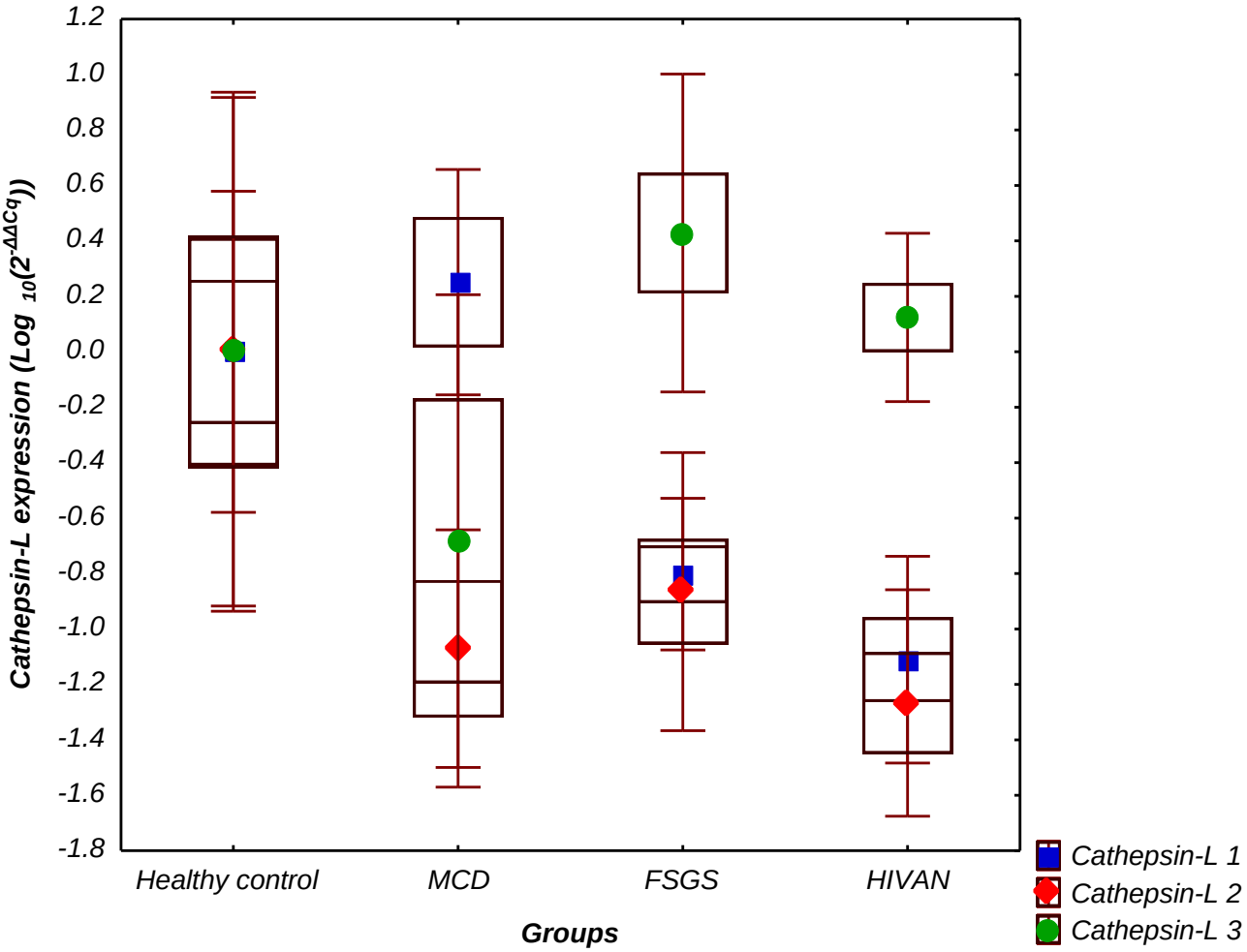

Figure 12: qPCR renal cathepsin-L expression

Plots of the three isoforms of cathepsin-L were superimposed to contrast expression of the various isoforms of the gene among the experimental groups. Cathepsin-L 1 was down-regulated in HIVAN and FSGS, and over-expressed in MCD. Cathepsin-L 3 was up-regulated in HIVAN and FSGS, and down-regulated in MCD, whereas, expression of cathepsin-L 2 was attenuated in all three proteinuric states. Graphs were plotted using median values of $Log_{10}(2^{-\Delta\Delta Cq})$ of each of the experimental groups as determined from the Kruskal-Wallis ANOVA test. Statistical analysis of data and graphs were plotted using Statistica12.5.192.5 analysis software (StatSoft).

Cathepsin-L 3 is more over-expressed in FSGS than in HIVAN. Similarly to cathepsin-L, expression of the three isoforms of dynamin was not significantly different between MCD and healthy controls, *p-value* > 0.05 (Table 16).

Dynamin 1 expression was slightly enhanced in HIVAN and MCD, relative to the healthy control group and significantly down-regulated in FSGS relative to MCD (Figure 13). Dynamin 3 was slightly down-regulated in all three proteinuric states, whereas isoform 2 was equally expressed between FSGS and healthy controls (*p-value* close to 1, i.e., 0.9755) but marginally down-regulated in MCD and HIVAN. In FSGS, over-expression of cathepsin-L 3 was accompanied by down-regulated expression of all 3 isoforms of dynamin as well as cathepsin-L 1 and 2. Similarly, enhanced expression of cathepsin-L 3 in HIVAN was complemented by down-regulation of isoforms 1 and 2, and dynamin 2 and 3. However, dynamin 1 expression was enhanced in HIVAN. Overall, dynamin expression was marginally down-regulated and cathepsin-L significantly enhanced in proteinuric kidney diseases compared to the healthy controls (Figure 13). Figure 12 and Figure 13 summarize cathepsin-L and dynamin expression in proteinuric diseases relative to the healthy non-proteinuric control group.

3.2.2. Western-blot validation of cathepsin-L and dynamin protein expression

To validate the mRNA expression levels of cathepsin-L and dynamin as observed in real-time qPCR experiments, western blotting technique was used. Western-blot experiments were carried-out as described in Section 2.11 using anti-cathepsin-L and anti-dynamin antibodies, respectively. Attenuated cathepsin-L protein levels were detected in healthy non-proteinuric controls and MCD as compared to FSGS and HIVAN (Figure 14A). Cathepsin-L was significantly over-expressed in HIVAN relative to all other study groups. In contrast, the expression levels of dynamin protein could not be validated in western-blots as expression levels seemed identical between all proteinuric states and the healthy non-proteinuric control (Figure 14B).

Table 16: Comparison of qPCR expression levels of dynamin in the kidneys of proteinuric groups and the healthy non-proteinuric controls.

	***p-values* between groups**											
Study group	***DYN-1***				***DYN-2***				***DYN-3***			
	Normal	**MCD**	**FSGS**	**HIVAN**	**Normal**	**MCD**	**FSGS**	**HIVAN**	**Normal**	**MCD**	**FSGS**	**HIVAN**
Normal	1.0000				1.0000				1.0000			
MCD	0.1428	1.0000			0.7857	1.0000			0.3928	1.0000		
FSGS	0.9755	**0.0166***	1.0000		0.9755	0.6666	1.0000		0.1490	0.5166	1.0000	
HIVAN	0.3290	0.2619	0.1014	1.0000	0.6623	0.7142	0.1806	1.0000	0.2467	0.9047	0.3660	1.0000

Mann-Whitney U-test was used to compare two independent groups. Significantly different protein localization in each group is marked: * *p-value* < 0.05; ** *p-value* < 0.01. Normal: healthy controls; MCD: minimal change disease; FSGS: focal and segmental glomerulosclerosis; HIVAN: human immunodeficiency virus-associated nephropathy. Normal n= 4; MCD n= 4; FSGS n= 7; HIVAN n=6.

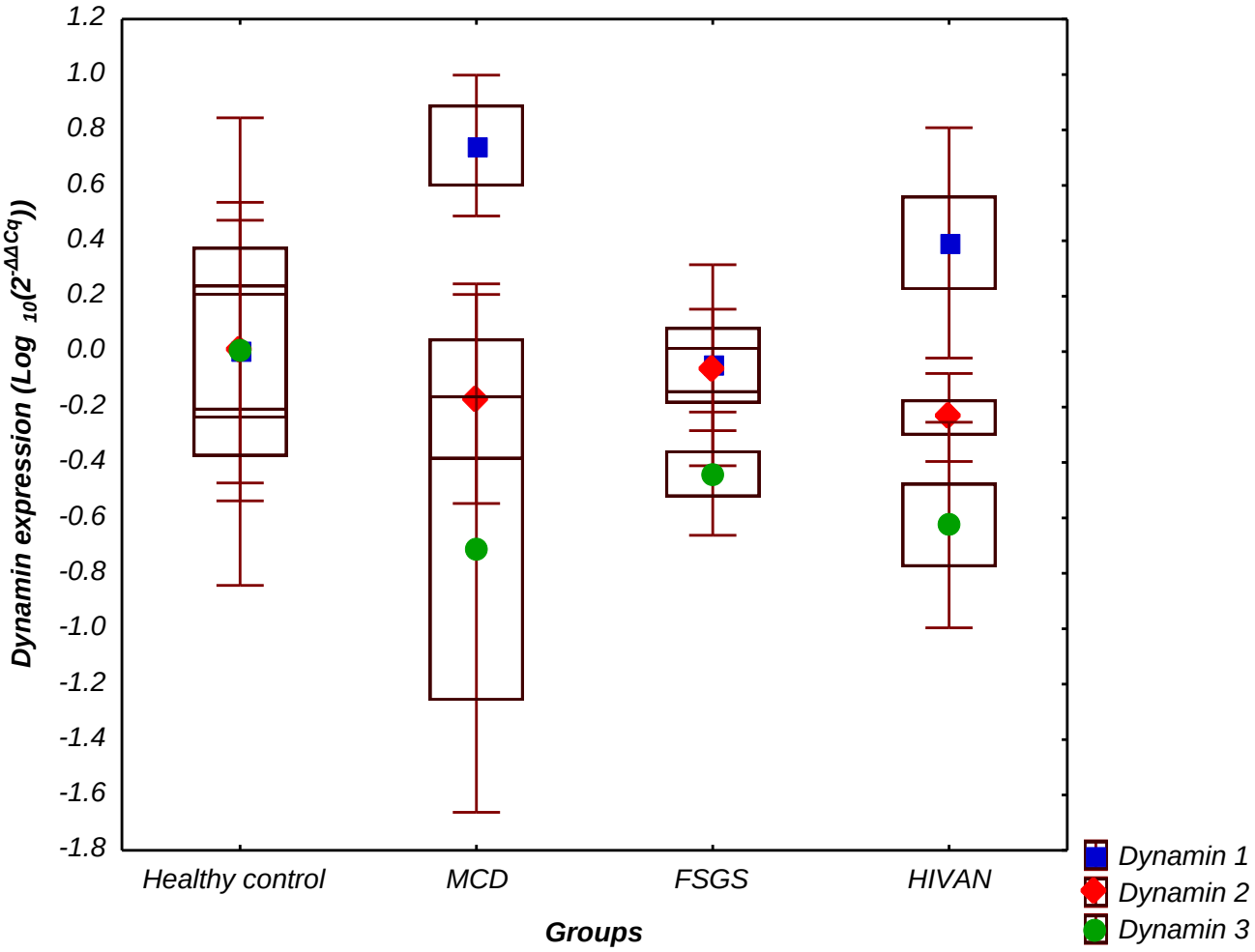

Figure 13: Box-Whisker plots of qPCR renal dynamin expression

Plots of all three dynamin isoforms were superimposed to contrast expression of various isoforms of the gene among the experimental groups. Dynamin 1 was over-expressed in MCD and HIVAN though slightly down-regulated in FSGS. Both isoform 2 and 3 of dynamin were down-regulated in all three proteinuric states. Graphs were plotted using median values of Log_{10} ($2^{-\Delta\Delta Cq}$) of each of the experimental groups as determined from the Kruskal-Wallis ANOVA test. Statistical analysis of data and graphs were plotted using Statistica12.5.192.5 analysis software (StatSoft).

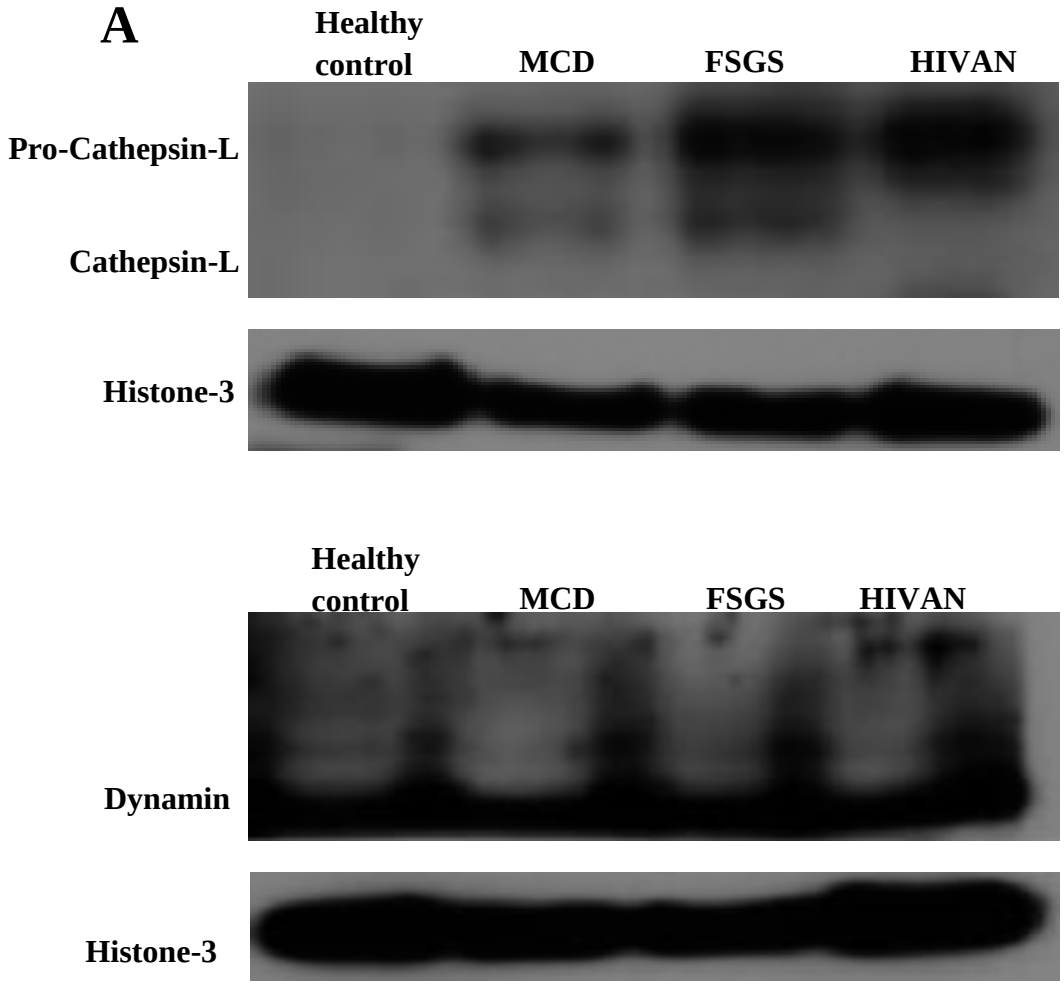

Figure 14: Western-blot analysis of cathepsin-L and dynamin expression

Cathepsin-L and dynamin protein expression levels in proteinuric kidney diseases were assessed relative to healthy controls. Each lane of the 10 % SDS-PAGE gel was loaded with 150 µg of total purified protein sample (**A**) Cathepsin-L (30 kDa) and pro-cathepsin-L (40 kDa) expression were over-expressed in proteinuric diseases, especially in HIVAN. In contrast, the expression of dynamin (100 kDa) was down-regulated in proteinuric kidney diseases as compared to the healthy controls (**B**). Consistent levels of the loading control, Histone-3, were detected across experimental groups (bottom panels). Histone-3 (18 kDa), labelled using anti-Histone-3 antibody and detected using goat anti-rabbit HRP-conjugated IgG was used as a loading control. All antibodies were prepared in 5 % fat-free milk dissolved in TTBS buffer.

3.3. Expression patterns of podocyte cytoskeleton proteins

Proteolysis of the actin-associated proteins, in the podocyte slit diaphragm, by cathepsin-L in renal cells leads to compromised cytoskeleton integrity and podocyte foot process effacement, and ultimately proteinuria. Primers for CD2AP, nephrin, podocin and synaptopodin were used in real-time quantitative PCR experiments to evaluate the expression of these genes at a transcriptional level. mRNA expression patterns of these actin-associated proteins were assessed in proteinuric kidney diseases relative to the healthy non-proteinuric control group. Real-time quantitative PCR results confirmed the hypothesis that actin-associated proteins are enzymatically cleaved by cathepsin-L in podocytopathy, as CD2AP, podocin, and synaptopodin were all down-regulated in proteinuric states (Figure 15). These proteins were significantly down-regulated in MCD as compared to other diseases and the healthy controls (Table 17). Nephrin was only over-expresed in HIV negative FSGS and down-regulated in both HIVAN and MCD as compared to the healthy controls. Overall, the expression levels of the cytoskeleton proteins were similar between FSGS and the healthy controls (*p-values* greater than 0.05) and significantly higher than in MCD (*p-values* ≤ 0.05) (Table 17).

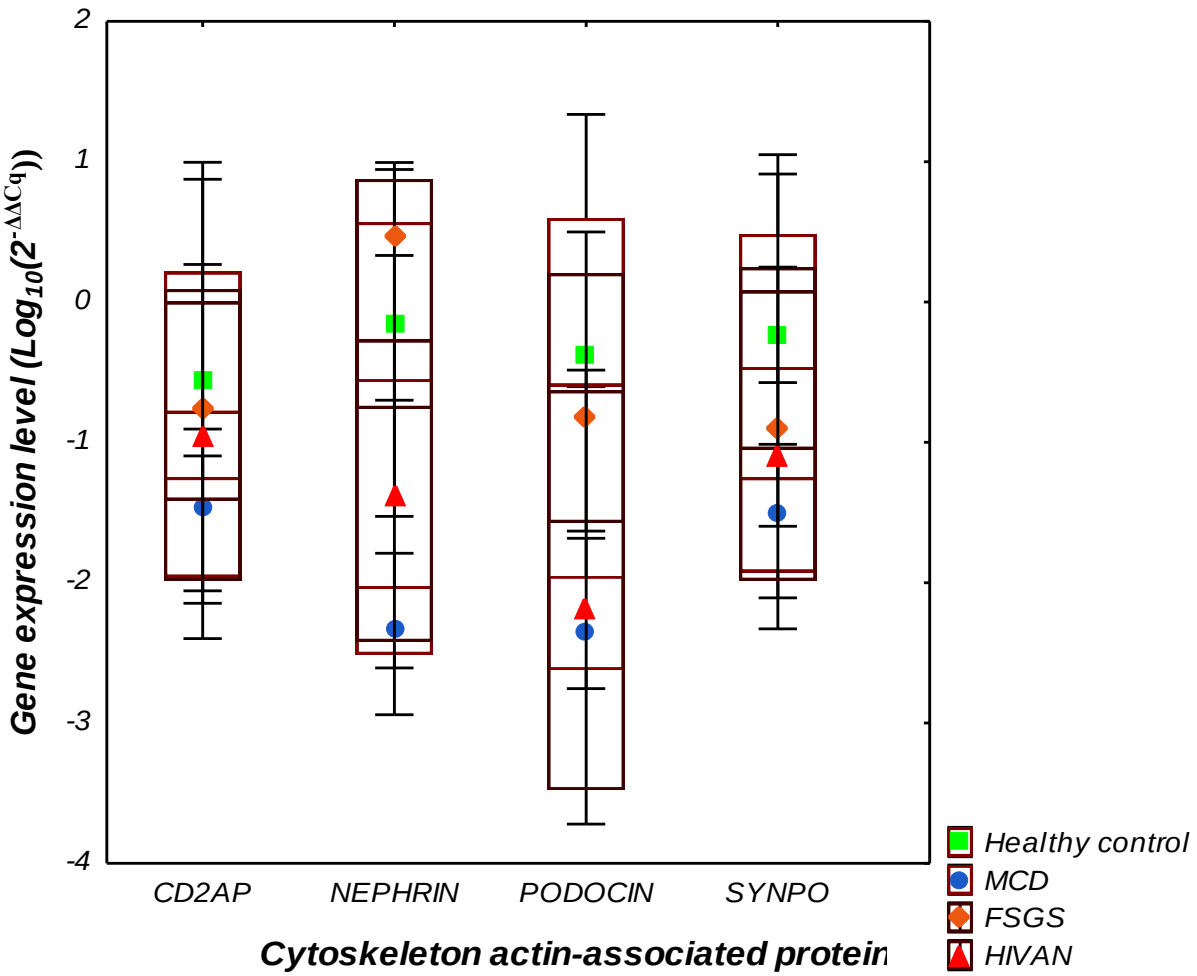

Figure 15: Expression patterns of podocyte cytoskeleton proteins

Box whisker plots of four actin-associated gene products in lipid rafts of the podocytes slit diaphragm were superimposed to compare expression levels of the genes. CD2AP, podocin and synaptopodin (SYNPO) expression levels were attenuated in all proteinuric states relative to the healthy controls. Nephrin expression was also down-regulated in HIVAN and MCD but up-regulated in FSGS compared to the control. Gene expression levels were normalized against three reference genes, i.e., *RPL13A*, *SDHA* and *YWHAZ*. Graphs were plotted using median values of $Log_{10}(2^{-\Delta\Delta Cq})$ of the experimental groups as determined from Kruskal-Wallis ANOVA test. Statistical analysis was performed using Statistica12.5.192.5 analysis software (StatSoft).

Table 17: Comparison of qPCR expression patterns of actin-associated podocyte cytoskeleton gene products in proteinuric kidney diseases and the healthy controls.

Study group	Gene product			
	CD2AP	**Nephrin**	**Podocin**	**Synaptopodin**
Healthy control vs MCD	**0.028571***	**0.028571***	**0.028571***	**0.028571***
Healthy control vs FSGS	0.412121	0.927273	0.163636	0.163636
Healthy control vs HIVAN	0.609524	0.057143	**0.038095***	0.476190
MCD vs FSGS	0.109091	**0.006061****	**0.006061****	0.072727
MCD vs HIVAN	0.609524	0.857143	0.915106	0.609524
FSGS vs HIVAN	0.730769	**0.033333***	0.234266	0.533800

Mann-Whitney U-test was used to compare two independent groups. Significantly different protein localization in each group is marked: * *p-value* < 0.05; ** *p-value* < 0.01. Healthy control: healthy controls; MCD: minimal change disease; FSGS: focal and segmental glomerulosclerosis; HIVAN: human immunodeficiency virus-associated nephropathy. Normal n= 4; MCD n= 4; FSGS n= 7; HIVAN n=6.

3.4. Polymerase chain reaction arrays

Gene expression patterns in HIVAN samples were compared to non-HIV FSGS tissues and healthy non-proteinuric controls. Changes in gene expression patterns in kidney tissues were assessed using RT^2 Profiler PCR Arrays. Real-time PCR cycling was performed using the 7500 Real Time PCR System and data analyzed using the 7500 real-time cycler software v2.0.5 and web-based software package (SABiosciences; QIAgen). Each assay had an end cycle number, the pre-set maximum number of cycles that real-time qPCR experiment performs for a specified assay, of 40. Raw data resulting from real-time qPCR were used in the real-time cycler software to calculate quantification cycle values (C_q), previously known as the cycle threshold values (C_t values) (Bustin *et al*., 2009). A C_q value is the point in the exponential phase of the curve where the PCR curve crosses the pre-set threshold. This represents the earliest PCR cycle at which point the amplification product of a sample is significantly different from the background fluorescence. Hence, C_q value is interpreted as the amount of mRNA detected in each assay. The smaller the C_q value (below 20, from a 40 cycles qPCR assay), the more mRNA detected since less amplification cycles are needed to detect fluorescence, thus the higher the gene expression. Similarly, the higher the C_q value (over 35), the lower the gene expression level. C_q cut-off values have been implemented to minimize the occurrence of flawed results and PCR outliers used in the downstream processing of real-time PCR results. In clinical research and genotyping studies, C_q cut-off values are used to increase the probability of true positive results being detected and to lessen the occurrence of false positives (Foy and Parkes, 2001; Burns *et al*., 2005). These values are subjective and justification for the exact value highly depends on the end-cycle value (Rodriguez-Lazaro *et al*., 2003). Too low a C_q cut-off values may be too stringent and erroneously omit true positive results. Furthermore, a too high value makes it less stringent but increases chances of incorporating false positives. The present study carefully selected C_q cut-off value of 35 in order to avoid either one of the two common errors of real-time PCR data analysis. This value was used in conjunction with the fold change value to filter results for downstream processing.

Using these parameters, we have identified HIV-1 disease- and TLR pathway-specific genes that were either up-regulated or down-regulated in HIVAN compared to non-HIV FSGS and healthy non-proteinuric controls. C_q values were calculated by firstly defining the baseline and the threshold based on the log view of the amplification plot. C_q values for all wells were

exported to Excel spreadsheet and subsequently uploaded to the RT^2 PCR Profiler Array System v4.0 (SABiosciences, QIAgen) web-based analysis software to calculate $\Delta\Delta C_q$-based fold-change. Catalogued PCR Arrays PAHS-051Z and PAHS-018Z were used for HIV Host Response Panel and TLR pathway analysis, respectively.

$\Delta\Delta C_q$-based fold-change represents the quotient of normalized gene expression in the test and control samples. Fold change values below 0.5 indicate a down-regulation in gene expression whereas, values greater than 2.0 indicate an up-regulation. Any fold-change values between 0.5 and 2.0 were considered insignificant and were excluded from further analyses. Samples were considered significant and eligible for further analyses when both fold-change and C_q value were less than or equal to 0.5 and greater than or equal to 2.0 (i.e., $0.5 \leq 2.0$), and less than 35, respectively.

3.4.1. HIV host response PCR arrays

The HIV Host Response PCR array panel was employed in real-time PCR to assess the expression of a focused panel of genes related to HIV infection and the host response. This array includes host genes that are involved in various stages of the HIV life-cycle and host cell infection, notably viral attachment, fusion, uncoating, reverse transcription, nuclear import, integration, transcription, RNA export, viral assembly and budding. Two genes (*CCL4* and *SLPI*) were up-regulated and one (*CXCL12*) was down-regulated in HIVAN relative to the HIV negative FSGS from the HIV Host Response panel of arrays (Figure 16).

When comparing the gene expression patterns of HIV-host response panel in HIV negative FSGS and HIVAN to healthy controls using RT^2 PCR arrays, we discovered that 2 genes were down-regulated and 3 were over-expressed in both proteinuric states relative to the controls (Figure 17). The two down-regulated genes were *CCL*3 and *CDKN*1*A*, and the over-expressed genes were *SERPINA*1, *STAT*1 and *TNFSF*10. Furthermore, the expression level of *TGF-β*1 was only up-regulated in HIV negative FSGS but not in HIVAN (Figure 17).

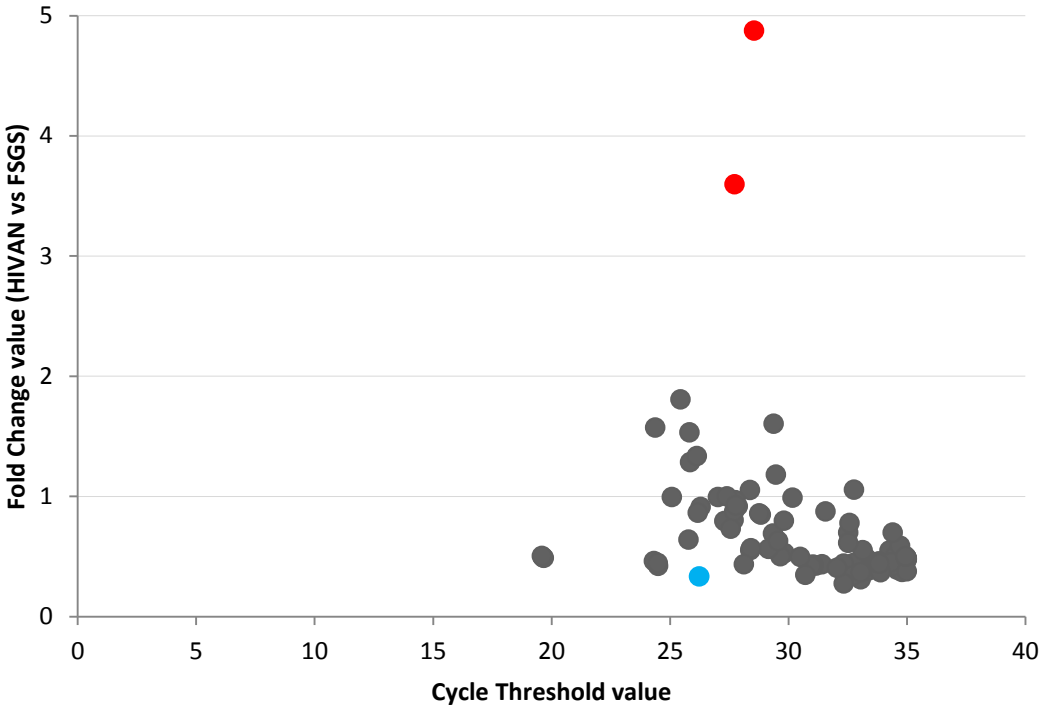

Figure 16: HIV Host Response Panel arrays gene expression pattern in HIVAN vs HIV negative FSGS

A gene was regarded as either down-regulated (blue dots) or up-regulated (red dots) when fold-change value was less than 0.51 or greater than 1.9, respectively. Data points with C_q values equal to or higher than the pre-set cycle cut-off point of 35 were considered to be false positives or negative test results and were excluded from downstream processing. Data points with C_q values less than the cycle cut-off point were regarded as positive test results. Positive results were considered significant and eligible for downstream analyses when fold-change value denoted either an up- or down-regulation of the gene expression. Two genes were up-regulated, i.e., *CCL4* and *SLPI*, whereas one was down-regulated, i.e., *CXCL12*, from the HIV Host Response panel of genes. Grey dots represent data points that were excluded from downstream processing due to either one (HIVAN or FSGS) of the C_q values being a false positive or the fold change value was $0.5 \leq 2.0$. Real-time qPCR data was collected from 7500 Real Time PCR System (Applied Biosystems) and analyzed using the 7500 Software v2.0.5 and web-based software package (RT^2 PCR Profiler Array System v4.0, SABiosciences; QIAgen). For web-based analysis of the HIV Host Response Panel, PAHS-051Z catalogued PCR Arrays were used. Data points for the graph were C_q values obtained from qPCR.

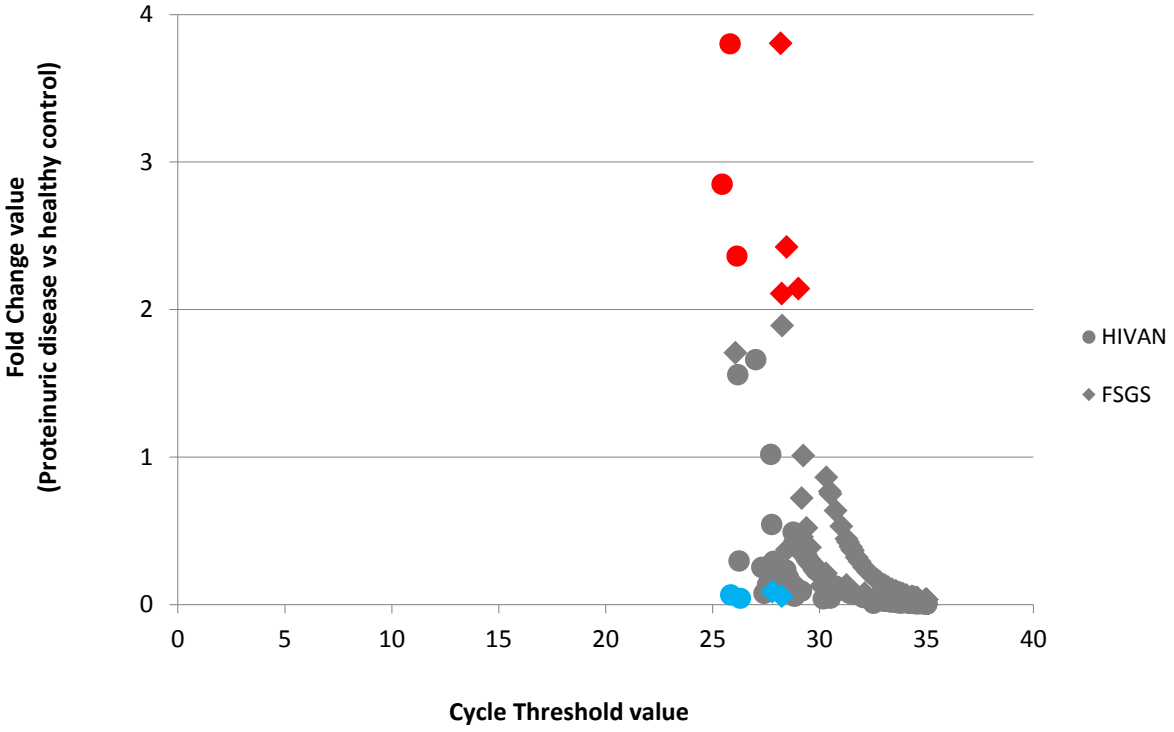

Figure 17: HIV Host Response Panel arrays gene expression pattern in HIVAN and HIV negative FSGS compared to the healthy non-proteinuric controls

A gene was regarded as either down-regulated (blue dots) or up-regulated (red dots) when fold-change value was less than 0.51 or greater than 1.9, respectively. Data points with C_q values less than the cycle cut-off point were regarded as positive test results. Positive results were considered significant and eligible for downstream analyses when fold-change value denoted either an up- or down-regulation of the gene expression. Grey dots represent data points that were excluded from downstream processing due to either one (HIVAN or FSGS) of the C_q values being a false positive or the fold change value was $0.5 \leq 2.0$. Two genes were down-regulated, i.e., *CCL3* and *CDKN1A*, whereas three were up-regulated, i.e., *SERPINA*1, *STAT*1 and *TNFSF*10, in both HIVAN and FSGS relative to the controls. *TGF-β1* was only up-regulated in the HIV negative FSGS. Real-time qPCR data was collected from 7500 Real Time PCR System (Applied Biosystems) and analyzed using the 7500 Software v2.0.5 and web-based software package (RT^2 PCR Profiler Array System v4.0, SABiosciences; QIAgen). For web-based analysis of the HIV Host Response Panel, PAHS-051Z catalogued PCR Arrays were used. Data points for the graph were C_q values obtained from qPCR.

3.4.1.1. qPCR validation of altered HIV-host response genes

From the HIV-host response panel of qPCR arrays, expression of 3 genes was altered in HIVAN compared to HIV negative FSGS (Figure 16). Additionally, expression of 5 other genes was altered in both HIVAN and the HIV negative FSGS, relative to the healthy non-proteinuric control group, and one more over-expressed only in HIV negative FSGS but not in HIVAN (Figure 17). Primers for all nine genes were designed using the Integrated DNA Technologies Primer Quest design tool and purchased (Whitehead Scientific) for use in qPCR experiments to elucidate the effect of HIV-1 infection on expression of these genes and to validate the arrays results.

Real-time quantitative PCR results of genes that were altered in HIVAN as compared to HIV negative FSGS confirmed the mRNA expression patterns though some discrepancies were observed (Figure 18). *CCL4* was only over-expressed in HIV negative FSGS and attenuated in HIVAN and MCD, relative to the healthy control. Comparing expression levels between groups, we discovered that *CCL4* expression patterns were not significantly different in all 4 groups. *CXCL12* was down-regulated across all proteinuric states and the difference was not statistically significant between the proteinuric states (Table 18). However, *CXCL12* expression levels were significantly down-regulated in all three proteinuric kidney disease states as compared to healthy controls; *p-values* between 0.0060 and 0.0286. *SLPI* levels were only up-regulated in MCD and down-regulated in HIV negative FSGS and HIVAN. Expression of SLPI was only significantly decreased in HIVAN and FSGS when compared to MCD but not the healthy controls (Table 18).

Real-time quantitative PCR results of genes that were altered in HIVAN and HIV negative FSGS as compared to the healthy controls revealed that mRNA expression levels of *CDKN1A*, *SERPINA1* and *TNFSF10* were down-regulated in all proteinuric states as compared to the healthy controls (Figure 19). *CCL3* was down-regulated in MCD only and over-expressed in HIVAN and HIV negative FSGS. Statistically significantly decreased expression of *CCL3* and *CDKN1A* was only observed between healthy controls and MCD groups, *p-value* 0.0286. Expression level of *STAT1* was moderately up-regulated in HIVAN and HIV negative FSGS. Expression of *TNFSF10* in MCD was significantly reduced relative to the healthy control (*p-value* 0.0286). *TGF-β1* was significantly over-expressed in FSGS as compared to MCD and comparable between FSGS and the healthy controls (Table 19).

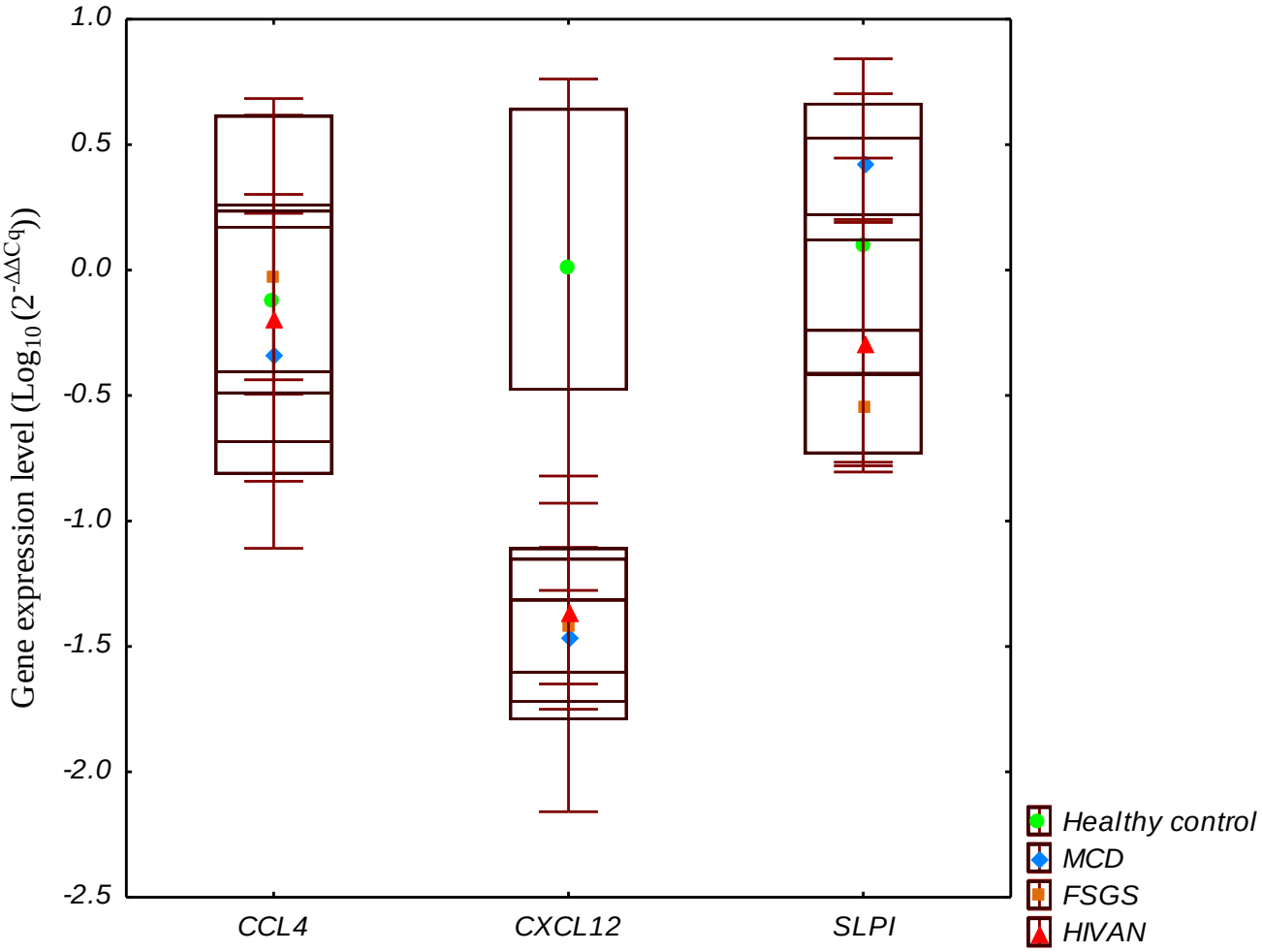

Figure 18: mRNA expression patterns of altered *CCL4*, *CXCL12* and *SLPI* from HIV-1 host response panel of arrays

Box-Whisker plots were constructed using Kruskal-Wallis ANOVA median values of qPCR results represented as Log_{10} ($2^{-\Delta\Delta Cq}$) of each experimental groups. *CCL4* and *SLPI* were overexpressed in all proteinuric states as compared to the healthy controls. Primers were designed based on intercalating dye (SYBR green) and mRNA transcripts of the Homo sapiens *CCL4*, *CXCL12* and *SLPI*. qPCR experiments were normalized against three reference genes, i.e., *RPL13A*, *SDHA* and *YWHAZ*. Primers were designed and ordered from Integrated DNA Technologies (Whitehead Scientific). Statistical analysis of data and graphs were plotted using Statistica12.5.192.5 analysis software (StatSoft).

Table 18: Comparison of qPCR expression patterns of CCL4, CXCL12 and SLPI genes in proteinuric kidney diseases and the healthy controls.

	***p-values* between groups**											
Study group	***CCL4***				***CXCL12***				***SLPI***			
	Normal	**MCD**	**FSGS**	**HIVAN**	**Normal**	**MCD**	**FSGS**	**HIVAN**	**Normal**	**MCD**	**FSGS**	**HIVAN**
Normal	1.0000				1.0000				1.0000			
MCD	0.6286	1.0000			**0.02856***	1.0000			0.4126	1.0000		
FSGS	0.8571	0.6857	1.0000		**0.0060****	0.7878	1.0000		0.3290	**0.0381***	1.0000	
HIVAN	0.9047	0.4762	0.9151	1.0000	**0.0190***	0.7619	0.6282	1.0000	0.2467	**0.0095****	0.4848	1.0000

Mann-Whitney U-test was used to compare two independent groups. Significance at $p < 0.05$. * *p-value* < 0.05; ** *p-value* < 0.01. *CCL4*: Chemokine (C-C Motif) Ligand 4; *CXCL12*: Chemokine (C-X-C Motif) Ligand 12; *SLPI*: Secretory Leukocyte Peptidase Inhibitor; Normal: healthy controls; MCD: minimal change disease; FSGS: focal and segmental glomerulosclerosis; HIVAN: human immunodeficiency virus-associated nephropathy. Normal n= 4; MCD n= 4; FSGS n= 7; HIVAN n=6

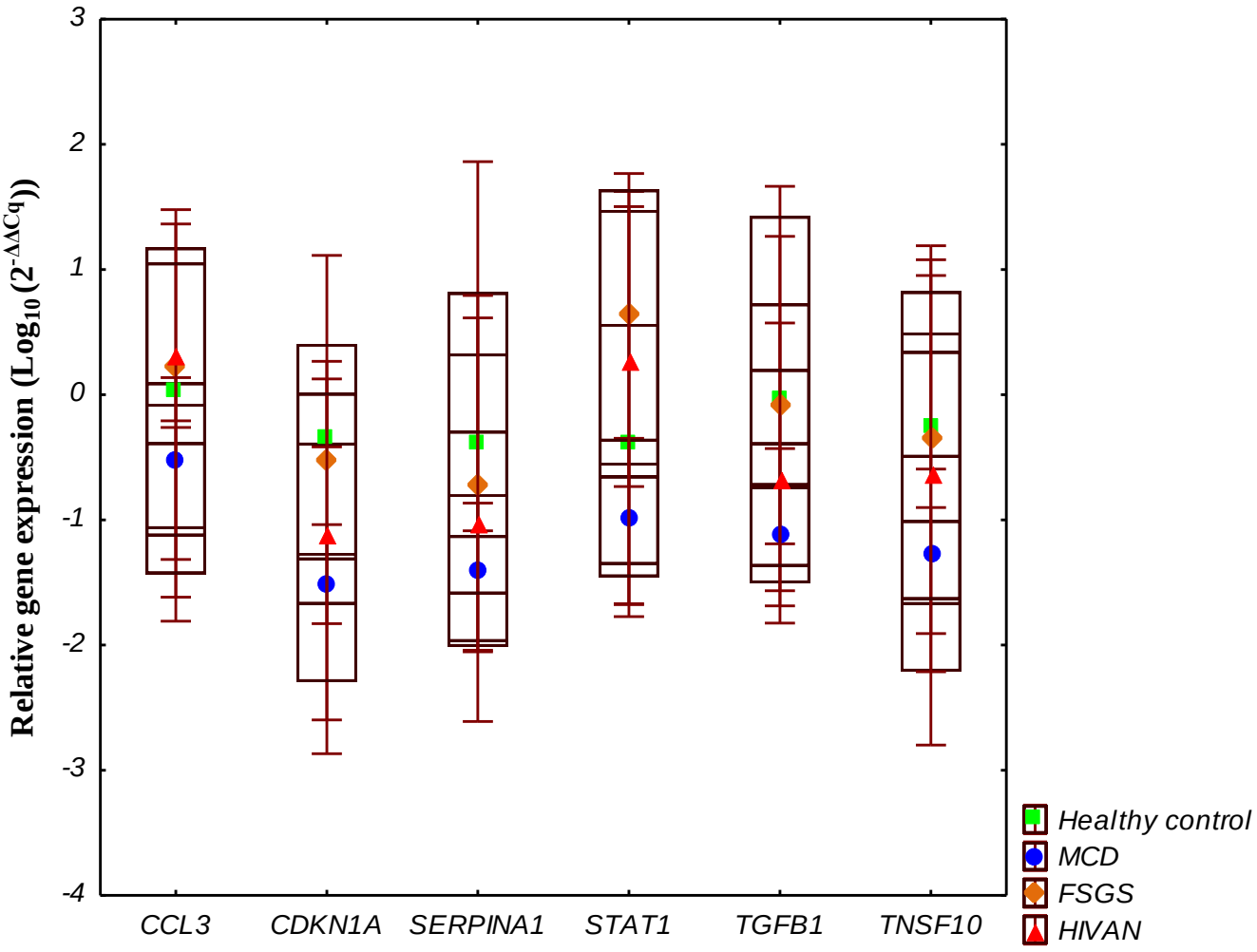

Figure 19: Altered HIV-host response genes in HIVAN and the HIV negative FSGS relative to healthy controls

Box-Whisker plots were constructed using Kruskal-Wallis ANOVA median values of qPCR results represented as Log_{10} ($2^{-\Delta\Delta Cq}$) of each experimental groups. *CCL3* and *STAT1* expression was down-regulated in MCD and up-regulated in HIVAN and HIV negative FSGS. *CDKN1A*, *SERPINA1*, *TGF-β1* and *TNFSF10* were down-regulated in all proteinuric states as compared to the healthy controls. Primers were designed based on intercalating dye (SYBR green) and mRNA transcripts of the *Homo sapiens* genes. qPCR experiments were normalized against three reference genes, i.e., *RPL13A*, *SDHA* and *YWHAZ*. Primers were designed and ordered from Integrated DNA Technologies (Whitehead Scientific). Statistical analysis of data and graphs were plotted using Statistica12.5.192.5 analysis software (StatSoft).

Table 19: Comparison of qPCR expression patterns of HIV-host response genes in proteinuric kidney diseases compared to healthy controls.

Study groups	*p-value* between groups					
	CCL3	***CDKN1A***	***SERPINA1***	***STAT1***	***TGF-β1***	***TNFSF10***
Healthy control vs MCD	**0.0286***	**0.0286***	**0.0286***	**0.0286***	0.2000	**0.0286***
Healthy control vs FSGS	0.4121	0.9272	0.1636	0.1636	0.9272	0.6484
Healthy control vs HIVAN	0.6095	0.0571	**0.0381***	0.4761	0.4762	0.6095
MCD vs FSGS	0.1090	**0.0060****	**0.0060****	0.0727	**0.0424***	0.3151
MCD vs HIVAN	0.6095	0.8571	0.9151	0.6095	0.3523	0.7619
FSGS vs HIVAN	0.7308	**0.0333***	0.2342	0.5338	0.4452	0.8356

Mann-Whitney U-test was used to compare two independent groups. Significantly different mRNA expression in each group is marked: * *p-value* < 0.05; ** *p-value* < 0.01. *CCL3*: Chemokine (C-C motif) ligand 3; *CDKN1A*: Cyclin-dependent kinase inhibitor 1A; *SERPINA1*: Serpin peptidase inhibitor, clade A (alpha-1 antiproteinase, antitrypsin), member 1; *STAT1*: Signal transducer and activator of transcription 1; *TGF-β1*: Transforming growth factor beta; *TNFSF10*: Tumor necrosis factor (ligand) superfamily , member 10; Healthy control: healthy controls; MCD: minimal change disease; FSGS: focal and segmental glomerulosclerosis; HIVAN: human immunodeficiency virus-associated nephropathy. Normal n= 4; MCD n= 4; FSGS n= 7; HIVAN n=6.

3.4.2. Toll-like receptor PCR arrays

Catalogued PCR Arrays used for web-based TLR pathway analysis were PAHS-018Z. In HIVAN, seven genes from the Toll-Like Receptor array were down-regulated and none up-regulated, as compared to the HIV negative FSGS (Figure 20). The down-regulated genes included *HMGB1*, *LY96*, *PELI1*, *SIGIRR*, *MAP3K1*, *MAP4K4* and *MAPK8*. Comparing the expression levels of TLR genes in proteinuric kidney diseases to the healthy controls, we showed that *CCL2* expression was down-regulated in both HIVAN and HIV negative FSGS, whereas REL1 was only up-regulated in HIV negative FSGS (Figure 21). Gene expression patterns were validated using specifically designed primers in real-time quantitative PCR assays and specific antibodies in western-blot experiments.

3.4.2.1. Western-blot validation of altered TLR proteins

To validate protein expression levels of the down-regulated TLR genes in HIVAN relative to HIV negative FSGS, western-blotting techniques were employed. Since most of the genes are involved in the JNK signaling pathway (as outlined in Figure 22), antibodies directed towards these epitopes were purchased (Cell Signaling, Anatech Instruments) and used to detect the amount of JNK and phospho-JNK present in each proteinuric disease state compared to the healthy controls. Western-blotting results were in agreement with the PCR observations, confirming that the JNK proteins are down-regulated in proteinuric kidney diseases, as protein signal was barely detected in MCD, FSGS and HIVAN (Figure 23 A). No phosphorylated JNK was detected in any of the experimental groups, including the healthy non-proteinuric control group (Figure 23 B).

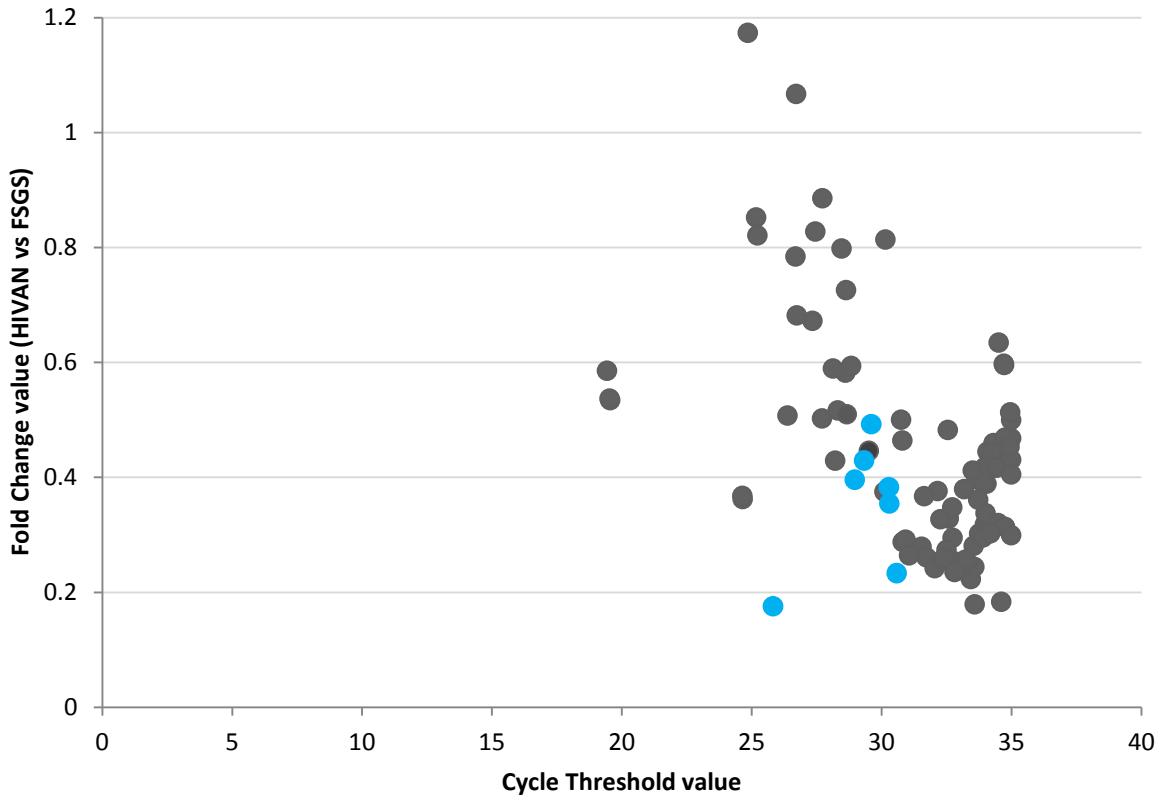

Figure 20: Toll-Like Receptor arrays gene expression pattern of HIVAN vs HIV negative FSGS

Data points with C_q values equal to or higher than the pre-set cycle cut-off point of 35 were considered to be false positives or negative test results and were excluded from downstream processing. Data points with C_q values less than the cycle cut-off point were regarded as positive test results. Positive results were considered significant and eligible for downstream analyses when fold-change value denoted either an up- or down-regulation of the gene. A gene was regarded as either down-regulated or up-regulated when fold-change value was less than 0.51 or greater than 1.9, respectively. Grey dots represent data points that were excluded from downstream processing due to either one (HIVAN or HIV negative FSGS) of the C_q values being a false positive or the fold change value was $0.5 \leq 2.0$. Blue dots denote down-regulated genes. Seven genes were down-regulated in the TLR receptor pathways and none up-regulated. Down-regulated genes included *HMGB1*, *LY96*, *PELI1*, *SIGIRR*, *MAP3K1*, *MAP4K4* and *MAPK8*. Real-time qPCR data was collected from 7500 Real Time PCR System (Applied Biosystems) and analyzed using the 7500 Software v2.0.5 and web-based software package (RT^2 PCR Profiler Array System v4.0 and PAHS-018Z catalogued PCR Arrays, SABiosciences; QIAgen).

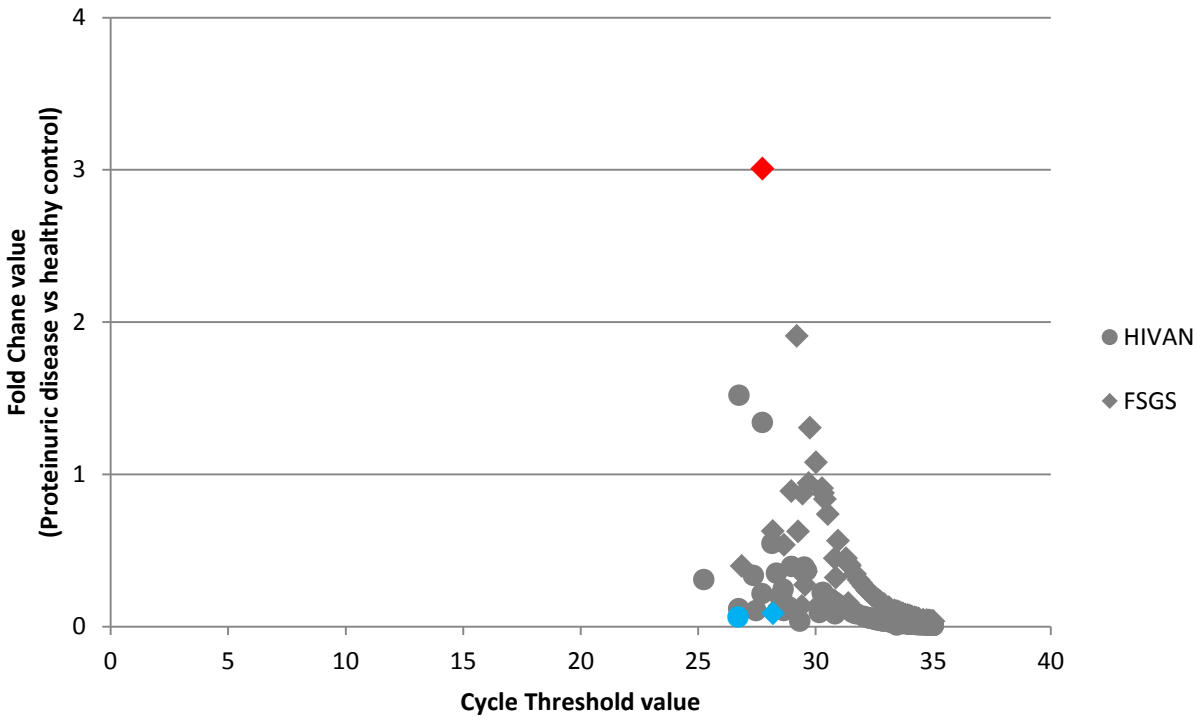

Figure 21: Toll-Like Receptor arrays gene expression pattern in HIVAN and HIV negative FSGS compared to the healthy non-proteinuric controls

A gene was regarded as either down-regulated (blue dots) or up-regulated (red dots) when fold-change value was less than 0.51 or greater than 1.9, respectively. Data points with C_q values less than the cycle cut-off point were regarded as positive outcomes. Positive outcomes were considered significant and eligible for downstream analyses when fold-change value denoted either an up- or down-regulation of the gene expression. Grey dots represent data points that were excluded from downstream processing due to either one (HIV negative FSGS, HIVAN or healthy controls) of the C_q values being a false positive or the fold change value was $0.5 \leq 2.0$. The expression of *CCL2* was down-regulated in both HIVAN and the HIV negative FSGS, whereas REL expression was only up-regulated in the HIV negative FSGS and remained unaltered in HIVAN. Real-time qPCR data was collected from a 7500 Real Time PCR System (Applied Biosystems) and analyzed using the 7500 Software v2.0.5 and web-based software package (RT^2 PCR Profiler Array System v4.0, SABiosciences; QIAgen). For web-based analysis of the HIV Host Response Panel, PAHS-018Z catalogued PCR Arrays were used. Data points for the graph were C_q values obtained from qPCR.

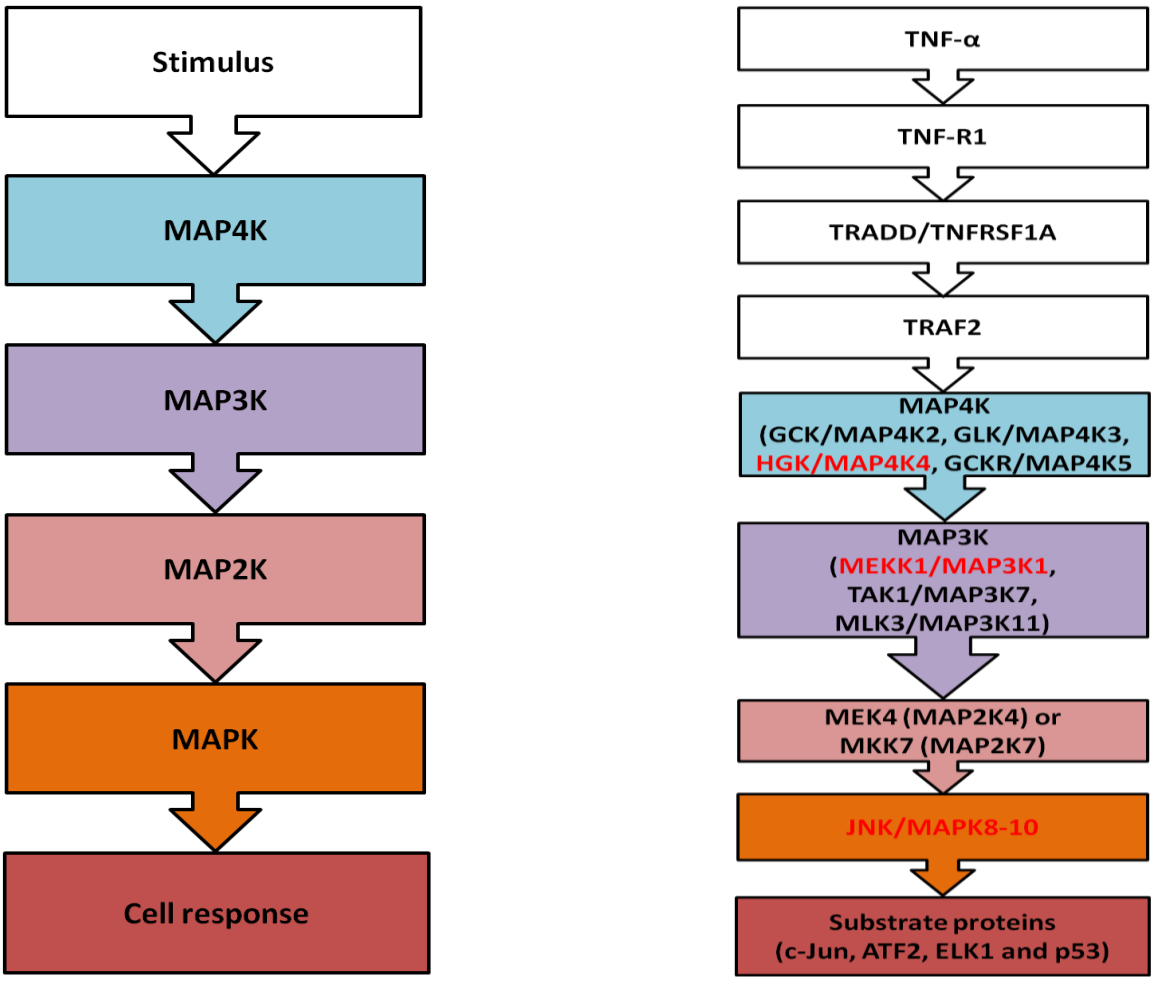

Figure 22: MAPK signaling pathway

MAPK pathways are fundamental components of signal transduction pathways activated by various extracellular and intracellular stimuli. Upon activation, the MAPK signaling pathways activate substrate proteins that regulate a variety of cellular activities such as proliferation, differentiation, survival, and death. **Left panel**: Representation of the MAPK signaling cascade. MAP4K is activated by a stimulus and in turn phosphorylates and activates MAP3K that will phosphorylate and activate MAP2K. MAPK (i.e. ERK, p38 or JNK) activated by phosphorylation on threonine and tyrosine residues by this MAP2K induces cellular response. **Right panel**: TNF-α-mediated JNK signaling pathway. Three of the genes that were perturbed (in red font) by HIV infection in the TLR arrays are associated with the MAPK signaling cascade, particularly the JNK pathway. Activation of the JNK pathway is primarily mediated by cytokines, i.e., TNF-α.

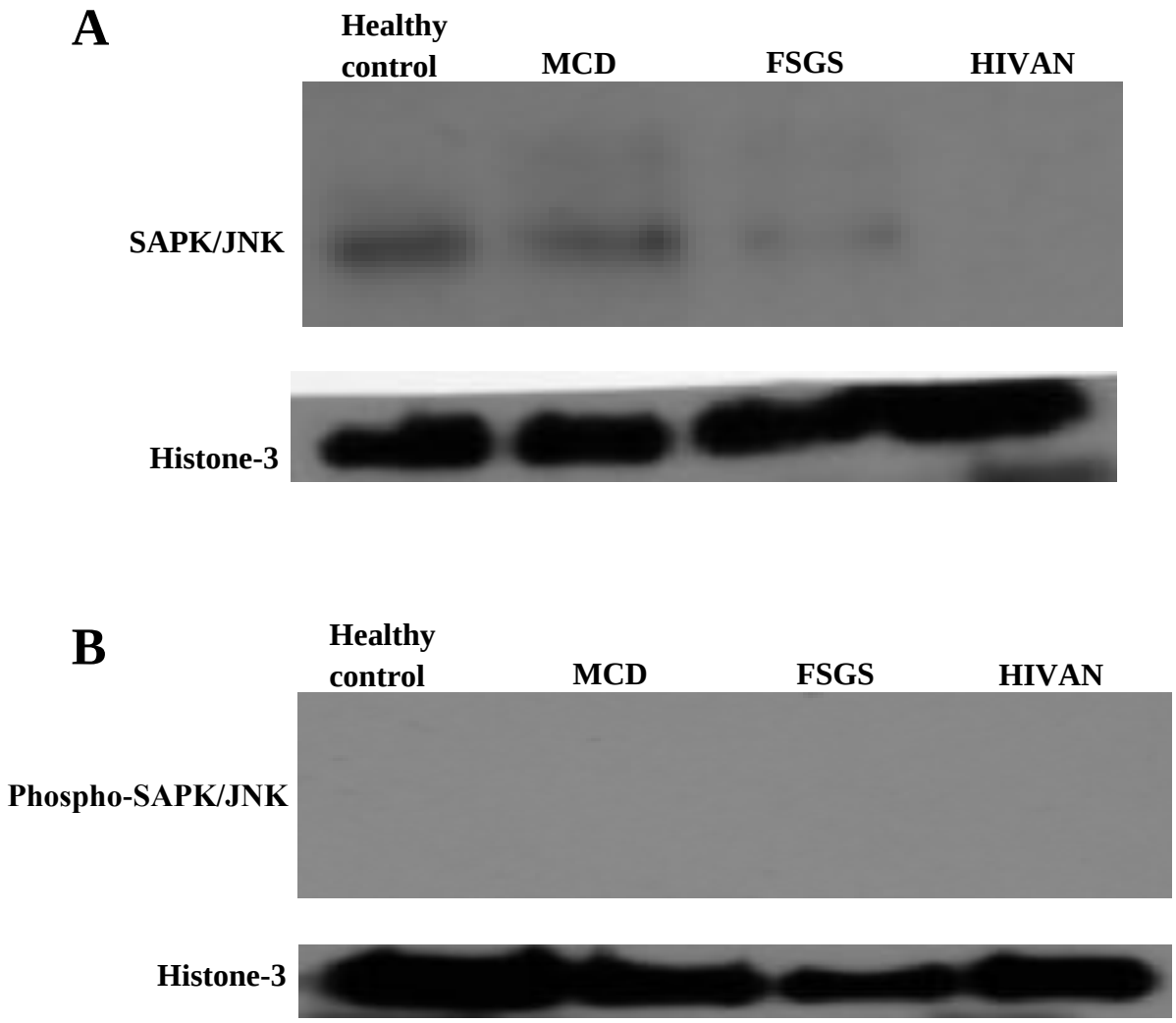

Figure 23: Western-blot analysis of JNK proteins

Expression levels of JNK proteins in proteinuric kidney diseases were assessed relative to healthy non-proteinuric controls. (**A**) SAPK/JNK (47 kDa) expression was down-regulated in proteinuric disease, especially in HIVAN. (**B**) Phospho-SAPK/JNK (T183/Y185) (47 kDa) was not detected in proteinuric kidney disease or in the healthy non-proteinuric control. Each lane of the 10 % SDS-PAGE gel was loaded with 150 µg of total purified protein sample. Proteins were labelled using anti-SAPK/JNK and anti-Phospho-SAPK/JNK (T183/Y185) antibodies, respectively. HRP-conjugated goat anti-rabbit and goat anti-mouse IgG were used to detect SAPK/JNK and Phospho-SAPK/JNK (T183/Y185), respectively. Consistent levels of the loading control, Histone-3, were detected across experimental groups. Histone-3 (18 kDa), was labelled using anti-Histone-3 antibody and detected using goat anti-rabbit HRP-conjugated IgG. All antibodies were prepared in 5 % fat-free milk dissolved in TTBS buffer.

3.4.2.2. qPCR validation of altered TLR genes

When gene expression patterns in proteinuric kidney diseases were compared to the healthy non-proteinuric control, 2 more genes, notably *CCL2* and *REL1*, were revealed to be altered in proteinuric kidney disease. Primers for the altered *CCL2* and *REL1* genes were designed and ordered for use in real-time quantitative PCR experiments to validate the expression patterns of these genes. Real-time quantitative PCR results confirmed the expression patterns observed from PCR arrays data though some discrepancies were noted. Both CCL2 and REL were up-regulated in FSGS compared to all study groups. CCL2 expression was attenuated in HIVAN but not in HIV negative FSGS, as compared to the healthy non-proteinuric controls. REL1 levels were attenuated in HIVAN and enhanced in HIV negative FSGS, relative to the healthy non-proteinuric controls (Figure 24). However, the difference was not statistically significant. Of the three proteinuric states investigated, MCD is the only one that showed significantly attenuated expression levels of CCL2 while HIVAN and the HIV negative FSGS were slightly moderated (Table 20).

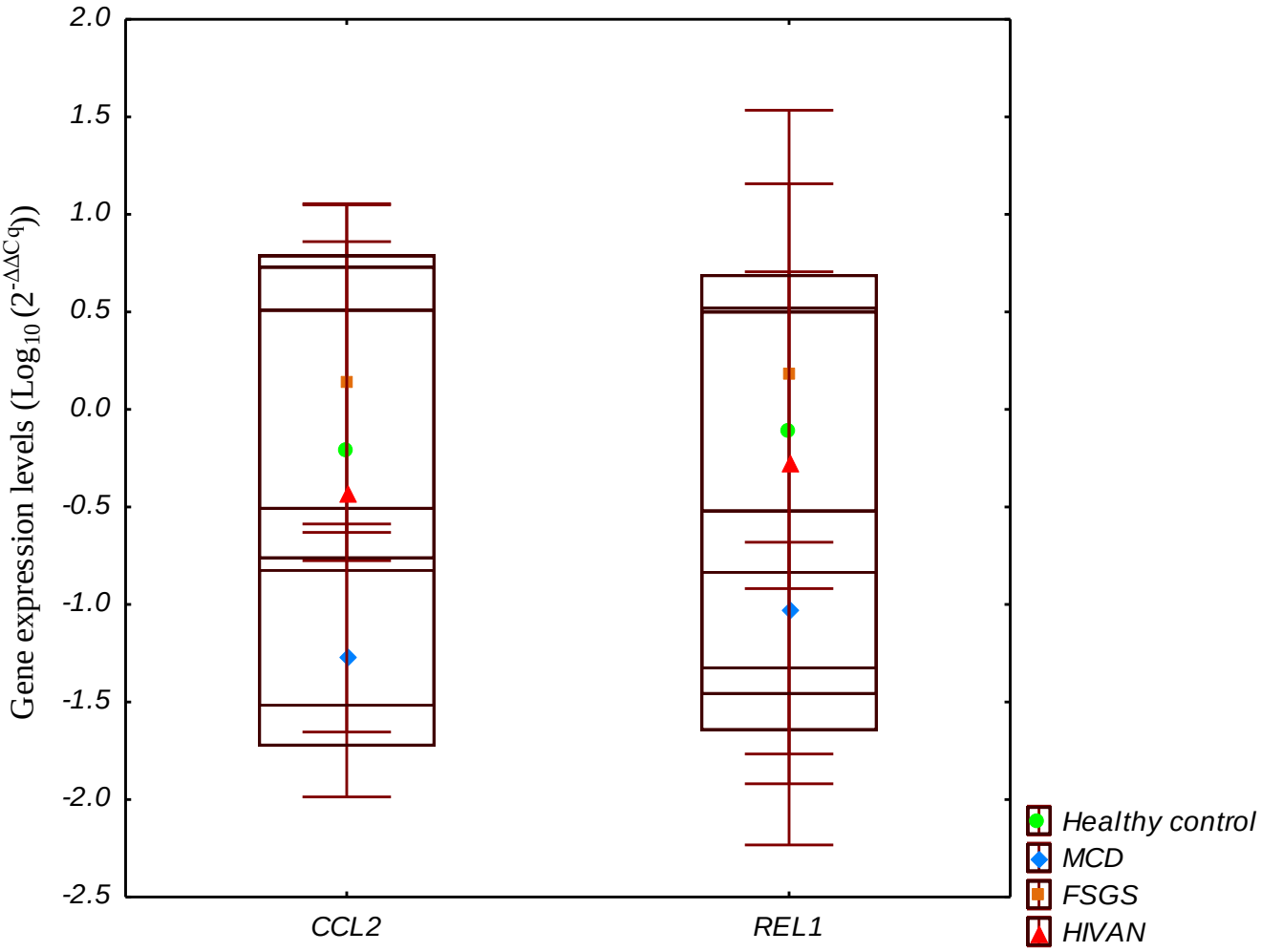

Figure 24: mRNA expression of altered TLR array genes in HIVAN and HIV negative FSGS relative to the healthy control.

Box-Whisker plots were constructed using Kruskal-Wallis ANOVA median values of qPCR results represented as Log_{10} ($2^{-\Delta\Delta Cq}$) of each experimental groups. CCL2 was down-regulated in MCD and HIVAN, significantly so in MCD, and over-expressed in HIV negative FSGS. *REL1* was only overexpressed in FSGS and down-regulated in MCD and HIVAN as compared to the healthy non-proteinuric control. Primers were designed based on intercalating dye (SYBR green) and mRNA transcripts of the *Homo sapiens* genes. qPCR experiments were normalized against three reference genes, i.e., *RPL13A*, *SDHA* and *YWHAZ*. Primers were designed and ordered from Integrated DNA Technologies (Whitehead Scientific). Statistical analysis of data and graphs were plotted using Statistica12.5.192.5 analysis software (StatSoft).

Table 20: Comparison of qPCR expression patterns of *CCL2* and *REL1* genes was assessed.

Study group	***p-value* between groups**							
	CCL2				***REL1***			
	Normal	**MCD**	**FSGS**	**HIVAN**	**Normal**	**MCD**	**FSGS**	**HIVAN**
Normal	1.0000				1.0000			
MCD	0.0571	1.0000			0.0571	1.0000		
FSGS	0.6484	**0.0242***	1.0000		0.9247	0.1636	1.0000	
HIVAN	0.6095	0.4762	0.1806	1.0000	0.6095	0.6095	0.9452	1.0000

Mann-Whitney U-test was used to compare two independent groups. Significance at $p < 0.05$. * *p-value* < 0.05; ** *p-value* < 0.01; *CCL2*: Chemokine (C-C Motif) Ligand 2; *REL1*: V-rel reticuloendotheliosis viral oncogene homolog (avian); Normal: healthy non-proteinuric control; MCD: minimal change disease; FSGS: focal and segmental glomerulosclerosis; HIVAN: human immunodeficiency virus-associated nephropathy. Normal n= 4; MCD n= 4; FSGS n= 7; HIVAN n=6

4. DISCUSSION

Dynamin localization in the kidney

In the current study, HIVAN and HIV negative FSGS biopsies presented with over 70 % of glomeruli collapsed and sclerosed in the analyzed tissue sections. Sclerosis and collapse of the glomerular tufts made it difficult to precisely determine the exact location of the immunolabelled proteins, i.e., cathepsin-L and dynamin, in these patients. In the glomeruli, dynamin plays a pivotal role in aiding the podocytes to maintain the filtration barrier through regulation of the actin-based cytoskeleton. Server *et al*., (2007) showed that dynamin serves as a substrate for cathepsin-L in the kidneys and it is susceptible to catabolism in proteinuric kidney diseases. Thus, dynamin was recognized as a critical regulator of the filtration barrier permselectivity. this study showed that dynamin levels remained unchanged in all three proteinuric states. However, dynamin 1 expression levels were in contrast with these findings. We showed that dynamin 1 levels were markedly enhanced in the renal tubules and glomeruli of HIVAN and MCD patients relative to the healthy controls. This suggested that the proteinuria detected in these proteinuric groups was not attributable to cleaved dynamin in the glomeruli. Discrepancies in dynamin localization were validated by comparing these proteinuric disease groups, histologically characterized by marked scarring (sclerosis) of the glomeruli, to other proteinuric disease states of different pathology. Significant amounts of dynamin were detected in FSGS and HIVAN populations but not in MCD and healthy controls. Dynamin is a positively charged protein, with affinity for negatively charged molecules (Hinshaw, 2000; McMahon and Gallop, 2005). Negatively charged dynamin species are unable to form necessary protein interactions that are crucial for dynamin action, i.e., maintaining the cytoskeleton integrity in this instance. An earlier study by Server *et al*., (2007) assessed the effects of a negatively charged dynamin mutants in proteinuria manifestation *in vivo* and *in vitro* using mice models and cultured podocytes, respectively. This study reported that expression of predominantly negative dynamin constructs caused podocyte injury through cytoskeleton reorganization and podocyte cell shape changes that altered podocyte function. These led us to postulate that proteinuria observed in the FSGS and HIVAN groups, in the current study, was due to severe podocyte injury that was demonstrated by the accumulation of predominantly negatively charged dynamin species expressed in the severe kidney disease patients.

Cathepsin-L localization in the kidney

The feasibility of cathepsins as a diagnostic tool was evaluated and revealed that serum levels of cathepsin-L may serve as a biomarker in the diagnosis of cardiac fibrosis, coronary artery disease and renal dysfunction (Liu *et al*., 2006; Bauer *et al*., 2011). Both *in vitro* and *in vivo* experiments have showed that serum cystatin-C and cathepsin-L are sensitive predictors of potential kidney injury and that increased urinary cathepsin-B levels are associated with membranous glomerulonephritis (Senatorski *et al*., 1998; Bauer *et al*., 2011; Takeuchi *et al*., 2011). Furthermore, increased levels of cathepsins-L and -S in proximal tubules and podocytes were shown to be indicative of proteinuric kidney disease (Rajashree *et al*., 1996; Schaefer *et al*., 1996). Similarly, this current study revealed that localization of renal cathepsin-L was significantly increased in FSGS and HIVAN relative to healthy controls. To elaborate on these observations, a group of proteinuric kidney disease patients, with intact glomeruli on light microscopy (absence of glomerular lesions or no sign of global sclerosis i.e., MCD) was assessed. Using immunohistochemistry, the minimal change disease population showed marker localization comparable to those reported for healthy non-proteinuric controls. In addition, as expected, renal function (blood urea and creatinine levels) in the majority of MCD patients was within the normal range. Although similar amounts of proteinuria were detected in all three proteinuric disease groups, there were major differences observed in renal function. HIVAN patients had severe renal dysfunction (over 5- and 3-folds increase in urea and creatinine levels) relative to MCD and FSGS patients, respectively (data not shown). Higher levels of cathepsin-L in proteinuric diseases are implicated in the collapse of the glomerular tuft observed HIVAN and HIV negative FSGS groups. These observations suggest that the proteinuria in HIVAN and HIV negative FSGS patients is due to collapse of the actin cytoskeleton, due to severe podocyte and glomerular disease and is associated with the up-regulated levels of glomerular cathepsin-L.

Cathepsin-L and dynamin expression levels in renal tissue

Over-expression of renal cathepsin-L is reported to be an indicator of podocyte injury, characterized by compromised actin-based cytoskeleton integrity and foot process effacement, as observed in proteinuric kidney diseases. Server *et al*., (2007) reported that dynamin serves as a substrate for cathepsin-L in kidneys and it is cleaved in proteinuric

kidney diseases. Cleavage of dynamin resulted from over-expressed renal cathepsin-L and led to attenuated levels of dynamin. In an effort to demonstrate how HIV infection compromises the actin cytoskeleton through down-regulation of the vitamin D receptor, Chandel *et al*., (2013) showed how podocytes lacking cathepsin-L presented with enhanced dynamin expression, whereas HIV-transduced podocytes expressing cathepsin-L displayed down-regulation of dynamin. The latter study further reported that HIV infection enhanced angiotensin II production thereby mediating podocyte injury through the renin-angiotensin system. Down-regulation of the vitamin D receptor by HIV activates the renin-angiotensin II system, thus inducing cathepsin-L over-expression which results in proteolyzed and down-regulated dynamin. This current study showed downregulated expression of cathepsin-L 1 in FSGS and HIVAN relative to MCD and normal tissue with cathepsin –L 2 and 3 remaining relatively unchanged. These findings report on the differential expression of the cathepsin-L in the various disease entities with the dynamin expression pattern remaining unchanged. These results elude to the important role that post-translational modification plays in the regulation of the cathepsin L1 in kidney disease since the expression at the RNA level does not recapitulate the findings at the protein level. Further studies are therefore required using larger sample sizes to validate these findings. Additionally dynamin protein expression needs to be investigated through the implementation of western-blot analysis. Most importantly the regulation of cathepsin-L expression during the development of proteinuria in kidney diasease needs to be elucidated.

Cathepsin-L enzymatic activity in the podocyte cytoskeleton

Although dynamin cleavage by enhanced cathespsin-L expression is the prevalent predictor of podocyte injury in proteinuric kidney diseases, studies have revealed that dynamin is not the sole substrate for cathepsin-L activity and that proteolysis of either of the other two substrates, i.e., synaptopodin and CD2AP, were also indicative of podocyte injury (Server *et al*., 2007; Faul *et al*., 2008; Yaddanapudi *et al*., 2011; Altintas *et al*., 2014). Interestingly, the present study demonstrated that dynamin 2 expression was barely altered across proteinuric states, compared to the healthy non-proteinuric controls. This implies that proteolysis of the actin-associated protein synaptopodin and/or slit diaphragm-associated CD2AP by the seemingly over-expressed cathepsin-L 1 and 3 was responsible for the proteinuria in FSGS, HIVAN and MCD. In FSGS, expression of all 3 isoforms of dynamin were marginally altered compared to the healthy non-proteinuric controls, pointing out that FSGS is not mediated by

dynamin cleavage but manifests through the apparently over-expressed cathepsin-L 3 cleavage of other substrates. For this reason, our study further assessed expression patterns of other documented cytoskeleton-associated gene products, i.e., CD2AP, nephrin, podocin and synaptopodin. In lipid rafts of the actin-based podocyte cytoskeleton, nephrin, a surface receptor transmitting extracellular signals from the slit diaphragm to the podocyte cytoskeketon, interacts with podocin and CD2AP. This protein association promotes nephrin signaling, and CD2AP binding anchors nephrin and podocin to the actin filaments, thus maintaining the structural and functional integrity of the slit diaphragm (Shih *et al*., 1999; Schwarz *et al*., 2001; Tryggvason *et al*., 2006b). CD2AP-deficient mice over-express TGF-β1, consequently, increasing cathepsin-L levels in glomerular podocytes (Woroniecki *et al*., 2006; Asanuma *et al*., 2007; Yaddanapudi *et al*., 2011). In line with these reports, the current study showed that CD2AP expression levels were down-regulated in all 3 studied proteinuric groups. Interestingly, the attenuated CD2AP mRNA levels were complemented by significantly down-regulated nephrin and podocin expression. This implicated the loss of structural integrity of the cytoskeleton manifested as the proteinuria observed in our study groups. However, the expression of TGF-β1 appeared to be up-regulated only in FSGS and attenuated in HIVAN and MCD. Together with the dynamin expression results, these results imply that FSGS manifests through the attenuated CD2AP, up-regulated TGF-β1 and cathepsin-L activity and not via dynamin degradation.

When assessing another cathepsin-L substrate, synaptopodin, our study showed that similarly to CD2AP, the expression of synaptopodin at transcriptional level is also down-regulated in all 3 studied proteinuric groups. Synaptopodin binds F-actinin and α-actin in the podocyte cytoskeleton, and thus regulates synaptic plasticity of the cytoskeketon. Attenuation of synaptopodin has been linked to impaired actin filament reformation (Yamazaki *et al*., 2001; Asanuma *et al*., 2005). Collectively, the attenuated mRNA expression levels of dynamin, CD2AP and synaptopodin in renal tissues of the three proteinuric groups validate that podocyte injury, in the form of loss of foot process integrity and slit diaphragm permeability, is caused by the over-expressed cathepsin-L enzymatic activity.

Altered host genes and pathways

HIV-1 infection of host cell is initiated by sequential binding of the viral gp120 to the host receptor, CD4, and chemokine co-receptors, CCR5 or CXCR4. Viral infectivity is hindered through binding of the chemokine gene products, CCL4 and CXCL12, to the co-receptors, CCR5 and CXCR4, respectively. Interestingly, our study showed that the expression pattern of chemokine genes, *CCL4* and *CXCL12*, is altered following HIV-1 infection in proteinuric kidney diseases. HIV-1 infection induced up-regulation and down-regulation of CCL4 and CXCL12, respectively. Up-regulation of CCL4 indicates that the immune response induced enhanced expression of this product to curb infection of nascent cells by the virus. Significant amounts of CCL4 in the host's system may imply that the majority of CCR5 co-receptors are bound by this protein, rendering the co-receptors inaccessible to viral gp120. Thus, CCR5-mediated entry of HIV into target CD4+ T cells was hampered. However, the observed down-regulation of CXCL12 suggested that a significant amount of CXCR4 was unbound and available to initiate viral infection of the host cell through these receptors. We recommend future studies to assess viral tropism in this regard.

HIV-1 infection of the cell results in reverse-transcription complex formation in which viral nucleic acids are synthesized. Synthesis and translocation of viral nucleic acids from cell membrane to the nucleus require cellular activation that is mediated by a virion-associated kinase (McCune, 1995). MAP kinases exist in all cell types and play a crucial role in regulating cell proliferation and differentiation (i.e., cell cycle, generation of phospholipid messenger, transcription and translation) in response to stimuli. MAPKs have been shown to play a role in regulating HIV-1 replication and infectivity through phosphorylation of viral proteins on threonine and serine residues (Yang and Gabuzda, 1999). Of the three MAPK pathways, notably JNK, p38, and extracellular signal-regulated kinase (ERK), the latter has been described as the HIV-1-associated kinase (Jacqué *et al*., 1998). Activation of the ERK MAPK signaling pathway activates HIV-1 replication and thus, modulates viral infectivity (Jacqué *et al*., 1998; Yang and Gabuzda, 1999). In contrast to these reports, our study showed that a number of genes whose expression was perturbed following HIV-1 infection in kidney diseases form part of the JNK and not the ERK cellular signaling pathway. Our study reports that mRNA transcriptional levels, determined using real-time quantitative PCR arrays, together with the protein expression levels, determined using western-blot experiments,

showed that *MAP3K1*, *MAP4K4* and *MAPK8* together with the two regulators of activaton of the JNK pathway, i.e., *PELI1* and *TNFSF10*, were down-regulated in the three proteinuric kidney diseases relative to the healthy non-proteinuric controls. SAPK/JNK was down-regulated in all proteinuric states relative to the healthy controls and the phospho-SAPK/JNK was not detected in any of the groups. He *et al*., (2004) showed that expression of the HIV-1 *nef* gene in podocytes phosphorylates and activates MAPK 1 and 2 via the Ras-c-Raf-MAPK pathway, leading to podocyte phenotypic changes. In contrast, our study showed that the MAPK pathway is down-regulated in HIVAN relative to the HIV negative FSGS. This predicted that the phosphorylation of the MAPK pathway was also decreased in HIVAN. However, the lack of phosphorylated SAPK/JNK protein in the current study, including in the healthy non-proteinuric control group, could be attributed to the use of FFPE biopsy specimens for protein extraction. Future studies are recommended to extract protein from fresh frozen renal cores to reduce variability. The dysregulation of the JNK pathway implies that in the presence of HIV, proteinuric kidney patients would be more susceptible to cancer development due to the lack of apoptotic factors. However, HIVAN patients do not live long if untreated. Ross *et al*., (2005) showed evidence for the role of NF-κB in Fas-mediated apoptosis in HIVAN. Further studies probing apoptotic gene expression will be beneficial in providing additional insight and validating these hypotheses in HIVAN and other proteinuric kidney diseases.

The ubiquitous SLPI principally functions as a protector of local tissue against degradation caused by inflammation. The enzyme also plays a major role in apoptosis and wound healing (Ashcroft *et al*., 2000; Odaka *et al*., 2003). SLPI has been profiled for its anti-fungal, anti-bacterial, anti-protease, anti-inflammatory and anti-viral efficacies (Eisenberg *et al*., 1990; Tomee *et al*., 1998; McNeely *et al*., 1995; Shugars, 1999; Hiemstra, 1999; Fahey and Wira, 2002; Challacombe and Sweet, 2002). The latter has been thoroughly investigated in HIV-1 but no activity against other retroviruses has been reported. The anti-HIV-1 activity of SLPI was demonstrated in monocytes and non-macrophage cells (McNeely *et al*., 1995; Shugars *et al*., 1997). SLPI is proposed to be the key inhibiting agent of HIV-1 transmission through oral secretions (Shugars *et al*., 1999; Chattopadhyay *et al*., 2004). Of the various innate inhibitory molecules, i.e., mucins, antibodies and thrombospodins, found in the saliva, SLPI was the most potent antiretroviral agent at physiological concentrations (McNeely *et al*., 1995). Similarly to the chemokine gene products, CCL4 and CXCL12, SLPI mechanism of HIV-1 acquisition inhibition involves the target host cell rather than the virus. This multifaceted

protein is also used as a biomarker in monitoring the progress of an infection or a malignant lesion and detection thereof is correlated with poor prognosis (Garver *et al*., 1994; Westin *et al*., 2002). Comparing *SLPI* gene expression in HIVAN to non-HIV FSGS patients, our study showed that HIV-1 infection increases expression of *SLPI* in kidney disease patients. SLPI levels were increased in HIVAN and decreased in HIV negative FSGS relative to the healthy non-proteinuric controls. Up-regulation of *SLPI* levels in this regard may be attributed to the compromised immunity following HIV-1 infection in proteinuric kidney diseases.

Interleukin-1 receptors and TLRs play a central role in innate immunity and inflammation by activating signaling pathways that induce activation of transcription factors associated with specific cellular responses. TLRs are pattern recognition receptors that bind conserved structural molecules found in large groups of pathogens, called pathogen-associated molecular patterns, and of necrotic cell-derived danger signals (Medzhitov and Janeway, 1997; Cavassani *et al*., 2008). Interleukin-1 receptor- and TLR-mediated signaling activate a variety of NF-κB-related genes that would in turn induce inflammatory responses in various organs (Medzhitov *et al*., 1997; Rock *et al*., 1998). Expression of these genes is often dysregulated in pathological conditions (Bsibsi *et al*., 2002; Sundstrom *et al*., 2004; Jung *et al*., 2005). Comparing gene expression levels in HIVAN to non-HIV FSGS, our study showed that expression of *CCL2*, *CCL3*, *CDKN1A*, *HMGB1*, *LY96*, *PELI1*, *REL*, *SIGIRR*, *STAT1* and *TGF-β1* immunoregulatory and inflammatory response-genes were down-regulated in the presence of HIV in proteinuric kidney disease. A glycoprotein LY96, also known as myeloid differentiation 2 (MD2), has an MD-2-related lipid-recognition domain that is implicated in the recognition of pathogen-related products, and thus endotoxin neutralization (Shimazu *et al*., 1999; Inohara and Nunez, 2002). The protein plays a fundamental role as an accessory protein of the TLR4 during LPS-mediated inflammatory responses through association with the ectodomain of TLR4 (Shimazu *et al*., 1999; Nagai *et al*., 2002). TLR4 signalling relies on this association to initiate a MyD88-dependent signalling cascade. Inhibition of this association by mutations on the LY96 sequence or peptides that compete for the LY96 or LPS binding significantly attenuates TLR4 signalling (Visintin *et al*., 2003; Nishitani *et al*., 2006; Schnabl *et al*., 2008). TLR4-LY96 complex is involved in the hyperactivation and dysregulation of the immune system in HIV-1-infected patients through interaction with the *tat* protein of the virus to induce proinflammatory and immunosuppressive cytokines, TNF-α, and IL-10, respectively (Ben Haij *et al*., 2013).

Activation of TLRs triggers HIV-1 replication in latently infected mast cells (Sundstrom *et al*., 2004). LY96 is also involved in the pathogenesis of chronic pain, sepsis and tumors (DeLeo *et al*., 2004; Leon *et al*., 2008; Grondin *et al*., 2011). Pellino 1 protein, encoded by the *PELI1* gene, is a vital component in the TLR- and interleukin-1 receptor-mediated signalling cascade (Moynagh, 2009). It regulates the TLR signalling by inducing degradation of Traf3 (TNF receptor-associated factor 3) and thus, MAPK activation. A single nucleotide polymorphism in the *PELI1* gene was reported to be a genetic risk factor in the pathogenesis of Kawasaki disease and coronary artery lesions in children (Kim *et al*., 2011). Elsewhere, Xiao *et al*., (2013) reported on PELI1 as a mediator for autoimmune neuroinflammation in glial cells. *HMGB1* and *SIGIRR* are ubiquitously expressed in all cells and have versatile functions. The former is well documented as a mediator of immune and inflammatory responses (Lotze and Tracey, 2005; Andersson and Tracey, 2011; Harris *et al*., 2012). This gene plays a pivotal role in a variety of host's inflammatory responses upon infection or toxic stress through the activation of cell surface innate immune receptors (Lotze and Tracey, 2005). A study investigating how HMGB1 contributes to protective or pathological responses, using mice models, reported that *HMGB1*-deficient mice are prone to macrophage cell death following endotoxin shock relative to the controls (Yanai *et al*., 2013). A recent study showed how the anti-cancer activity of TNFSF10 is induced through the suppression of the PARP1-HMGB1 pathway (Yang *et al*., 2015). Uncontrolled activation and induction of immunity and inflammatory responses by TLRs and interleukin-1 receptors through signaling cascades is potentially harmful to the host. Thus, it is tightly regulated at various stages by receptor antagonists, decoy receptors and miRNAs to prevent possible tissue damage and acute or chronic inflammatory disorders (Mantovani *et al*., 2001; Kobayashi *et al*., 2002; Janssens *et al*., 2003). SIGIRR functions as a negative regulator of inflammatory responses through maintaining a balance between activation and inhibition of the innate immune response in various organs (Liew *et al*., 2005). Attenuation of *SIGIRR* enhances LPS-induced inflammatory responses whereas over-expression hampers these responses through inhibition of the TLR-induced NF-κB activation (Qin *et al*., 2005; Lech *et al*., 2007). Collectively, our findings suggest that uncontrolled activation and induction of immunity and inflammatory responses, demonstrated by down-regulated *SIGIRR*, together with the decrease in expression levels of the inflammatory response genes detected following HIV infection, are responsible for the weakened host immunity, resulting in the severe renal lesions observed in HIVAN. These results demonstrate that HIV-1 infection modulates expression patterns of the genes that are involved in immunity and inflammatory responses in proteinuric kidney disease,

compromising the structure and function not only of the kidney but of the entire immune system. These findings indicate that TLR-mediated gene expression pattern changes significantly contribute to the development and pathogenesis of HIV-associated nephropathy.

Concluding remarks

Renal cathepsin-L, notably isoform 3, expression in the tubules and glomeruli is enhanced in proteinuric kidney diseases, thereby compromising integrity of the actin cytoskeleton, represented by loss of foot process integrity and slit diaphragm permeability, through cleavage of either of the substrates, i.e., dynamin, CD2AP and synaptopodin. Our study also showed that a number of genes, whose expression was perturbed following HIV-1 infection in the proteinuric kidney diseases, form part of the immunity and inflammatory responses and the JNK cellular signaling pathway. Our findings suggest that a decrease in expression levels of the inflammatory genes detected following HIV infection in proteinuric kidney diseases is responsible for the weakened host immunity resulting in the severe renal pathology as observed in HIVAN. These results demonstrate that HIV-1 infection modulates expression patterns of the genes that are involved in immunity and inflammatory responses in proteinuric kidney disease, thereby compromising the structure and function not only of the kidney but of the entire immune system. We report that TLR-mediated gene expression pattern changes significantly contribute to the development and pathogenesis of HIV-associated nephropathy. Our study postulates the mechanism outlined in Figure 25 in the pathogenesis of HIVAN.

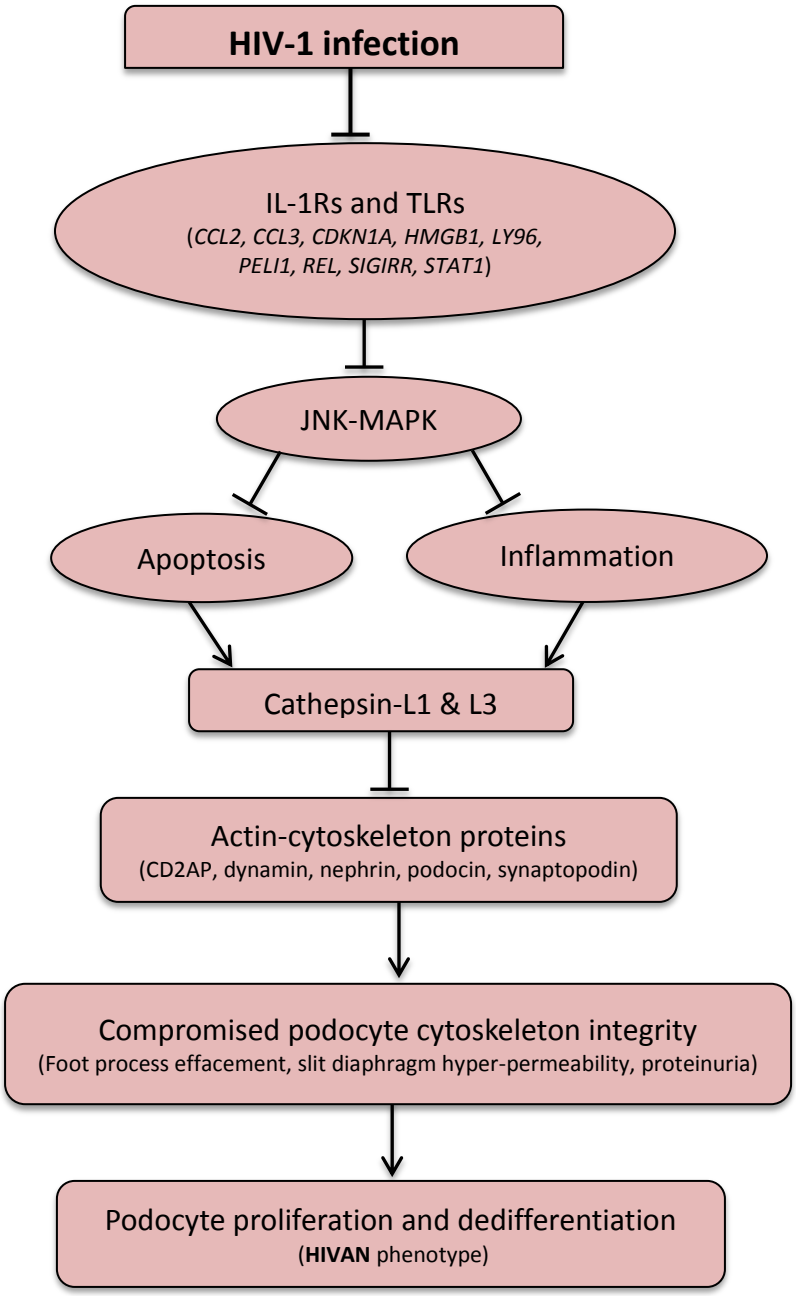

Figure 25: Gene expression pattern changes in HIV-1-associated kidney disease

Interleukin-1 receptor- and TLR-mediated signaling activates a variety of NF-κB-related genes that would in turn induce inflammatory responses. However, this signaling cascade is dysregulated in disease states. HIV-1 infection attenuates expression levels of innate immunity and inflammatory response mediators, consequently leading to podocyte proliferation and dedifferentiation, characteristic of the HIVAN pathology.

Study limitations and future work

Some PCR array data were not correlated in real-time qPCR experiments. The discrepancies observed between the PCR array data and the qPCR validation results may be attributed to the various reference genes that were used for normalization. Our study employed three kidney specific reference genes whereas PCR array data analysis may be using various ones that are not kidney specific. Additionally, the study was based on a relatively small sample size and the results on which the conclusions were drawn were interpreted based on the trends observed from Box-Whisker plots of median values of Log_{10} ($2^{-\Delta\Delta Cq}$) of each of the experimental groups as determined from the Kruskal-Wallis ANOVA test. We recommend that further studies be conducted using larger sample sizes. Dynamin protein expression needs to be correlated using western-blot. Beyond the scope of this degree, phospho-SAPK/JNK western-blot validations have to be performed using fresh tissue or cell culture and not FFPE tissue, as performed in the current study, as phosphorylation is significantly diminished upon tissue fixation.

5. REFERENCES

Addis MF, Tanca A, Pagnozzi D, Crobu S, Fanciulli G, Cossu-Rocca P, Uzzau S: Generation of high-quality protein extracts from formalin-fixed, paraffin-embedded tissues. *Proteomics* 2009; **9**(15):3815-3823.

Altintas MM, Moriwaki K, Wei C, Moller CC, Flesche J, Li J, Yaddanapudi S, Faridi MH, Godel M, Huber TB, Preston RA, Jiang JX, Kerjaschki D, Sever S, Reiser J: Reduction of proteinuria through podocyte alkalinization. *J Biol Chem* 2014; **289**(25):17454-17467.

Andersson U, Tracey KJ: HMGB1 is a therapeutic target for sterile inflammation and infection. *Ann Rev Immunol* 2011; **29**:139-162.

Asanuma K, Mundel P: The role of podocytes in glomerular pathobiology. *Journal of Clinical and Experimental Nephrology* 2003; **7**(4):255-259.

Asanuma K, Kim K, Oh J, Giardino L, Chabanis S, Faul C, Reiser J, Mundel P: Synaptopodin regulates the actin-bundling activity of α-actinin in an isoform-specific manner. *The Journal of Clinical Investigation* 2005; **115**(5):1188-1198.

Asanuma K, Campbell KN, Kim K, Faul C, Mundel P: Nuclear relocation of the nephrin and CD2AP-binding protein dendrin promotes apoptosis of podocytes. *Proceedings of the National Academy of Sciences* 2007; **104**(24):10134-10139.

Ashcroft GS, Lei K, Jin W, Longenecker G, Kulkarni AB, Greenwell-Wild T, Hale-Donze H, McGrady G, Song XY, Wahl SM: Secretory leukocyte protease inhibitor mediates non-redundant functions necessary for normal wound healing. *Nat Med* 2000; **6**(10):1147-1153.

Ballermann BJ: Glomerular endothelial cell differentiation. *Kidney Int* 2005; **67**(5):1668-1671.

Barletta GM, Kovari IA, Verma RK, Kerjaschki D, Holzman LB: Nephrin and Neph1 co-localize at the podocyte foot process intercellular junction and form cis hetero-oligomers. *J Biol Chem* 2003; **278**(21):19266-19271.

Barrett AJ, Kirschke H: Cathepsin B, Cathepsin H, and cathepsin L. *Methods Enzymol* 1981; **80**:535-561.

Barisoni L, Kriz W, Mundel P, D'Agati V: The dysregulated podocyte phenotype: a novel concept in the pathogenesis of collapsing idiopathic focal segmental glomerulosclerosis and HIV-associated nephropathy. *J Am Soc Nephrol* 1999; **10**(1):51-61.

Bauer Y, Hess P, Qiu C, Klenk A, Renault B, Wanner D, Studer R, Killer N, Stalder AK, Stritt M, Strasser DS, Farine H, Kauser K, Clozel M, Fischli W, Nayler O: Identification of cathepsin L as a potential sex-specific biomarker for renal damage. *Hypertension* 2011; **57**(4):795-801.

Ben Haij N, Leghmari K, Planes R, Thieblemont N, Bahraoui E: HIV-1 Tat protein binds to TLR4-MD2 and signals to induce TNF-alpha and IL-10. *Retrovirology* 2013; **10**(123):1742-4690.

Birkeland SA, Lokkegaard H, Storm HH: Cancer risk in patients on dialysis and after renal transplantation: Lancet. 2000 May 27;355(9218):1886-7.

Bourgoignie JJ, Pardo V: The nephropathology in human immunodeficiency virus (HIV-1) infection. *Kidney Int Suppl* 1991; **35**:S19-23.

Boute N, Gribouval O, Roselli S, Benessy F, Lee H, Fuchshuber A, Dahan K, Gubler MC, Niaudet P, Antignac C: NPHS2, encoding the glomerular protein podocin, is mutated in autosomal recessive steroid-resistant nephrotic syndrome. *Nat Genet* 2000; **24**(4):349-354.

Bruggeman LA, Ross MD, Tanji N, Cara A, Dikman S, Gordon RE, Burns GC, D'Agati VD, Winston JA, Klotman ME, Klotman PE: Renal epithelium is a previously unrecognized site of HIV-1 infection. *J Am Soc Nephrol* 2000; **11**(11):2079-2087.

Bruggeman LA, Nelson PJ: Controversies in the pathogenesis of HIV-associated renal diseases. *Nature reviews Nephrology* 2009; **5**(10):574-581.

Bsibsi M, Ravid R, Gveric D, van Noort JM: Broad expression of Toll-like receptors in the human central nervous system. *J Neuropathol Exp Neurol* 2002; **61**(11):1013-1021.

Burns GC, Paul SK, Toth IR, Sivak SL: Effect of angiotensin-converting enzyme inhibition in HIV-associated nephropathy. *J Am Soc Nephrol* 1997; **8**(7):1140-1146.

Burns MJ, Nixon GJ, Foy CA, Harris N: Standardisation of data from real-time quantitative PCR methods - evaluation of outliers and comparison of calibration curves. *BMC Biotechnol* 2005; **5**:31.

Bustin SA, Benes V, Garson JA, Hellemans J, Huggett J, Kubista M, Mueller R, Nolan T, Pfaffl MW, Shipley GL, Vandesompele J, Wittwer CT: The MIQE guidelines: minimum information for publication of quantitative real-time PCR experiments. *Clin Chem* 2009; **55**(4):611-622.

Cantor KP, Weiss SH, Goedert JJ, Battjes RJ: HTLV-I/II seroprevalence and HIV/HTLV coinfection among U.S. intravenous drug users. *J Acquir Immune Defic Syndr* 1991; **4**(5):460-467.

Caridi G, Bertelli R, Scolari F, Sanna-Cherchi S, Di Duca M, Ghiggeri GM: Podocin mutations in sporadic focal-segmental glomerulosclerosis occurring in adulthood: Kidney Int. 2003 Jul;64(1):365.

Cavassani KA, Ishii M, Wen H, Schaller MA, Lincoln PM, Lukacs NW, Hogaboam CM, Kunkel SL: TLR3 is an endogenous sensor of tissue necrosis during acute inflammatory events. *J Exp Med* 2008; **205**(11):2609-2621.

Centers for Disease Control and Prevention, 2014 - http://www.cdc.gov, accessed February 2015.

Challacombe SJ, Sweet SP: Oral mucosal immunity and HIV infection: current status. *Oral Dis* 2002; **2**:55-62.

Chandel N, Sharma B, Husain M, Salhan D, Singh T, Rai P, Mathieson PW, Saleem MA, Malhotra A, Singhal PC: HIV compromises integrity of the podocyte actin cytoskeleton through downregulation of the vitamin D receptor. *Am J Physiol Renal Physiol* 2013; **304**(11):6.

Chapman HA, Jr., Munger JS, Shi GP: The role of thiol proteases in tissue injury and remodeling. *Am J Respir Crit Care Med* 1994; **150**(6 Pt 2):S155-159.

Chattopadhyay A, Gray LR, Patton LL, Caplan DJ, Slade GD, Tien HC, Shugars DC: Salivary secretory leukocyte protease inhibitor and oral candidiasis in human immunodeficiency virus type 1-infected persons. *Infect Immun* 2004; **72**(4):1956-1963.

Chen P, Chen BK, Mosoian A, Hays T, Ross MJ, Klotman PE, Klotman ME: Virological Synapses Allow HIV-1 Uptake and Gene Expression in Renal Tubular Epithelial Cells. *Journal of the American Society of Nephrology : JASN* 2011; **22**(3):496-507.

Cheng XW, Obata K, Kuzuya M, Izawa H, Nakamura K, Asai E, Nagasaka T, Saka M, Kimata T, Noda A, Nagata K, Jin H, Shi GP, Iguchi A, Murohara T, Yokota M: Elastolytic

cathepsin induction/activation system exists in myocardium and is upregulated in hypertensive heart failure. *Hypertension* 2006; **48**(5):979-987.

Chun MJ, Korbet SM, Schwartz MM, Lewis EJ: Focal segmental glomerulosclerosis in nephrotic adults: presentation, prognosis, and response to therapy of the histologic variants. *J Am Soc Nephrol* 2004; **15**(8):2169-2177.

Coffin JM, Hughes SH, Varmus HE, editors. Retroviruses. Cold Spring Harbor (NY): Cold Spring Harbor Laboratory Press; 1997. Virion Proteins. Available from: http://www.ncbi.nlm.nih.gov/books/NBK19464/

Cohen SD, Kimmel PL: Immune complex renal disease and human immunodeficiency virus infection. *Semin Nephrol* 2008; **28**(6):535-544.

Connell BJ, Lortat-Jacob H: Human Immunodeficiency Virus and Heparan Sulfate: from attachment to entry inhibition. *Frontiers in Immunology* 2013; **4**.

Coresh J, Astor BC, Greene T, Eknoyan G, Levey AS: Prevalence of chronic kidney disease and decreased kidney function in the adult US population: Third National Health and Nutrition Examination Survey. *Am J Kidney Dis* 2003; **41**(1):1-12.

Costiniuk CT, Jenabian MA: Cell-to-cell transfer of HIV infection: implications for HIV viral persistence. *J Gen Virol* 2014; **95**(Pt 11):2346-2355.

Crie JS, Morton P, Wildenthal K: Changes in cardiac cathepsin B activity in response to interventions that alter heart size or protein metabolism: comparison with cathepsin D. *J Mol Cell Cardiol* 1983; **15**(8):487-494.

D'Agati VD, Kaskel FJ, Falk RJ: Focal segmental glomerulosclerosis. *N Engl J Med* 2011; **365**(25):2398-2411.

Debouck C, Gorniak JG, Strickler JE, Meek TD, Metcalf BW, Rosenberg M: Human immunodeficiency virus protease expressed in Escherichia coli exhibits autoprocessing and specific maturation of the gag precursor. *Proc Natl Acad Sci U S A* 1987; **84**(24):8903-8906.

DeLeo JA, Tanga FY, Tawfik VL: Neuroimmune activation and neuroinflammation in chronic pain and opioid tolerance/hyperalgesia. *Neuroscientist* 2004; **10**(1):40-52.

Deller T, Merten T, Roth SU, Mundel P, Frotscher M: Actin-associated protein synaptopodin in the rat hippocampal formation: localization in the spine neck and close association with the spine apparatus of principal neurons. *J Comp Neurol* 2000; **418**(2):164-181.

Deller T, Bas Orth C, Del Turco D, Vlachos A, Burbach GJ, Drakew A, Chabanis S, Korte M, Schwegler H, Haas CA, Frotscher M: A role for synaptopodin and the spine apparatus in hippocampal synaptic plasticity. *Ann Anat* 2007; **189**(1):5-16.

Detwiler RK, Falk RJ, Hogan SL, Jennette JC: Collapsing glomerulopathy: a clinically and pathologically distinct variant of focal segmental glomerulosclerosis. *Kidney Int* 1994; **45**(5):1416-1424.

Drenckhahn D, Franke RP: Ultrastructural organization of contractile and cytoskeletal proteins in glomerular podocytes of chicken, rat, and man. *Lab Invest* 1988; **59**(5):673-682.

Drueke TB, Eckardt KU: Role of secondary hyperparathyroidism in erythropoietin resistance of chronic renal failure patients. *Nephrol Dial Transplant* 2002; **5**:28-31.

Drumond MC, Deen WM: Structural determinants of glomerular hydraulic permeability. *Am J Physiol* 1994; **266**(1 Pt 2):F1-12.

Dustin ML, Olszowy MW, Holdorf AD, Li J, Bromley S, Desai N, Widder P, Rosenberger F, van der Merwe PA, Allen PM, Shaw AS: A novel adaptor protein orchestrates receptor patterning and cytoskeletal polarity in T-cell contacts. *Cell* 1998; **94**(5):667-677.

Ebert BL, Bunn HF: Regulation of the Erythropoietin Gene, vol. 94; 1999.

Eisenberg SP, Hale KK, Heimdal P, Thompson RC: Location of the protease-inhibitory region of secretory leukocyte protease inhibitor. *Journal of Biological Chemistry* 1990; **265**(14):7976-7981.

Eitner F, Cui Y, Hudkins KL, Stokes MB, Segerer S, Mack M, Lewis PL, Abraham AA, Schlondorff D, Gallo G, Kimmel PL, Alpers CE: Chemokine receptor CCR5 and CXCR4 expression in HIV-associated kidney disease. *J Am Soc Nephrol* 2000; **11**(5):856-867.

Engelman A, Cherepanov P: The structural biology of HIV-1: mechanistic and therapeutic insights. *Nat Rev Micro* 2012; **10**(4):279-290.

Fahey JV, Wira CR: Effect of menstrual status on antibacterial activity and secretory leukocyte protease inhibitor production by human uterine epithelial cells in culture. *J Infect Dis* 2002; **185**(11):1606-1613.

Farquhar MG: Editorial: The primary glomerular filtration barrier--basement membrane or epithelial slits? *Kidney Int* 1975; **8**(4):197-211.

Faul C, Asanuma K, Yanagida-Asanuma E, Kim K, Mundel P: Actin up: regulation of podocyte structure and function by components of the actin cytoskeleton. *Trends in Cell Biology* 2007; **17**(9):428-437.

Faul C, Donnelly M, Merscher-Gomez S, Chang YH, Franz S, Delfgaauw J, Chang JM, Choi HY, Campbell KN, Kim K, Reiser J, Mundel P: The actin cytoskeleton of kidney podocytes is a direct target of the antiproteinuric effect of cyclosporine A. *Nat Med* 2008; **14**(9):931-938.

Fine DM, Perazella MA, Lucas GM, Atta MG: Renal disease in patients with HIV infection: Epidemiology, pathogenesis and management. *Drugs* 2008; **68**(7):963-980.

Foy CA, Parkes HC: Emerging homogeneous DNA-based technologies in the clinical laboratory. *Clin Chem* 2001; **47**(6):990-1000.

Foy MC, Estrella MM, Lucas GM, Tahir F, Fine DM, Moore RD, Atta MG: Comparison of risk factors and outcomes in HIV immune complex kidney disease and HIV-associated nephropathy. *Clin J Am Soc Nephrol* 2013; **8**(9):1524-1532.

Frade JM, Llorente M, Mellado M, Alcami J, Gutierrez-Ramos JC, Zaballos A, Real G, Martinez AC: The amino-terminal domain of the CCR2 chemokine receptor acts as coreceptor for HIV-1 infection. *J Clin Invest* 1997; **100**(3):497-502.

Gallo RC: HIV--the cause of AIDS: an overview on its biology, mechanisms of disease induction, and our attempts to control it. *J Acquir Immune Defic Syndr* 1988; **1**(6):521-535.

Gallo RC, Montagnier L: AIDS in 1988. *Sci Am* 1988; **259**(4):41-48.

Garver RI, Jr., Goldsmith KT, Rodu B, Hu PC, Sorscher EJ, Curiel DT: Strategy for achieving selective killing of carcinomas. *Gene Ther* 1994; **1**(1):46-50.

Ge J, Zhao G, Chen R, Li S, Wang S, Zhang X, Zhuang Y, Du J, Yu X, Li G, Yang Y: Enhanced myocardial cathepsin B expression in patients with dilated cardiomyopathy. *Eur J Heart Fail* 2006; **8**(3):284-289.

Gerntholtz TE, Goetsch SJ, Katz I: HIV-related nephropathy: a South African perspective. *Kidney Int* 2006; **69**:1885-1891.

Gharavi AG, Ahmad T, Wong RD, Hooshyar R, Vaughn J, Oller S, Frankel RZ, Bruggeman LA, D'Agati VD, Klotman PE, Lifton RP: Mapping a locus for susceptibility to HIV-1-

associated nephropathy to mouse chromosome 3. *Proc Natl Acad Sci U S A* 2004; **101**(8):2488-2493.

Goretzki L, Schmitt M, Mann K, Calvete J, Chucholowski N, Kramer M, Gunzler WA, Janicke F, Graeff H: Effective activation of the proenzyme form of the urokinase-type plasminogen activator (pro-uPA) by the cysteine protease cathepsin L. *FEBS Lett* 1992; **297**(1-2):112-118.

Gottesman MM, Cabral F: Purification and characterization of a transformation-dependent protein secreted by cultured murine fibroblasts. *Biochemistry* 1981; **20**(6):1659-1665.

Grondin V, Seksik P, Dumont S, Thomas G, Trugnan G, Flejou JF, Masliah J, Wendum D, Bachelet M: Regulation of colon cancer cell proliferation and migration by MD-2 activity. *Innate Immun* 2011; **17**(4):414-422.

Grunkemeyer JA, Kwoh C, Huber TB, Shaw AS: CD2-associated protein (CD2AP) expression in podocytes rescues lethality of CD2AP deficiency. *J Biol Chem* 2005; **280**(33):29677-29681.

Gu L, Dai Y, Xu J, Mallipattu S, Kaufman L, Klotman PE, He JC, Chuang PY: Deletion of podocyte STAT3 mitigates the entire spectrum of HIV-1-associated nephropathy. *Aids* 2013; **27**(7):1091-1098.

Hall A, Hakansson K, Mason RW, Grubb A, Abrahamson M: Structural basis for the biological specificity of cystatin C. Identification of leucine 9 in the N-terminal binding region as a selectivity-conferring residue in the inhibition of mammalian cysteine peptidases. *J Biol Chem* 1995; **270**(10):5115-5121.

Harris HE, Andersson U, Pisetsky DS: HMGB1: a multifunctional alarmin driving autoimmune and inflammatory disease. *Nat Rev Rheumatol* 2012; **8**(4):195-202.

He JC, Husain M, Sunamoto M, D'Agati VD, Klotman ME, Iyengar R, Klotman PE: Nef stimulates proliferation of glomerular podocytes through activation of Src-dependent Stat3 and MAPK1,2 pathways. *J Clin Invest* 2004; **114**(5):643-651.

Hiemstra PS, Maassen RJ, Stolk J, Heinzel-Wieland R, Steffens GJ, Dijkman JH: Antibacterial activity of antileukoprotease. *Infection and Immunity* 1996; **64**(11):4520-4524.

Hinshaw JE: Dynamin and its role in membrane fission. *Annu Rev Cell Dev Biol* 2000; **16**:483-519.

Howie AJ, Brewer DB: The glomerular tip lesion: a previously undescribed type of segmental glomerular abnormality. *J Pathol* 1984; **142**(3):205-220.

Huber TB, Simons M, Hartleben B, Sernetz L, Schmidts M, Gundlach E, Saleem MA, Walz G, Benzing T: Molecular basis of the functional podocin-nephrin complex: mutations in the NPHS2 gene disrupt nephrin targeting to lipid raft microdomains. *Hum Mol Genet* 2003; **12**(24):3397-3405.

Huber TB, Benzing T: The slit diaphragm: a signaling platform to regulate podocyte function. *Curr Opin Nephrol Hypertens* 2005; **14**(3):211-216.

Hübner W, McNerney GP, Chen P, Dale BM, Gordon RE, Chuang FYS, Li X-D, Asmuth DM, Huser T, Chen BK: Quantitative 3D Video Microscopy of HIV Transfer Across T Cell Virological Synapses. *Science (New York, NY)* 2009; **323**(5922):1743-1747.

Huggett J, Dheda K, Bustin S, Zumla A: Real-time RT-PCR normalisation; strategies and considerations. *Genes Immun* 2005; **6**(4):279-284.

Husain M, Gusella GL, Klotman ME, Gelman IH, Ross MD, Schwartz EJ, Cara A, Klotman PE: HIV-1 Nef induces proliferation and anchorage-independent growth in podocytes. *J Am Soc Nephrol* 2002; **13**(7):1806-1815.

Ifudu O, Friedman EA: Kidney injury, electrolyte and acid-base abnormalities associated with use of alternative medicine products. *Dialysis & Transplantation* 2009; **38**(4):124-127.

Ifudu O, Rao TK, Tan CC, Fleischman H, Chirgwin K, Friedman EA: Zidovudine is beneficial in human immunodeficiency virus associated nephropathy. *Am J Nephrol* 1995; **15**(3):217-221.

Inohara N, Nunez G: ML -- a conserved domain involved in innate immunity and lipid metabolism. *Trends Biochem Sci* 2002; **27**(5):219-221.

Jacqué JM, Mann A, Enslen H, Sharova N, Brichacek B, Davis RJ, Stevenson M: Modulation of HIV-1 infectivity by MAPK, a virion–associated kinase, vol. 17; 1998.

Janssens S, Burns K, Vercammen E, Tschopp J, Beyaert R: MyD88S, a splice variant of MyD88, differentially modulates NF-kappaB- and AP-1-dependent gene expression. *FEBS Lett* 2003; **548**(1-3):103-107.

Johnson SC, Benson CA, Johnson DW, Weinberg A: Recurrences of cytomegalovirus retinitis in a human immunodeficiency virus-infected patient, despite potent antiretroviral therapy and apparent immune reconstitution. *Clin Infect Dis* 2001; **32**(5):815-819.

Kambham N, Markowitz GS, Valeri AM, Lin J, D'Agati VD: Obesity-related glomerulopathy: an emerging epidemic. *Kidney Int* 2001; **59**(4):1498-1509.

Kestila M, Lenkkeri U, Mannikko M, Lamerdin J, McCready P, Putaala H, Ruotsalainen V, Morita T, Nissinen M, Herva R, Kashtan CE, Peltonen L, Holmberg C, Olsen A, Tryggvason K: Positionally cloned gene for a novel glomerular protein--nephrin--is mutated in congenital nephrotic syndrome. *Mol Cell* 1998; **1**(4):575-582.

Kim JJ, Hong YM, Sohn S, Jang GY, Ha KS, Yun SW, Han MK, Lee KY, Song MS, Lee HD, Kim DS, Lee JE, Shin ES, Jang JH, Lee YS, Kim SY, Lee JY, Han BG, Wu JY, Kim KJ, Park YM, Seo EJ, Park IS, Lee JK: A genome-wide association analysis reveals 1p31 and 2p13.3 as susceptibility loci for Kawasaki disease. *Hum Genet* 2011; **129**(5):487-495.

Klein DE, Lee A, Frank DW, Marks MS, Lemmon MA: The pleckstrin homology domains of dynamin isoforms require oligomerization for high affinity phosphoinositide binding. *J Biol Chem* 1998; **273**(42):27725-27733.

Kobayashi K, Hernandez LD, Galan JE, Janeway CA, Jr., Medzhitov R, Flavell RA: IRAK-M is a negative regulator of Toll-like receptor signaling. *Cell* 2002; **110**(2):191-202.

Kretzler M: Regulation of adhesive interaction between podocytes and glomerular basement membrane. *Microsc Res Tech* 2002; **57**(4):247-253.

Kriz W, Hackenthal E, Nobiling R, Sakai T, Elger M, Hahnel B: A role for podocytes to counteract capillary wall distension. *Kidney Int* 1994; **45**(2):369-376.

Kuwabara A, Satoh M, Tomita N, Sasaki T, Kashihara N: Deterioration of glomerular endothelial surface layer induced by oxidative stress is implicated in altered permeability of macromolecules in Zucker fatty rats. *Diabetologia* 2010; **53**(9):2056-2065.

Laemmli UK: Cleavage of structural proteins during the assembly of the head of bacteriophage T4. *Nature* 1970; **227**(5259):680-685.

Laguette N, Bregnard C, Benichou S, Basmaciogullari S: Human immunodeficiency virus (HIV) type-1, HIV-2 and simian immunodeficiency virus Nef proteins. *Mol Aspects Med* 2010; **31**(5):418-433.

Lamprecht MR, Sabatini DM, Carpenter AE: CellProfiler: free, versatile software for automated biological image analysis. *Biotechniques* 2007; **42**(1):71-75.

Lawn SD, Wood R: Incidence of Tuberculosis during Highly Active Antiretroviral Therapy in High-Income and Low-Income Countries. *Clinical Infectious Diseases* 2005; **41**(12):1783-1786.

Lech M, Garlanda C, Mantovani A, Kirschning CJ, Schlondorff D, Anders HJ: Different roles of TiR8/Sigirr on toll-like receptor signaling in intrarenal antigen-presenting cells and tubular epithelial cells. *Kidney Int* 2007; **72**(2):182-192.

Lenkkeri U, Mannikko M, McCready P, Lamerdin J, Gribouval O, Niaudet PM, Antignac CK, Kashtan CE, Homberg C, Olsen A, Kestila M, Tryggvason K: Structure of the gene for congenital nephrotic syndrome of the finnish type (NPHS1) and characterization of mutations. *Am J Hum Genet* 1999; **64**(1):51-61.

Leon CG, Tory R, Jia J, Sivak O, Wasan KM: Discovery and development of toll-like receptor 4 (TLR4) antagonists: a new paradigm for treating sepsis and other diseases. *Pharm Res* 2008; **25**(8):1751-1761.

Levey AS, Coresh J, Balk E, Kausz AT, Levin A, Steffes MW, Hogg RJ, Perrone RD, Lau J, Eknoyan G: National Kidney Foundation practice guidelines for chronic kidney disease: evaluation, classification, and stratification. *Ann Intern Med* 2003; **139**(2):137-147.

Levidiotis V, Power DA: New insights into the molecular biology of the glomerular filtration barrier and associated disease. *Nephrology (Carlton)* 2005; **10**(2):157-166.

Li C, Ruotsalainen V, Tryggvason K, Shaw AS, Miner JH: CD2AP is expressed with nephrin in developing podocytes and is found widely in mature kidney and elsewhere. *Am J Physiol Renal Physiol* 2000; **279**(4):F785-792.

Liew FY, Xu D, Brint EK, O'Neill LA: Negative regulation of toll-like receptor-mediated immune responses. *Nat Rev Immunol* 2005; **5**(6):446-458.

Lisowski P, Pierzchala M, Goscik J, Pareek CS, Zwierzchowski L: Evaluation of reference genes for studies of gene expression in the bovine liver, kidney, pituitary, and thyroid. *J Appl Genet* 2008; **49**(4):367-372.

Liu J, Sukhova GK, Yang JT, Sun J, Ma L, Ren A, Xu WH, Fu H, Dolganov GM, Hu C, Libby P, Shi GP: Cathepsin L expression and regulation in human abdominal aortic aneurysm, atherosclerosis, and vascular cells. *Atherosclerosis* 2006; **184**(2):302-311.

Livak KJ, Schmittgen TD: Analysis of relative gene expression data using real-time quantitative PCR and the 2(-Delta Delta C(T)) Method. *Methods* 2001; **25**(4):402-408.

Lotze MT, Tracey KJ: High-mobility group box 1 protein (HMGB1): nuclear weapon in the immune arsenal. *Nat Rev Immunol* 2005; **5**(4):331-342.

Louis JM, Oroszlan S, Tozser J: Stabilization from autoproteolysis and kinetic characterization of the human T-cell leukemia virus type 1 proteinase. *J Biol Chem* 1999; **274**(10):6660-6666.

Luban J, Lee C, Goff SP: Effect of linker insertion mutations in the human immunodeficiency virus type 1 gag gene on activation of viral protease expressed in bacteria. *J Virol* 1993; **67**(6):3630-3634.

Lucas GM, Eustace JA, Sozio S, Mentari EK, Appiah KA, Moore RD: Highly active antiretroviral therapy and the incidence of HIV-1-associated nephropathy: a 12-year cohort study. *AIDS* 2004; **18**:541-546.

Maciewicz RA, Etherington DJ, Kos J, Turk V: Collagenolytic cathepsins of rabbit spleen: a kinetic analysis of collagen degradation and inhibition by chicken cystatin. *Coll Relat Res* 1987; **7**(4):295-304.

Mandayam S, Shahinian VB: Are chronic dialysis patients at increased risk for cancer? *J Nephrol* 2008; **21**(2):166-174.

Mantovani A, Locati M, Vecchi A, Sozzani S, Allavena P: Decoy receptors: a strategy to regulate inflammatory cytokines and chemokines. *Trends Immunol* 2001; **22**(6):328-336.

Marras D, Bruggeman LA, Gao F, Tanji N, Mansukhani MM, Cara A, Ross MD, Gusella GL, Benson G, D'Agati VD, Hahn BH, Klotman ME, Klotman PE: Replication and compartmentalization of HIV-1 in kidney epithelium of patients with HIV-associated nephropathy. *Nat Med* 2002; **8**(5):522-526.

Mason DY, Sammons R: Alkaline phosphatase and peroxidase for double immunoenzymatic labelling of cellular constituents. *Journal of Clinical Pathology* 1978; **31**(5):454-460.

Mason RW, Gal S, Gottesman MM: The identification of the major excreted protein (MEP) from a transformed mouse fibroblast cell line as a catalytically active precursor form of cathepsin L. *Biochem J* 1987; **248**(2):449-454.

Mason RW: Interaction of lysosomal cysteine proteinases with alpha 2-macroglobulin: conclusive evidence for the endopeptidase activities of cathepsins B and H. *Arch Biochem Biophys* 1989; **273**(2):367-374.

McCoy K, Gal S, Schwartz RH, Gottesman MM: An acid protease secreted by transformed cells interferes with antigen processing. *J Cell Biol* 1988; **106**(6):1879-1884.

McCune JM: Viral latency in HIV disease. *Cell* 1995; **82**(2):183-188.

McMahon HT, Gallop JL: Membrane curvature and mechanisms of dynamic cell membrane remodelling. *Nature* 2005; **438**(7068):590-596.

McNeely TB, Dealy M, Dripps DJ, Orenstein JM, Eisenberg SP, Wahl SM: Secretory leukocyte protease inhibitor: a human saliva protein exhibiting anti-human immunodeficiency virus 1 activity in vitro. *J Clin Invest* 1995; **96**(1):456-464.

Medapalli RK, He JC, Klotman PE: HIV- Associated Nephropathy: Pathogenesis. *Current opinion in nephrology and hypertension* 2011; **20**(3):306-311.

Medzhitov R, Janeway CA, Jr.: Innate immunity: the virtues of a nonclonal system of recognition. *Cell* 1997; **91**(3):295-298.

Medzhitov R, Preston-Hurlburt P, Janeway CA, Jr.: A human homologue of the Drosophila Toll protein signals activation of adaptive immunity. *Nature* 1997; **388**(6640):394-397.

Meyrier A: Sarcoidosis: the nephrologist's view. *Ann Med Interne (Paris)* 2001; **152**(1):45-50.

Mikulak J, Singhal PC: HIV-1 entry into human podocytes is mediated through lipid rafts: Kidney Int. 2010 Jan;77(1):72-3; author reply 73-4. doi: 10.1038/ki.2009.366.

Modi WS, Lautenberger J, An P, Scott K, Goedert JJ, Kirk GD, Buchbinder S, Phair J, Donfield S, O'Brien SJ, Winkler C: Genetic variation in the CCL18-CCL3-CCL4 chemokine gene cluster influences HIV Type 1 transmission and AIDS disease progression. *Am J Hum Genet* 2006; **79**(1):120-128. find paper asap

Montaner JS, Hogg R, Wood E, Kerr T, Tyndall M, Levy AR, Harrigan PR: The case for expanding access to highly active antiretroviral therapy to curb the growth of the HIV epidemic. *Lancet* 2006; **368**(9534):531-536.

Moynagh PN: The Pellino family: IRAK E3 ligases with emerging roles in innate immune signalling. *Trends Immunol* 2009; **30**(1):33-42.

Mundel P, Gilbert P, Kriz W: Podocytes in glomerulus of rat kidney express a characteristic 44 KD protein. *J Histochem Cytochem* 1991; **39**(8):1047-1056.

Mundel P, Kriz W: Structure and function of podocytes: an update. *Anat Embryol (Berl)* 1995; **192**(5):385-397.

Mundel P, Reiser J, Zuniga Mejia Borja A, Pavenstadt H, Davidson GR, Kriz W, Zeller R: Rearrangements of the cytoskeleton and cell contacts induce process formation during differentiation of conditionally immortalized mouse podocyte cell lines. *Exp Cell Res* 1997; **236**(1):248-258.

Mundel P, Shankland SJ: Podocyte Biology and Response to Injury. *Journal of the American Society of Nephrology* 2002; **13**(12):3005-3015.

Nagai Y, Akashi S, Nagafuku M, Ogata M, Iwakura Y, Akira S, Kitamura T, Kosugi A, Kimoto M, Miyake K: Essential role of MD-2 in LPS responsiveness and TLR4 distribution. *Nat Immunol* 2002; **3**(7):667-672.

Nakane PK, Pierce GB, Jr.: Enzyme-labeled antibodies for the light and electron microscopic localization of tissue antigens. *J Cell Biol* 1967; **33**(2):307-318.

National Institute for Health and Care Excellence, 2015 - http://www.nice.org.uk, accessed February 2015.

Nishitani C, Mitsuzawa H, Sano H, Shimizu T, Matsushima N, Kuroki Y: Toll-like receptor 4 region Glu24-Lys47 is a site for MD-2 binding: importance of CYS29 and CYS40. *J Biol Chem* 2006; **281**(50):38322-38329.

Niu B, Lu L, Liu L, Gu TH, Feng KY, Lu WC, Cai YD: HIV-1 protease cleavage site prediction based on amino acid property. *J Comput Chem* 2009; **30**(1):33-39.

Nochy D, Glotz D, Dosquet P, Pruna A, Guettier C, Weiss L, Hinglais N, Idatte J-M, Méry J-P, Kazatchkine M, Druet P, Bariéty J: Renal disease associated with HIV infection: a multicentric study of 60 patients from Paris hospitals. *Nephrology Dialysis Transplantation* 1993; **8**(1):11-19.

Odaka C, Mizuochi T, Yang J, Ding A: Murine macrophages produce secretory leukocyte protease inhibitor during clearance of apoptotic cells: implications for resolution of the inflammatory response. *J Immunol* 2003; **171**(3):1507-1514.

Orth JD, McNiven MA: Dynamin at the actin-membrane interface. *Curr Opin Cell Biol* 2003; **15**(1):31-39.

Papeta N, Chan KT, Prakash S, Martino J, Kiryluk K, Ballard D, Bruggeman LA, Frankel R, Zheng Z, Klotman PE, Zhao H, D'Agati VD, Lifton RP, Gharavi AG: Susceptibility loci for murine HIV-associated nephropathy encode trans-regulators of podocyte gene expression. *J Clin Invest* 2009; **119**(5):1178-1188.

Patel V, Hedayati SS: Lactic acidosis in an HIV-infected patient receiving highly active antiretroviral therapy. *Nat Clin Pract Neph* 2006; **2**(2):109-114.

Pavenstadt H, Kriz W, Kretzler M: Cell biology of the glomerular podocyte. *Physiol Rev* 2003; **83**(1):253-307.

Percherancier Y, Lagane B, Planchenault T, Staropoli I, Altmeyer R, Virelizier JL, Arenzana-Seisdedos F, Hoessli DC, Bachelerie F: HIV-1 entry into T-cells is not dependent on CD4 and CCR5 localization to sphingolipid-enriched, detergent-resistant, raft membrane domains. *J Biol Chem* 2003; **278**(5):3153-3161.

Popik W, Alce TM: CD4 receptor localized to non-raft membrane microdomains supports HIV-1 entry. Identification of a novel raft localization marker in CD4. *J Biol Chem* 2004; **279**(1):704-712.

Qin J, Qian Y, Yao J, Grace C, Li X: SIGIRR inhibits interleukin-1 receptor- and toll-like receptor 4-mediated signaling through different mechanisms. *J Biol Chem* 2005; **280**(26):25233-25241.

Rajashree S, Puvanakrishnan R: Alterations in certain lysosomal glycohydrolases and cathepsins in rats on dexamethasone administration. *Mol Cell Biochem* 1996; **154**(2):165-170.

Rao TK, Filippone EJ, Nicastri AD, Landesman SH, Frank E, Chen CK, Friedman EA: Associated focal and segmental glomerulosclerosis in the acquired immunodeficiency syndrome. *N Engl J Med* 1984; **310**(11):669-673.

Reid W, Sadowska M, Denaro F, Rao S, Foulke J, Jr., Hayes N, Jones O, Doodnauth D, Davis H, Sill A, O'Driscoll P, Huso D, Fouts T, Lewis G, Hill M, Kamin-Lewis R, Wei C, Ray P, Gallo RC, Reitz M, Bryant J: An HIV-1 transgenic rat that develops HIV-related pathology and immunologic dysfunction. *Proc Natl Acad Sci U S A* 2001; **98**(16):9271-9276.

Reiser J, Kriz W, Kretzler M, Mundel P: The glomerular slit diaphragm is a modified adherens junction. *J Am Soc Nephrol* 2000; **11**(1):1-8.

Robinson PJ: Dephosphin, a 96,000 Da substrate of protein kinase C in synaptosomal cytosol, is phosphorylated in intact synaptosomes. *FEBS Lett* 1991; **282**(2):388-392.

Robker RL, Russell DL, Espey LL, Lydon JP, O'Malley BW, Richards JS: Progesterone-regulated genes in the ovulation process: ADAMTS-1 and cathepsin L proteases. *Proc Natl Acad Sci U S A* 2000; **97**(9):4689-4694.

Rock FL, Hardiman G, Timans JC, Kastelein RA, Bazan JF: A family of human receptors structurally related to Drosophila Toll. *Proc Natl Acad Sci U S A* 1998; **95**(2):588-593.

Rockwood N, Mandalia S, Bower M, Gazzard B, Nelson M: Ritonavir-boosted atazanavir exposure is associated with an increased rate of renal stones compared with efavirenz, ritonavir-boosted lopinavir and ritonavir-boosted darunavir. *AIDS* 2011; **25**(13):1671-1673.

Rodriguez-Lazaro D, Hernandez M, Esteve T, Hoorfar J, Pla M: A rapid and direct real time PCR-based method for identification of Salmonella spp. *J Microbiol Methods* 2003; **54**(3):381-390.

Romanowski T, Markiewicz A, Bednarz N, Bielawski KP: [Housekeeping genes as a reference in quantitative real-time RT-PCR]. *Postepy Hig Med Dosw* 2007; **61**:500-510.

Ronco P: Proteinuria: is it all in the foot? *Journal of Clinical Investigation* 2007; **117**(8):2079-2082.

Rosenstiel P, Gruosso T, Letourneau A, Chan J, LeBlanc A, Husain M, Najfeld V, Planelles V, D'Agati V, Klotman M, Klotman PE: HIV-1 vpr inhibits cytokinesis in human proximal tubule cells. *Kidney international* 2008; **74**(8):1049-1058.

Ross MJ, Martinka S, D'Agati VD, Bruggeman LA: NF-kappaB regulates Fas-mediated apoptosis in HIV-associated nephropathy. *J Am Soc Nephrol* 2005; **16**(8):2403-2411.

Ruotsalainen V, Ljungberg P, Wartiovaara J, Lenkkeri U, Kestila M, Jalanko H, Holmberg C, Tryggvason K: Nephrin is specifically located at the slit diaphragm of glomerular podocytes. *Proc Natl Acad Sci U S A* 1999; **96**(14):7962-7967.

Sarnak MJ, Levey AS, Schoolwerth AC, Coresh J, Culleton B, Hamm LL, McCullough PA, Kasiske BL, Kelepouris E, Klag MJ, Parfrey P, Pfeffer M, Raij L, Spinosa DJ, Wilson PW: Kidney disease as a risk factor for development of cardiovascular disease: a statement from the American Heart Association Councils on Kidney in Cardiovascular Disease, High Blood Pressure Research, Clinical Cardiology, and Epidemiology and Prevention. *Hypertension* 2003; **42**(5):1050-1065.

Salim K, Bottomley MJ, Querfurth E, Zvelebil MJ, Gout I, Scaife R, Margolis RL, Gigg R, Smith CI, Driscoll PC, Waterfield MD, Panayotou G: Distinct specificity in the recognition of phosphoinositides by the pleckstrin homology domains of dynamin and Bruton's tyrosine kinase. *Embo J* 1996; **15**(22):6241-6250.

Schaefer L, Han X, Gretz N, Schaefer RM: Alterations of cathepsins B, H and L in proximal tubules from polycystic kidneys of the Han:SPRD rat. *Kidney Int* 1996; **50**(2):424-431.

Schnabl B, Brandl K, Fink M, Gross P, Taura K, Gabele E, Hellerbrand C, Falk W: A TLR4/MD2 fusion protein inhibits LPS-induced pro-inflammatory signaling in hepatic stellate cells. *Biochem Biophys Res Commun* 2008; **375**(2):210-214.

Schoolwerth AC, Engelgau MM, Rufo KH, Vinicor F, Hostetter TH, Chianchiano D, McClellan WM, Warnock DG: Chronic Kidney Disease: A Public Health Problem That Needs a Public Health Action Plan. *Preventing Chronic Disease* 2006; **3**(2):A57.

Schwarz K, Simons M, Reiser J, Saleem MA, Faul C, Kriz W, Shaw AS, Holzman LB, Mundel P: Podocin, a raft-associated component of the glomerular slit diaphragm, interacts with CD2AP and nephrin. *J Clin Invest* 2001; **108**(11):1621-1629.

Schwartz EJ, Szczech LA, Ross MJ, Klotman ME, Winston JA, Klotman PE: Highly active antiretroviral therapy and the epidemic of HIV+ end-stage renal disease. *J Am Soc Nephrol* 2005; **16**(8):2412-2420.

Senatorski G, Paczek L, Sulowicz W, Gradowska L, Bartlomiejczyk I: Urine activity of cathepsin B, collagenase and urine excretion of TGF-beta 1 and fibronectin in membranous glomerulonephritis. *Res Exp Med* 1998; **198**(4):199-206.

Sever S, Muhlberg AB, Schmid SL: Impairment of dynamin's GAP domain stimulates receptor-mediated endocytosis. *Nature* 1999; **398**(6727):481-486.

Sever S, Altintas MM, Nankoe SR, Moller CC, Ko D, Wei C, Henderson J, del Re EC, Hsing L, Erickson A, Cohen CD, Kretzler M, Kerjaschki D, Rudensky A, Nikolic B, Reiser J: Proteolytic processing of dynamin by cytoplasmic cathepsin L is a mechanism for proteinuric kidney disease. *J Clin Invest* 2007; **117**(8):2095-2104.

Sharifi HJ, Furuya AM, de Noronha CMC: The Role of HIV-1 Vpr in Promoting the Infection of non-dividing Cells and in Cell Cycle Arrest. *Current opinion in HIV and AIDS* 2012; **7**(2):187-194.

Shih NY, Li J, Karpitskii V, Nguyen A, Dustin ML, Kanagawa O, Miner JH, Shaw AS: Congenital nephrotic syndrome in mice lacking CD2-associated protein. *Science* 1999; **286**(5438):312-315.

Shih N-Y, Li J, Cotran R, Mundel P, Miner JH, Shaw AS: CD2AP Localizes to the Slit Diaphragm and Binds to Nephrin via a Novel C-Terminal Domain. *The American Journal of Pathology* 2001; **159**(6):2303-2308.

Shimazu R, Akashi S, Ogata H, Nagai Y, Fukudome K, Miyake K, Kimoto M: MD-2, a molecule that confers lipopolysaccharide responsiveness on Toll-like receptor 4. *J Exp Med* 1999; **189**(11):1777-1782.

Shugars DC, Alexander AL, Fu K, Freel SA: Endogenous salivary inhibitors of human immunodeficiency virus. *Arch Oral Biol* 1999; **44**(6):445-453.

Shugars DC, Sauls DL, Weinberg JB: Secretory leukocyte protease inhibitor blocks infectivity of primary monocytes and mononuclear cells with both monocytotropic and lymphocytotropic strains of human immunodeficiency virus type I. *Oral Diseases* 1997; **3**(SUPPL. 1):S70-S72.

Sloane BF, Moin K, Krepela E, Rozhin J: Cathepsin B and its endogenous inhibitors: the role in tumor malignancy. *Cancer Metastasis Rev* 1990; **9**(4):333-352.

Smith MC, Austen JL, Carey JT, Emancipator SN, Herbener T, Gripshover B, Mbanefo C, Phinney M, Rahman M, Salata RA, Weigel K, Kalayjian RC: Prednisone improves renal function and proteinuria in human immunodeficiency virus-associated nephropathy. *Am J Med* 1996; **101**(1):41-48.

Smoyer WE, Mundel P, Gupta A, Welsh MJ: Podocyte alpha-actinin induction precedes foot process effacement in experimental nephrotic syndrome. *Am J Physiol* 1997; **273**(1 Pt 2):F150-157.

Snyder A, Alsauskas ZC, Leventhal JS, Rosenstiel PE, Gong P, Chan JJ, Barley K, He JC, Klotman ME, Ross MJ, Klotman PE: HIV-1 viral protein r induces ERK and caspase-8-dependent apoptosis in renal tubular epithelial cells. *Aids* 2010; **24**(8):1107-1119.

Stokes MB, Valeri AM, Markowitz GS, D'Agati VD: Cellular focal segmental glomerulosclerosis: Clinical and pathologic features. *Kidney Int* 2006; **70**(10):1783-1792.

Stypmann J, Glaser K, Roth W, Tobin DJ, Petermann I, Matthias R, Monnig G, Haverkamp W, Breithardt G, Schmahl W, Peters C, Reinheckel T: Dilated cardiomyopathy in mice deficient for the lysosomal cysteine peptidase cathepsin L. *Proc Natl Acad Sci U S A* 2002; **99**(9):6234-6239.

Sundstrom P, Juto P, Wadell G, Hallmans G, Svenningsson A, Nystrom L, Dillner J, Forsgren L: An altered immune response to Epstein-Barr virus in multiple sclerosis: a prospective study. *Neurology* 2004; **62**(12):2277-2282.

Sweet DE: Metabolic complications of antiretroviral therapy. *Top HIV Med* 2005; **13**(2):70-74.

Szczech LA, Edwards LJ, Sanders LL, van der Horst C, Bartlett JA, Heald AE, Svetkey LP: Protease inhibitors are associated with a slowed progression of HIV-related renal diseases. *Clin Nephrol* 2002; **57**(5):336-341.

Taggart CC, Lowe GJ, Greene CM, Mulgrew AT, O'Neill SJ, Levine RL, McElvaney NG: Cathepsin B, L, and S cleave and inactivate secretory leucoprotease inhibitor. *J Biol Chem* 2001; **276**(36):33345-33352.

Takeda T, McQuistan T, Orlando RA, Farquhar MG: Loss of glomerular foot processes is associated with uncoupling of podocalyxin from the actin cytoskeleton. *J Clin Invest* 2001; **108**(2):289-301.

Takeuchi T, Isobe S, Sato K, Kato MI, Kasai NN, Ohyama H, Yoshikawa D, Ishii H, Matsubara T, Murohara T: Cystatin C: a possible sensitive marker for detecting potential kidney injury after computed tomography coronary angiography. *J Comput Assist Tomogr* 2011; **35**(2):240-245.

Tanner GA: Glomerular sieving coefficient of serum albumin in the rat: a two-photon microscopy study. *Am J Physiol Renal Physiol* 2009; **296**(6):11.

Tomee JF, Koeter GH, Hiemstra PS, Kauffman HF: Secretory leukoprotease inhibitor: a native antimicrobial protein presenting a new therapeutic option? *Thorax* 1998; **53**(2):114-116.

Towbin H, Staehelin T, Gordon J: Electrophoretic transfer of proteins from polyacrylamide gels to nitrocellulose sheets: procedure and some applications. *Proc Natl Acad Sci U S A* 1979; **76**(9):4350-4354.

Tryggvason K, Patrakka J, Wartiovaara J: Hereditary proteinuria syndromes and mechanisms of proteinuria. *N Engl J Med* 2006a; **354**(13):1387-1401.

Tryggvason K, Pikkarainen T, Patrakka J: Nck links nephrin to actin in kidney podocytes. *Cell* 2006b; **125**(2):221-224.

Turk B, Bieth JG, Bjork I, Dolenc I, Turk D, Cimerman N, Kos J, Colic A, Stoka V, Turk V: Regulation of the activity of lysosomal cysteine proteinases by pH-induced inactivation

and/or endogenous protein inhibitors, cystatins. *Biol Chem Hoppe Seyler* 1995; **376**(4):225-230.

Verma DP: Cytokinesis and Building of the Cell Plate in Plants. *Annu Rev Plant Physiol Plant Mol Biol* 2001; **52**:751-784.

Verma SK, Leikina E, Melikov K, Chernomordik LV: Late stages of the synchronized macrophage fusion in osteoclast formation depend on dynamin. *Biochem J* 2014; **464**(3):293-300.

Visintin A, Latz E, Monks BG, Espevik T, Golenbock DT: Lysines 128 and 132 enable lipopolysaccharide binding to MD-2, leading to Toll-like receptor-4 aggregation and signal transduction. *J Biol Chem* 2003; **278**(48):48313-48320.

Wali RK, Drachenberg CI, Papadimitriou JC, Keay S, Ramos E: HIV-1-associated nephropathy and response to highly-active antiretroviral therapy: Lancet. 1998 Sep 5;352(9130):783-4.

Wei A, Burns GC, Williams BA, Mohammed NB, Visintainer P, Sivak SL: Long-term renal survival in HIV-associated nephropathy with angiotensin-converting enzyme inhibition. *Kidney Int* 2003; **64**(4):1462-1471.

Weiss A, Hollander H, Stobo J: Acquired immunofefeciency syndrome: epidemiology, virology, and immunology. *Annu Rev Med* 1985; **36**, 545-562.

Westin U, Nystrom M, Ljungcrantz I, Eriksson B, Ohlsson K: The presence of elafin, SLPI, IL1-RA and STNFalpha RI in head and neck squamous cell carcinomas and their relation to the degree of tumour differentiation. *Mediators Inflamm* 2002; **11**(1):7-12.

Winston JA, Burns GC, Klotman PE: The human immunodeficiency virus (HIV) epidemic and HIV-associated nephropathy. *Semin Nephrol* 1998; **18**(4):373-377.

Winston JA, Bruggeman LA, Ross MD, Jacobson J, Ross L, D'Agati VD, Klotman PE, Klotman ME: Nephropathy and establishment of a renal reservoir of HIV type 1 during primary infection. *N Engl J Med* 2001; **344**(26):1979-1984.

Wong ED, Wagner JA, Scott SV, Okreglak V, Holewinske TJ, Cassidy-Stone A, Nunnari J: The intramitochondrial dynamin-related GTPase, Mgm1p, is a component of a protein complex that mediates mitochondrial fusion. *J Cell Biol* 2003; **160**(3):303-311.

World Health Organization, 2015 - http://www.who.int/gho/hiv/en, accessed February 2015.

Woroniecki RP, Schiffer M, Shaw AS, Kaskel FJ, Bottinger EP: Glomerular expression of transforming growth factor-beta (TGF-beta) isoforms in mice lacking CD2-associated protein. *Pediatr Nephrol* 2006; **21**(3):333-338.

Xiao Y, Jin J, Chang M, Chang JH, Hu H, Zhou X, Brittain GC, Stansberg C, Torkildsen O, Wang X, Brink R, Cheng X, Sun SC: Peli1 promotes microglia-mediated CNS inflammation by regulating Traf3 degradation. *Nat Med* 2013; **19**(5):595-602.

Yaddanapudi S, Altintas MM, Kistler AD, Fernandez I, xF, ller CC, Wei C, Peev V, Flesche JB, Forst A-L, Li J, Patrakka J, Xiao Z, Grahammer F, Schiffer M, Lohm, xFc, ller T, Reinheckel T, Gu C, Huber TB, Ju W, Bitzer M, Rastaldi MP, Ruiz P, Tryggvason K, Shaw AS, Faul C, Sever S, Reiser J: CD2AP in mouse and human podocytes controls a proteolytic program that regulates cytoskeletal structure and cellular survival. *The Journal of Clinical Investigation* 2011; **121**(10):3965-3980.

Yamazaki M, Matsuo R, Fukazawa Y, Ozawa F, Inokuchi K: Regulated expression of an actin-associated protein, synaptopodin, during long-term potentiation. *J Neurochem* 2001; **79**(1):192-199.

Yanai H, Matsuda A, An J, Koshiba R, Nishio J, Negishi H, Ikushima H, Onoe T, Ohdan H, Yoshida N, Taniguchi T: Conditional ablation of HMGB1 in mice reveals its protective function against endotoxemia and bacterial infection. *Proceedings of the National Academy of Sciences of the United States of America* 2013; **110**(51):20699-20704.

Yang X, Gabuzda D: Regulation of human immunodeficiency virus type 1 infectivity by the ERK mitogen-activated protein kinase signaling pathway. *J Virol* 1999; **73**(4):3460-3466.

Yang M, Liu L, Xie M, Sun X, Yu Y, Kang R, Yang L, Zhu S, Cao L, Tang D: Poly-ADP-ribosylation of HMGB1 regulates TNFSF10/TRAIL resistance through autophagy. *Autophagy* 2015; **21**:0.

Zhong J, Zuo Y, Ma J, Fogo AB, Jolicoeur P, Ichikawa I, Matsusaka T: Expression of HIV-1 genes in podocytes alone can lead to the full spectrum of HIV-1-associated nephropathy. *Kidney Int* 2005; **68**(3):1048-1060.

Appendix

Ethics clearance certificate

HUMAN RESEARCH ETHICS COMMITTEE (MEDICAL)

CLEARANCE CERTIFICATE NO. M131062

NAME: (Principal Investigator)	Lerato Mpye
DEPARTMENT:	Department of Internal Medicine CM Johannesburg Academic Hospital
PROJECT TITLE:	The Role of Cathepsin L and Dynamin the Pathogenesis of HIV Related Kidney Disease (Previously M070916 Dr G Saleshando)
DATE CONSIDERED:	Ad hoc
DECISION:	Approved unconditionally
CONDITIONS:	
SUPERVISOR:	Prof S Naicker
APPROVED BY:	Professor PE Cleaton-Jones, Chairperson, HREC (Medical)

DATE OF APPROVAL: 22/11/2013

This clearance certificate is valid for 5 years from date of approval. Extension may be applied for.

DECLARATION OF INVESTIGATORS

To be completed in duplicate and **ONE COPY** returned to the Secretary in Room 10004, 10th floor, Senate House, University.

I/we fully understand the conditions under which I am/we are authorized to carry out the above-mentioned research and I/we undertake to ensure compliance with these conditions. Should any departure be contemplated, from the research protocol as approved, I/we undertake to resubmit the application to the Committee. **I agree to submit a yearly progress report**.

Principal Investigator Signature M131062Date

PLEASE QUOTE THE PROTOCOL NUMBER IN ALL ENQUIRIES

Copyright certification

Permission to reproduce the images used was granted by the respective publishers (certificates attached).

NATURE PUBLISHING GROUP LICENSE TERMS AND CONDITIONS

Mar 30, 2015

This is a License Agreement between KELEABETSWE LERATO MPYE ("You") and Nature Publishing Group ("Nature Publishing Group") provided by Copyright Clearance Center ("CCC"). The license consists of your order details, the terms and conditions provided by Nature Publishing Group, and the payment terms and conditions.

All payments must be made in full to CCC. For payment instructions, please see information listed at the bottom of this form.

License Number	3587040500655
License date	Mar 13, 2015
Licensed content publisher	Nature Publishing Group
Licensed content publication	Nature Reviews Microbiology
Licensed content title	The structural biology of HIV-1: mechanistic and therapeutic insights
Licensed content author	Alan Engelman and Peter Cherepanov
Licensed content date	Apr 1, 2012
Volume number	10
Issue number	4
Type of Use	reuse in a dissertation / thesis
Requestor type	academic/educational
Format	print and electronic
Portion	figures/tables/illustrations
Number of figures/tables/illustrations	1
High-res required	no
Figures	Figure 1 | Schematic overview of the HIV-1 replication cycle.
Author of this NPG article	no
Your reference number	None
Title of your thesis / dissertation	Profiling Gene Expression Pattern Changes in HIV-1-Associated Kidney Diseases
Expected completion date	Mar 2015
Estimated size (number of pages)	150
Total	0.00 USD
Terms and Conditions	

Terms and Conditions for Permissions

Nature Publishing Group hereby grants you a non-exclusive license to reproduce this

Copyright Clearance Center

Back to view orders

Copy order

Print this page
Print terms & conditions
Print citation information
(What's this?)

Confirmation Number: 11316984
Order Date: 03/13/2015

Customer Information

Customer: KELEABETSWE MPYE
Account Number: 3000897104
Organization: KELEABETSWE MPYE
Email:
keleabetswe.mpye@students.wits.ac.za
Phone: +27 735070111

Search order details by: Choose One Go

This is not an invoice

Order Details

JOURNAL OF CLINICAL INVESTIGATION. ONLINE

Billing Status: **N/A**

Order detail ID: 66399676
ISSN: 1558-8238
Publication Type: e-Journal
Volume:
Issue:
Start page:
Publisher: AMERICAN SOCIETY FOR CLINICAL INVESTIGATION

Permission Status: Granted
Permission type: Republish or display content
Type of use: Republish in a thesis/dissertation
Order License Id: 3587010816195

Hide details

Requestor type	Author of requested content
Format	Print, Electronic
Portion	image/photo
Number of images/photos requested	1
Title or numeric reference of the portion(s)	Proteinuria: is it all in the foot? Figure 1
Title of the article or chapter the portion is from	Figure 1, The glomerular filtration barrier.
Editor of portion(s)	N/A
Author of portion(s)	Pierre Ronco
Volume of serial or monograph	117
Page range of portion	2080
Publication date of portion	August 2007
Rights for	Main product
Duration of use	Life of current edition
Creation of copies for the disabled	no

With minor editing privileges	yes
For distribution to	Worldwide
In the following language(s)	Original language of publication
With incidental promotional use	no
Lifetime unit quantity of new product	Up to 499
Made available in the following markets	Academic
The requesting person/organization	Keleabetswe Lerato Mpye, University of the Witwatersrand, Johannesburg
Order reference number	
Author/Editor	KELEABETSWE LERATO MPYE
The standard identifier	PhD thesis
Title	Profiling Gene Expression Pattern Changes in HIV-1-Associated Kidney Diseases
Publisher	University of the Witwatersrand, Johannesburg
Expected publication date	Mar 2015
Estimated size (pages)	150

Copyright Clearance Center

Back to view orders

Copy order

Print this page
Print terms & conditions
Print citation information
(What's this?)

Confirmation Number: 11313441
Order Date: 03/10/2015

Customer Information

Customer: KELEABETSWE MPYE
Account Number: 3000897104
Organization: KELEABETSWE MPYE
Email:
keleabetswe.mpye@students.wits.ac.za
Phone: +27 735070111

Search order details by: Choose One Go

This is not an invoice

Order Details

Journal of the American Society of Nephrology

Billing Status: **N/A**

Order detail ID: 66350133
ISSN: 1533-3450
Publication Type: e-Journal
Volume:
Issue:
Start page:
Publisher: AMERICAN SOCIETY OF NEPHROLOGY
Author/Editor: American Society of Nephrology

Permission Status: Granted
Permission type: Republish or display content
Type of use: Thesis/Dissertation
Order License Id: 3585300486244

Hide details

Requestor type	Author of requested content
Format	Print, Electronic
Portion	image/photo
Number of images/photos requested	1
Title or numeric reference of the portion(s)	Figure 1. Molecular anatomy of the podocyte foot process (FP) actin cytoskeleton
Title of the article or chapter the portion is from	Podocyte Biology and Response to Injury
Editor of portion(s)	N/A
Author of portion(s)	N/A
Volume of serial or monograph	N/A
Page range of portion	3006
Publication date of portion	2002
Rights for	Main product
Duration of use	Life of current edition
Creation of copies for	

the disabled	no
With minor editing privileges	no
For distribution to	Worldwide
In the following language(s)	Original language of publication
With incidental promotional use	no
Lifetime unit quantity of new product	Up to 499
Made available in the following markets	Academic
The requesting person/organization	Keleabetswe Lerato Mpye, University of the Witwatersrand, Johannesburg
Order reference number	
Author/Editor	KELEABETSWE LERATO MPYE
The standard identifier	PhD thesis
Title	Profiling Gene Expression Pattern Changes in HIV-1-Associated Kidney Diseases
Publisher	University of the Witwatersrand, Johannesburg
Expected publication date	Mar 2015
Estimated size (pages)	150

Immunohistochemistry

All solutions and antibodies used, excluding the antigen retrieval buffer, were prepared in 1 × PBS. The entire experimental procedure was carried out at room temperature unless specified otherwise. Each run included a negative control, in which either a primary or secondary antibody was omitted.

Buffer	Components
Antigen retrieval buffer (Tris-EDTA)	10 mM Tris base, 1 mM EDTA, 0.05 % Tween-20, pH 9.0.
Wash buffer	1 × PBS, pH 7.4.

RNA isolation, purification and quantification

RNA was extracted from FFPE renal tissue of HIVAN, FSGS, MCD and healthy control biopsies using the AllPrep DNA/RNA FFPE kit (QIAgen, Whitehead Scientific) as per manufacturer's instruction (See detailed protocol in the appendix). Briefly, tissue sections were deparaffinized in an eppendorf following trimming of excess paraffin off the sample block. Deparaffinization solution (SABiosciences, QIAgen) was added to the sample, the mixture vigorously vortexed and incubated at 56 °C for 15 minutes. Sample was pelleted by centrifugation for 2 minutes at 12 000 x g after cooling at room temperature. Supernatant was carefully decanted and residual deparaffinization solution removed using a fine pipette without disturbing the pellet. Pellet was dried by incubating the open tube at 37 °C for 10 minutes and resuspended in buffer PKD. Proteinase K was added and mixed by vortexing. The mixture was incubated at 56 °C for 15 minutes to lyse the tissue and cooled on ice for 3 minutes. The DNA-containing pellet was precipitated by centrifugation at 20 000 x g for 15 minutes. All centrifugation steps were performed using BOECO M-24A (Germany) mini centrifuge, unless stated otherwise.

RNA-containing supernatant was transferred to a new 2 mℓ microcentrifuge tube for total RNA purification. The procedure was initiated by partially reversing formaldehyde modification of nucleic acids through heating of the supernatant for 15 minutes at 80 °C followed by

adding 320 µℓ buffer RLT to adjust binding conditions. Absolute ethanol, 720 µℓ, was added to the mixture and vortexed before transferring the sample onto an RNeasy MinElute spin column placed in a 2 mℓ collection tube. Sample was passed through the spin column by centrifugation. Flow-through was discarded and more sample added onto the column. The step was repeated until the entire sample had passed through the column. RNA, bound to the column, was washed with 350 µℓ buffer FRN added to the RNeasy MinElute spin column and centrifuged. Contaminating DNA was subsequently digested by adding DNase I solution directly onto the column membrane and incubated for 15 minutes at room temperature. Spin column membrane was washed by adding 500 µℓ buffer RPE and centrifuged. Flow-throw was discarded and same step repeated with fresh buffer RPE. All centrifugation was performed at 8 000 x g for 15 seconds at room temperature, unless specified otherwise. RNeasy MinElute spin column was placed in a new collection tube and spun at 12 000 x g for 5 minutes while open to dry residual ethanol from the column membrane. Following incubation of the spin column with 20 µℓ RNase-free water for 1 minute at room temperature, RNA was eluted into a new 1.5 mℓ collection tube by centrifugation for 1 minute at 12 000 x g. RNA-containing eluate was reapplied to the column, to retrieve residual RNA from the column, and centrifuged for a minute at 12 000 x g. RNA was quantified and stored at -80 °C prior to downstream application.

Template preparation

cDNA was reverse transcribed from total RNA using High Capacity cDNA Reverse Transcription kit (Applied Biosystems) according to manufacturers' instructions. cDNA reverse transcription (RT) reaction was set-up by initially preparing a 2 × RT master mix on ice. The 2 × RT master mix was prepared by adding equal volumes of the 10 × RT buffer and 10 × RT random primers to 100 mM dNTP mix, MultiScribe^{TM} reverse transcriptase and nuclease-free water (as indicated in Table 1). RT master mix was aliquoted accordingly and diluted to 1 × reaction mix by pipetting equal volume of extracted RNA sample from section 2.3. The reaction mix was homogenized by pipetting up and down twice and followed by brief centrifugation to eliminate air bubbles. The reaction mix was subjected to thermal cycling under the conditions outlined in Table 2. For transcription control (NRT) experiments, reverse transcriptase was

omitted and volume made-up with nuclease-free water. Non-reverse transcriptase (NRT) controls were included to monitor genomic DNA contamination. RNA samples were used at final concentration of 200 ng in all RT experiments. At the end of the run the reverse transcription reaction (cDNA) was removed from the thermocycler, MJ Mini^{TM} Personal Thermal Cycler (BIO-RAD), and stored at -20 °C prior to use.

PCR arrays

Changes in gene expression patterns of host kidney cells were determined using RT^2 Profiler PCR arrays (SABiosciences, Whitehead Scientific) in real-time qPCR experiments. The RT^2 Profiler PCR Arrays incorporate a panel of relevant optimized primers for monitoring pathway- or disease-focused gene expression patterns in cells and tissues. The two arrays selected for this study are Human Toll-Like Receptor and HIV Host Response panels. The latter PCR array profiles the expression of genes that are involved in the response of the host to HIV infection and includes genes implicated in both innate and adaptive immunity, as well as cellular co-factor implicated in HIV replication. The Toll-Like Receptor (TLR) signaling pathway array profiles genes that are crucial in TLR-meditated signal transduction and includes members of the TLR family as well as various adaptor and effector proteins. Each PCR Array profiles expression of 84 disease- or pathway-specific genes plus 8 control genes. PCR array experiments were divided into 3 parts, notably first-strand cDNA synthesis, cDNA target template pre-amplification and real-time qPCR.

Manufacturers' functional gene grouping list:

HIV HOST RESPONSE PCR ARRAY

Position	Symbol	Description
A01	APEX1	APEX nuclease (multifunctional DNA repair enzyme) 1
A02	APOBEC3G	Apolipoprotein B mRNA editing enzyme, catalytic polypeptide-like 3G
A03	BAD	BCL2-associated agonist of cell death

A04	BANF1	Barrier to autointegration factor 1
A05	BAX	BCL2-associated X protein
A06	BCL11B	B-cell CLL/lymphoma 11B (zinc finger protein)
A07	BCL2	B-cell CLL/lymphoma 2
A08	BTRC	Beta-transducin repeat containing
A09	CASP3	Caspase 3, apoptosis-related cysteine peptidase
A10	CASP8	Caspase 8, apoptosis-related cysteine peptidase
A11	CBX5	Chromobox homolog 5
A12	CCL2	Chemokine (C-C motif) ligand 2
B01	CCL3	Chemokine (C-C motif) ligand 3
B02	CCL4	Chemokine (C-C motif) ligand 4
B03	CCL5	Chemokine (C-C motif) ligand 5
B04	CCL8	Chemokine (C-C motif) ligand 8
B05	CCNT1	Cyclin T1
B06	CCR2	Chemokine (C-C motif) receptor 2
B07	CCR3	Chemokine (C-C motif) receptor 3
B08	CCR4	Chemokine (C-C motif) receptor 4
B09	CCR5	Chemokine (C-C motif) receptor 5
B10	CD209	CD209 molecule
B11	CD247	CD247 molecule
B12	CD4	CD4 molecule
C01	CD44	CD44 molecule (Indian blood group)
C02	CD69	CD69 molecule
C03	CD74	CD74 molecule, major histocompatibility complex, class II invariant chain
C04	CDK7	Cyclin-dependent kinase 7
C05	CDK9	Cyclin-dependent kinase 9
C06	CDKN1A	Cyclin-dependent kinase inhibitor 1A (p21, Cip1)
C07	CEBPB	CCAAT/enhancer binding protein (C/EBP), beta
C08	COPS6	COP9 constitutive photomorphogenic homolog subunit 6

		(Arabidopsis)
C09	CR2	Complement component (3d/Epstein Barr virus) receptor 2
C10	CREBBP	CREB binding protein
C11	CX3CL1	Chemokine (C-X3-C motif) ligand 1
C12	CXCL12	Chemokine (C-X-C motif) ligand 12
D01	CXCR4	Chemokine (C-X-C motif) receptor 4
D02	ELANE	Elastase, neutrophil expressed
D03	EP300	E1A binding protein p300
D04	FCAR	Fc fragment of IgA, receptor for
D05	FOS	FBJ murine osteosarcoma viral oncogene homolog
D06	GADD45A	Growth arrest and DNA-damage-inducible, alpha
D07	HCK	Hemopoietic cell kinase
D08	HTATSF1	HIV-1 Tat specific factor 1
D09	IFNA1	Interferon, alpha 1
D10	IFNB1	Interferon, beta 1, fibroblast
D11	IFNG	Interferon, gamma
D12	IL10	Interleukin 10
E01	IL12B	Interleukin 12B (natural killer cell stimulatory factor 2, cytotoxic lymphocyte maturation factor 2, p40)
E02	IL16	Interleukin 16
E03	IL1B	Interleukin 1, beta
E04	IL2	Interleukin 2
E05	IL8	Interleukin 8
E06	IRF1	Interferon regulatory factor 1
E07	IRF2	Interferon regulatory factor 2
E08	KLRD1	Killer cell lectin-like receptor subfamily D, member 1
E09	LTBR	Lymphotoxin beta receptor (TNFR superfamily, member 3)
E10	MAP3K5	Mitogen-activated protein kinase kinase kinase 5
E11	MBL2	Mannose-binding lectin (protein C) 2, soluble
E12	NFATC1	Nuclear factor of activated T-cells, cytoplasmic, calcineurin-

		dependent 1
F01	NFKB1	Nuclear factor of kappa light polypeptide gene enhancer in B-cells 1
F02	NFKBIA	Nuclear factor of kappa light polypeptide gene enhancer in B-cells inhibitor, alpha
F03	PPIA	Peptidylprolyl isomerase A (cyclophilin A)
F04	PRDX1	Peroxiredoxin 1
F05	PTK2B	PTK2B protein tyrosine kinase 2 beta
F06	RBL2	Retinoblastoma-like 2 (p130)
F07	SELL	Selectin L
F08	SERPINA1	Serpin peptidase inhibitor, clade A (alpha-1 antiproteinase, antitrypsin), member 1
F09	SERPINC1	Serpin peptidase inhibitor, clade C (antithrombin), member 1
F10	SLPI	Secretory leukocyte peptidase inhibitor
F11	SMARCB1	SWI/SNF related, matrix associated, actin dependent regulator of chromatin, subfamily b, member 1
F12	STAT1	Signal transducer and activator of transcription 1, 91kDa
G01	STAT3	Signal transducer and activator of transcription 3 (acute-phase response factor)
G02	TFCP2	Transcription factor CP2
G03	TGFB1	Transforming growth factor, beta 1
G04	TNF	Tumor necrosis factor
G05	TNFRSF1B	Tumor necrosis factor receptor superfamily, member 1B
G06	TNFSF10	Tumor necrosis factor (ligand) superfamily, member 10
G07	TRIM5	Tripartite motif containing 5
G08	TSG101	Tumor susceptibility gene 101
G09	VPS4A	Vacuolar protein sorting 4 homolog A (S. cerevisiae)
G10	XCL1	Chemokine (C motif) ligand 1
G11	XPO1	Exportin 1 (CRM1 homolog, yeast)
G12	YY1	YY1 transcription factor

H01	ACTB	Actin, beta
H02	B2M	Beta-2-microglobulin
H03	GAPDH	Glyceraldehyde-3-phosphate dehydrogenase
H04	HPRT1	Hypoxanthine phosphoribosyltransferase 1
H05	RPLP0	Ribosomal protein, large, P0
H06	HGDC	Human Genomic DNA Contamination
H07	RTC	Reverse Transcription Control
H08	RTC	Reverse Transcription Control
H09	RTC	Reverse Transcription Control
H10	PPC	Positive PCR Control
H11	PPC	Positive PCR Control
H12	PPC	Positive PCR Control

TOLL-LIKE RECEPTOR PCR ARRAY

Position	**Symbol**	**Description**
A01	BTK	Bruton agammaglobulinemia tyrosine kinase
A02	CASP8	Caspase 8, apoptosis-related cysteine peptidase
A03	CCL2	Chemokine (C-C motif) ligand 2
A04	CD14	CD14 molecule
A05	CD180	CD180 molecule
A06	CD80	CD80 molecule
A07	CD86	CD86 molecule
A08	CHUK	Conserved helix-loop-helix ubiquitous kinase
A09	CLEC4E	C-type lectin domain family 4, member E
A10	CSF2	Colony stimulating factor 2 (granulocyte-macrophage)
A11	CSF3	Colony stimulating factor 3 (granulocyte)
A12	CXCL10	Chemokine (C-X-C motif) ligand 10
B01	ECSIT	ECSIT homolog (Drosophila)

B02	EIF2AK2	Eukaryotic translation initiation factor 2-alpha kinase 2
B03	ELK1	ELK1, member of ETS oncogene family
B04	FADD	Fas (TNFRSF6)-associated via death domain
B05	FOS	FBJ murine osteosarcoma viral oncogene homolog
B06	HMGB1	High mobility group box 1
B07	HRAS	V-Ha-ras Harvey rat sarcoma viral oncogene homolog
B08	HSPA1A	Heat shock 70kDa protein 1A
B09	HSPD1	Heat shock 60kDa protein 1 (chaperonin)
B10	IFNA1	Interferon, alpha 1
B11	IFNB1	Interferon, beta 1, fibroblast
B12	IFNG	Interferon, gamma
C01	IKBKB	Inhibitor of kappa light polypeptide gene enhancer in B-cells, kinase beta
C02	IL10	Interleukin 10
C03	IL12A	Interleukin 12A (natural killer cell stimulatory factor 1, cytotoxic lymphocyte maturation factor 1, p35)
C04	IL1A	Interleukin 1, alpha
C05	IL1B	Interleukin 1, beta
C06	IL2	Interleukin 2
C07	IL6	Interleukin 6 (interferon, beta 2)
C08	IL8	Interleukin 8
C09	IRAK1	Interleukin-1 receptor-associated kinase 1
C10	IRAK2	Interleukin-1 receptor-associated kinase 2
C11	IRAK4	Interleukin-1 receptor-associated kinase 4
C12	IRF1	Interferon regulatory factor 1
D01	IRF3	Interferon regulatory factor 3

D02	JUN	Jun proto-oncogene
D03	LTA	Lymphotoxin alpha (TNF superfamily, member 1)
D04	LY86	Lymphocyte antigen 86
D05	LY96	Lymphocyte antigen 96
D06	MAP2K3	Mitogen-activated protein kinase kinase 3
D07	MAP2K4	Mitogen-activated protein kinase kinase 4
D08	MAP3K1	Mitogen-activated protein kinase kinase kinase 1
D09	MAP3K7	Mitogen-activated protein kinase kinase kinase 7
D10	MAP4K4	Mitogen-activated protein kinase kinase kinase kinase 4
D11	MAPK8	Mitogen-activated protein kinase 8
D12	MAPK8IP3	Mitogen-activated protein kinase 8 interacting protein 3
E01	MYD88	Myeloid differentiation primary response gene (88)
E02	NFKB1	Nuclear factor of kappa light polypeptide gene enhancer in B-cells 1
E03	NFKB2	Nuclear factor of kappa light polypeptide gene enhancer in B-cells 2 (p49/p100)
E04	NFKBIA	Nuclear factor of kappa light polypeptide gene enhancer in B-cells inhibitor, alpha
E05	NFKBIL1	Nuclear factor of kappa light polypeptide gene enhancer in B-cells inhibitor-like 1
E06	NFRKB	Nuclear factor related to kappaB binding protein
E07	NR2C2	Nuclear receptor subfamily 2, group C, member 2
E08	PELI1	Pellino homolog 1 (Drosophila)
E09	PPARA	Peroxisome proliferator-activated receptor alpha
E10	PRKRA	Protein kinase, interferon-inducible double

		stranded RNA dependent activator
E11	PTGS2	Prostaglandin-endoperoxide synthase 2 (prostaglandin G/H synthase and cyclooxygenase)
E12	REL	V-rel reticuloendotheliosis viral oncogene homolog (avian)
F01	RELA	V-rel reticuloendotheliosis viral oncogene homolog A (avian)
F02	RIPK2	Receptor-interacting serine-threonine kinase 2
F03	SARM1	Sterile alpha and TIR motif containing 1
F04	SIGIRR	Single immunoglobulin and toll-interleukin 1 receptor (TIR) domain
F05	TAB1	TGF-beta activated kinase 1/MAP3K7 binding protein 1
F06	TBK1	TANK-binding kinase 1
F07	TICAM1	Toll-like receptor adaptor molecule 1
F08	TICAM2	Toll-like receptor adaptor molecule 2
F09	TIRAP	Toll-interleukin 1 receptor (TIR) domain containing adaptor protein
F10	TLR1	Toll-like receptor 1
F11	TLR10	Toll-like receptor 10
F12	TLR2	Toll-like receptor 2
G01	TLR3	Toll-like receptor 3
G02	TLR4	Toll-like receptor 4
G03	TLR5	Toll-like receptor 5
G04	TLR6	Toll-like receptor 6
G05	TLR7	Toll-like receptor 7
G06	TLR8	Toll-like receptor 8
G07	TLR9	Toll-like receptor 9
G08	TNF	Tumor necrosis factor

G09	TNFRSF1A	Tumor necrosis factor receptor superfamily, member 1A
G10	TOLLIP	Toll interacting protein
G11	TRAF6	TNF receptor-associated factor 6
G12	UBE2N	Ubiquitin-conjugating enzyme E2N
H01	ACTB	Actin, beta
H02	B2M	Beta-2-microglobulin
H03	GAPDH	Glyceraldehyde-3-phosphate dehydrogenase
H04	HPRT1	Hypoxanthine phosphoribosyltransferase 1
H05	RPLP0	Ribosomal protein, large, P0
H06	HGDC	Human Genomic DNA Contamination
H07	RTC	Reverse Transcription Control
H08	RTC	Reverse Transcription Control
H09	RTC	Reverse Transcription Control
H10	PPC	Positive PCR Control
H11	PPC	Positive PCR Control
H12	PPC	Positive PCR Control

Sodium dodecyl sulphate polyacrylamide gel electrophoresis

Sodium dodecyl sulphate polyacrylamide gel electrophoresis (SDS-PAGE) is a discontinuous buffer system that was initially defined by Laemmli (1970) to separate protein subunits based on their molecular weights. The technique uses SDS, an anionic detergent, to denature proteins. Upon binding to and denaturation by SDS, the proteins acquire a rod-like shape with an overall negative charge. The charged particles migrate towards the electrode of opposite charge in an electric field. Inter- and intra-molecular disulphide bonds within the proteins are reduced by adding β-mercaptoethanol in the sample loading buffer. The protein samples were diluted five-fold in 5 × loading buffer and boiled for five minutes to denature the proteins before loading onto the gel. A 10 % SDS-PAGE gel was prepared in a 1.55 mm casting plate and used to separate the protein subunits. Electrode buffer was added into the gel chamber and electrophoresis was performed at 120 volts for 90 minutes using a Bio-rad system. The sizes of the proteins were

determined in relation to a set of standard proteins, of known molecular weight, electrophoresed under the same denaturing conditions. The protein molecular weight marker used was a Precision Plus Protein™ Dual Color Standards (Bio-Rad). Immediately after electrophoresis, the gel was assembled for protein transfer.

Buffer	Components
5 × loading buffer	0.5 mM Tris-HCl, pH 6.8, 20 % (v/v) glycerol, 10 % (w/v) SDS, 100 mM β-mercaptoethanol, 0.05 % (w/v) bromophenol blue.
10 % SDS-PAGE separating gel	6.15 mℓ H_2O, 3.75 mℓ 1.5 M Tris-HCl, pH 8.8, 150 µℓ 10 % (w/v) SDS, 4.95 mℓ Acrylamide/Bis-acrylamide (30 %/0.8 % w/v), 75 µℓ 10 % (w/v) APS, 20 µℓ TEMED
Stacking gel	3.075 mℓ H_2O, 1.25 mℓ 0.5 M Tris-HCl, pH 6.8, 25 µℓ 10 % (w/v) SDS, 67 µℓ Acrylamide/Bis-acrylamide (30 %/0.8 % w/v), 25 µℓ 10 % (w/v) APS, 5 µℓ TEMED
Electrode buffer	0.192 M glycine, 0.124 M Tris base, 0.5% (w/v) SDS, pH 8.3

Western-blotting

Buffer	Components
Transfer buffer	1 × SDS electrode buffer, 20 % (v/v) methanol
10 × TBS	88 g (w/v) NaCl, 24 (w/v) Tris, pH 7.6
TTBS	1 × TBS + 0.1 % Tween-20
Blocking buffer	5 % (w/v) fat-free milk, 0.1 % (v/v) Tween-20, 1 × TBS
Wash buffer	1 × TBS, 0.1 % (v/v) Tween-20